IRF4-DRIVEN EPIGENETIC CHANGES IN MELANOMA CELLS: UNDERSTANDING DOWNSTREAM EFFECTS FOR TARGETED THERAPY

by

Ulduz Sobhi Afshar

B.S., Cellular and Molecular Biology, University of Tehran, 2011

M.S., Molecular Biology and Genetics, Boğaziçi University, 2015

Submitted to the Institute for Graduate Studies in
Science and Engineering in partial fulfillment of
the requirements for the degree of
Doctor of Philosophy

Graduate Program in Molecular Biology and Genetics

Boğaziçi University

2023

ACKNOWLEDGEMENTS

No words can express and describe my gratitude and respect to my supervisor, Assoc. Prof. Tolga Emre. Who I am as a scientist and researcher today is mostly because of his mentoring through the years. During the last 10 years, in every mind-blowing discussion, every brainstorming session, and all the ups and downs, with Tolga hocam, I always learned something not only about my project but also about myself and who I am. Although the chapter of my life as a member of his group has come to an end, nevertheless, I am sure career-wise, at the key moments, he would be one of the people whom I will ask for his opinion and guidance.

This endeavor would not have been possible without guidance from my thesis progress jury members Prof. Tamer Önder and Prof. Arzu Çelik. During my Ph.D. journey, their knowledge, guidance, and suggestions during every thesis progress have helped me to do better experiments, prepare better figures, and become a better scientist. I would also like to thank all my thesis jury members, Assoc. Prof. Elif Nur Fırat Karalar, Assoc. Prof. Ibrahim Yaman, and Assist. Prof. Şükrü Anıl Doğan, for their time, reading and evaluating my thesis and for giving valuable, constructive criticisms. I would also like to give my special thanks to Assist. Prof. Tolga Sütlü for his invaluable guidance during CRISPR/Cas9 screening.

In the lab, I am most grateful to Laila Hedaya and Anna Ogmen, Betül Çakıcı, and Ali Gülhan. At the time they were part of the lab, I had the best memories and got the most scientific and non-scientific help from these four amazing humans. Their friendship and help through the years have helped me learn to laugh in the darkest days. I would also like to extend my sincere thanks to many previous lab members, Asya Evcil, Sedef Sarac, Erdem Yilmaz, Cansu Yerinde, Nalan Yildiz Ayhan, Ipek Selçen, Mustafa Can Ayhan, Ekin Ece Erkan, Ahmet Bugra Tufan, Beyza Dedeoğlu, Begüm Alankuş, Nazilla Moghtaran, Ilgın Karaoğlu, Elifsu Kartal and so many more for their friendship, and help.

I cannot describe it with words the following people mean to me. They have become my chosen family. They are among the most precious people in my life: Ilke, Emre, Oğuz, Elif Ç, Zeynep E, Zeynep K, Emir, Selif, Kübra, Can, İbrahim, Harun, Duygu, Olay, Ecem, Bilal, MehmetCan, Özen, Şiran, Efe, Öykü, Hilal, Sevgi, Farukcan and Davod. In this department, I have met many amazing friends and created many friendships which have lasted until today and hopefully will continue in the future. Therefore, my sincerest thanks and appreciation go to Elif D, Semanur K, Bircan, Ece K, Kardelen, Öykü, Yiğit, Farzaneh, Bahriye, Zeynep D, Burcin D, Uğurcan, Gizem G, Zeynep Ö, Mesut, Tuncay, Berfin, Anastasia, Sinan, Asli abla, Egeman Ş, and many more people. Please know I value you, your friendship, and your help throughout my life in the department.

None of this would have been possible without the love, support, patience, and kindness of my family. Nihal, my person, has been through a lot with me during the last three years of this journey. I hope the future will have many happy and joyful days for both of us. My mom, Sholeh, all this happened because of your unconditional love and support, there is no way to describe how close we are and how much she means to me. To my uncles_ Mohammad, Manochehr, and my dearest twin uncle and aunt, Shahram and Shahla, to Martina my deepest thanks and love to you all. You have always been there for me through this journey, helping me to overcome one obstacle after the other. To my dearest talented, awesome brother, Aydin, nobody can annoy me the way he does. I am lucky and grateful to have you as my brother. I love you more than you can imagine. I am also forever thankful to my father, Mohsen, who helped me through the years.

The work presented here was mostly supported by funds from the Scientific and Technological Research Council of Türkiye (TÜBITAK-ARDEB-1001 grant 218Z040) and the Boğaziçi University Research Projects funds (BÜ-BAP grants 18681, 12752).

ABSTRACT

IRF4-DRIVEN EPIGENETIC CHANGES IN MELANOMA CELLS: UNDERSTANDING DOWNSTREAM EFFECTS FOR TARGETED THERAPY

Despite recent advances in melanoma treatment, mortality rates for metastatic melanoma remain high, which indicates the need to identify new melanoma-critical genes and novel targeted therapies. Melanoma, like other cancers, is driven by driver mutations and the deregulation of epigenome and signaling pathways. Transcription factor IRF4 has been identified as a pivotal player in the development and maintenance of different cells, such as immune cells and melanocytes. Studies showed that IRF4 is an essential component of the survival and maintenance of hematopoietic cancers such as multiple myeloma. Different GWAS studies indicate a strong link between a variation in the IRF4 intronic region with pigmentation in melanocytes and predisposition to melanoma. In this thesis, analysis of patient data from The Cancer Genome Atlas and the integration of RNA-seq and ChIP-seq approaches have led to the identification of IRF4-regulated genes and pathways. Our data demonstrate that IRF4 is a modulator of epigenetic silencing in melanoma. Furthermore, we report that IRF4 is a key modulator of DNA methylation machinery and polycomb repressive complex, which subsequently results in global changes in the epigenetic suppressive marks in the cells. Also, we identify a subset of tumor suppressor genes (TSG) silenced through IRF4-mediated changes of these epigenetic marks. These TSGs are regulators of the cell cycle, PI3K-AKT pathway, and ciliogenesis in melanoma. Moreover, with CRISPR knockout screening, we set out to discover IRF4 synthetic lethal partners. Consistent with our findings, the screening results suggest a critical role for IRF4 as a regulator of the cell cycle and homeostasis pathways in melanoma cells.

ÖZET

MELANOM HÜCRELERİNDE IRF4'ÜN YÖNETTİĞİ EPİGENETİK DEĞİŞİKLİKLER: YENİ HEDEFLİ TEDAVİLER İÇİN ALT YOLAKLARIN İNCELENMESİ

Melanom tedavisindeki son gelişmelere rağmen, metastatik melanom için ölüm oranları hala yüksektir. Bu nedenle, yeni hedefli tedavilerle , melanom açısından kritik genlerin tanımlanmasına ihtiyaç vardır. Melanom, diğer kanserler gibi, sürücü mutasyonlar, epigenom ve sinyal yolaklarının bozulması tarafından yönlendirilir. IRF4'ün, bağışıklık hücreleri, ve melanositler gibi farklı hücrelerin gelişimi ve sürerliliği açısından çok önemli bir rolü vardır. Çalışmalar, IRF4'ün multipl miyelom gibi hematopoietik kanserlerin sağkalımı ve sürdürülmesi için temel bir bileşen olduğunu göstermiştir. Çeşitli GWAS çalışmaları, IRF4'ün intronik bölgesindeki bir varyasyonun, melanositlerdeki pigmentasyon ve melanom yatkınlığı arasında güçlü bir bağlantı olduğunu gösteriyor. Bu çalışmada, Kanser Genom Atlası'ndan alınan hasta verilerinin analizi ve RNA-seq ve ChIP-seq yaklaşımların entegrasyonu, IRF4 kontröllu genlerin ve yolakların tanımlanmasına yol açmıştır. Verilerimiz, IRF4'ün melanomda epigenetik susturma modülatörü olduğunu gösteriyor. IRF4'ün, melanom hücrelerinde epigenetik susturma imlerde genom çapında değişiklikleri yöneten, DNA metilasyon makinesinin ve polycomb kompleksinin önemli üyelerini düzenlediğini göste-rmekteyiz. IRF4 yoluyla bu epigenetik imlerin değişimi sonucunda bir kaç susturulmuş tümör baskılayıcı genlerini (TSG) tanımladık. Bu TSG'ler, hücre döngüsü, PI3K-AKT yolağı ve siliyogenez düzenleyicileridir. Ayrıca, CRISPR Knockout tarama yöntemiyle, melanomdaki IRF4 sentetik ölümcül ortaklarının keşifi gerçekleştirilmiştir. Tarama sonuçları, bulgularımızla uyumlu olarak IRF4'ün melanom da hücre döngüsünün ve homeostazi yolların regülasyonunda kritik bir rol önermektedır.

TABLE OF CONTENTS

LIST OF FIGURES

LIST OF TABLES

LIST OF SYMBOLS

bp	Base Pair
cm	Centimeter
g	Gravitational force
gr	Gram
hr	Hour
kbp	Kilo Base Pair
kDa	Kilo Dalton
M	Molar
mg	Milligram
ml	Milliliter
mM	Millimolar
min	Minute
ng	Nanogram
nM	Nanomolar
RPM	Revolutions Per Minute
RT	Room Temperature
sec	Second
V	Volt
μg	Microgram
μl	Micrliter
μM	Micromolar
$^{\circ}$C	Degree Celcius

LIST OF ACRONYMS/ABBREVIATIONS

ABC-DLBCL	Activated B-Cell subset of Diffuse Large B Cell Lymphoma
AF	Alexa fluor
App.	Application
BCA assay	Bicinchoninic Acid assay
Cas9	CRISPR-associated protein 9
CCLE	Cancer Cell Line Encyclopedia
cDNA	Complementary DNA
ChIP-Seq	Chromatin ImmunoPrecipitation-followed by Sequencing
co-IP	Co-Immunoprecipitation
CRISPR	Clustered Regularly Interspaced Short Palindromic Repeat
DepMap	Dependency Map
ddH2O	Double Distilled Water
DMEM	Dulbecco's Modified Eagle Medium
DNA	DeoxyriboNucleic Acid
DMSO	Dimethyl Sulfoxide
DNMT	DNA methyltransferase
Dox	Doxycycline
dCas9	dead Cas9
EDTA	Ethylenediamine Tetraacetic Acid
EV	Empty Vector
Exprs.	Expression
EZH2	Enhancer of Zeste Homolog 2
FBS	Fetal Bovine Serum
GFP	Green Fluorescent Protein
GWAS	Genome Wide Association Studies
HRP	Horse Radish Peroxidase
IF	Immunofluorescent
IRF	Interferon Regulatory Factor

ISRE	Interferon-Stimulated Response Elements
KD	Knock-down
KO	Knock-out
LSIRF	Lymphocyte-Specific Interferon Regulatory Factor
MFI	Mean Fluorescence Intensity
mRNA	messenger RNA
MSRE	Methylation-sensitive Restriction Enzyme Digestion
MUM1	Multiple Myeloma Oncogene 1
NaCl	Sodium Chloride
NF-EM5	Nuclear Factor Enhancer Motif 5
NGS	next-generation sequencing
OE	Over-Expression
ORF	Open Reading Frame
PAGE	Polyacrylamide Gel Electrophoresis
PBS	Phosphate Buffered Saline
PCR	Polymerase Chain Reaction
qPCR	quantitative PCR
PRC	polycomb repressive complex
RNA	RiboNucleic Acid
SDS	Sodium Dodecyl Sulfate
sgRNA	single guide RNA
shRNA	short hairpin RNA
SNP	Single Nucleotide Polymorphism
TAE	Tris Acetate EDTA
TBS	Tris Buffered Saline
TCGA	The Cancer Genome Atlas
TF	Transcription Factor
UT	Untransduced
WB	Western Blot

1. INTRODUCTION

1.1. Melanoma

The Greek physician Hippocrates first described melanoma in the fifth century B.C. Although there is little archaeological evidence of cancer, however, tumors can be diagnosed from the skeletons with osteolytic bone metastases. The oldest physical evidence of melanoma is from a 2400-year-old pre-Columbian mummy with diffuse melanotic metastases found in Peru (Urteaga et al., 1966).

Melanoma, the malignant neoplasm arising from melanocytes, is currently recognized as the most lethal form of skin cancer. Melanoma is also known as the most aggressive form of skin cancer due to its ability to metastasize early in the tumorigenesis process. Melanoma comprises 5.6% of US and 4% of Europe cancer diagnoses, according to 2020 data from European Cancer Information System (ECIS) and The Surveillance, Epidemiology, and End Results (SEER) (Cronin et al., 2022). One in every 74 and 66 women and men, respectively, have a lifetime risk of getting skin cancer (ECIS, 2021). In the US, the current 5-year survival if diagnosed at stages I-II is 99.4%, and at stage IV, 29.8% (Cronin et al., 2022). Mortality rates have been in decline since the emergence of targeted therapy and immunotherapy drugs in 2011 (Saginala et al., 2021). The number of naevi, skin color, and environmental factors such as UV exposure are key host factors that affect the susceptibility to cutaneous melanoma (Gandi et al., 2005; Mitra et al., 2012). Among environmental risk factors, due to an ongoing increase in the popularity of sunbathing and indoor sun-tanning beds, the peak in the number of melanoma incidences is yet to happen. The peak in melanoma cases is estimated to happen in the US until 2026 and in Europe until 2031 (Whiteman et al., 2016; Saginala et al., 2021). Considering the continuous increase in global diagnosis, melanoma has become a burden for public health due to its high mortality at advanced stages and cost of care.

Additionally, despite the development and approval of novel drugs targeting signaling pathways and immune checkpoints, the complexity of melanoma tumors and the rise of therapeutic resistance in recurring tumors have become a major concern. Therefore, expanding the prognostic, diagnostic, and therapeutic toolkits will facilitate the management of melanoma both at the patient level and as a public health burden. Research endeavors are still needed to determine the prognosis at earlier stages, to decrease the chance of re-occurrence, and develop breakthrough therapeutic strategies to get around therapy resistance. For many researchers in the field of cancer research, some of the fascinating targets to study are members of transcriptional regulatory machinery. Particularly transcription factors with potential roles in phenotype plasticity and tumorigenesis (Rambow et al., 2019) and chromatin modifiers, which reshape the chromatin landscape during tumorigenesis (Emran et al., 2019; Zob et al., 2023).

1.1.1. Genetic Landscape in Melanoma

Genome-wide association studies (GWAS) have revealed more than 50 melanoma-predisposition loci, which can influence these host risk factors and other biological processes to affect the likelihood of melanomagenesis (Landi et al., 2020). Several studies have reported that more than 80% of melanoma tumors carry BRAF or NRAS mutations together with highly active mitogen-activated protein kinase (MAPK) and phosphoinositide-3-kinase (PI3-AKT) pathways (Chin et al., 1998; Davies et al., 2002; Tsao et al., 2012). However, one of the most in-depth comprehensive studies on understanding genetic risk factors was published in 2015 by The Cancer Genome Atlas Consortium (TCGA). The TCGA study categorized cutaneous melanoma into four subtypes based on mutational profile: BRAFmt (mutant), NRASmt, NF1mt, and triple WT (Wild type) (Akbani et al., 2015). In 2017, ten other genes, apart from BRAF, NRAS, and NF1, were also validated as significantly mutated genes (SMG) by whole genome sequencing (WGS). These genes include CDKN2A, encoding p16 and p14 cell cycle checkpoint kinase inhibitors; TP53, the most frequently mutated gene in cancers and known as the guardian of the genome; ARID2, a subunit of the SWI/SNF complex, functions in nucleosome rearrangement and transcriptional activation; PTEN, the

negative regulator of PI3K-AKT pathway; and RB, the retinoblastoma protein and a known tumor suppressor with a key role in regulation of cell cycle (Hayward et al., 2017). The outcome of mutations in each of these SMGs has an impact on the activity of the pathway it is related to, which consequently contributes to the phenotype and behavior of the tumor. The role of many of these genetic risk factors in prognosis and melanoma biology still needs to be better understood.

1.1.2. Overview of Signaling Pathways in Melanoma

As mentioned previously, approximately 60% of the cutaneous melanoma tumors harbor a mutation in BRAF kinase (Ribas et al., 2011; Akbani et al., 2015). The V600E substitution mutation is an activating mutation in BRAF. Constitutively active BRAFV600E, the upstream activator of MAPK, contributes to many key features of melanomagenesis. Besides survival and an increase in cell proliferation rate, BRAFV600E also contributes to the migration and invasive behaviors of melanoma cells (Ribas et al., 2011). Due to the activating role of this mutation, BRAF inhibitors (BRAFi) became the first choice of treatment in tumors with BRAFV600E. After some time, cells become resistant to BRAFi. Then the BRAFi-resistant cells switch to ERK to reactivate MAPK (Trunzer et al., 2013; Shi et al., 2014). Therefore, therapy continues with mitogen-activated extracellular signal-regulated kinase kinase inhibitors (MEKi) (Ribas et al., 2014). Melanoma cells acquire cross-resistance toward BRAF and MEK inhibitors (Penna et al., 2015).

After MAPK, the second critical signaling pathway in melanoma is the PI3K-AKT pathway. The activation of the pathway is primarily due to loss-of-function mutations and copy number variation in upstream regulators of the pathways, such as PTEN, a negative regulator (Paraiso et al., 2011; Kwong et al., 2013). PTEN downregulation is observed in up to 30% of cutaneous melanoma tumors. In PTEN wild-type tumors, its expression is suppressed by hypermethylation of the promoter (Wu et al., 2003; Akbani et al., 2015). Furthermore, resistance to BRAFi, MEKi, and immune checkpoint inhibitors will enhance PI3K-AKT activity (Shi et al., 2014; Van Allen et

al., 2014; Trujillo et al., 2019). AKT kinase regulates multiple biological processes through its downstream effectors. AKT is at the nexus of various biological processes such as protein synthesis, survival, migration, proliferation, and glucose metabolism. Its function as a kinase can activate or inactivate its target proteins. For example, phosphorylation of FOXO1, a pro-apoptotic protein, leads to its inactivation and proteasomal degradation. Phosphorylation of mTORC1 by AKT leads to phosphorylation of p70S6K, another kinase. The final product of this phosphorylation cascade is the activation of the S6 ribosomal protein, which regulates global protein synthesis (Carnero et al., 2008; Hers et al., 2011).

Deregulation of canonical WNT- βCatenin pathway is frequent across cancers (Cui et al., 2018; Dzobo et al., 2019). From the Initial state of melanomagenesis to the invasive transformation of the tumor, the canonical WNT pathway has a critical role (Delmas et al., 2007). The canonical WNT pathway, through regulation of Microphthalmia-associated transcription factor (MITF), is one of the pivotal players in phenotype switching from proliferative to invasive or vice versa (Webster et al., 2015). In summary, the interplay between these oncogenic pathways and the transcriptional regulatory network drives melanomagenesis. However, there are still unknown players and members of this organization that are yet to be characterized.

1.1.3. Epigenetic Landscape of Melanoma

Epigenome modifications are at the center of the initiation and development of tumors and their progression to metastasis. In malignancies, alterations in the epigenome have become targets for novel targeted therapies. Epigenetic modification can be a representative marker for the diagnosis and prognosis of cancer (Hatzimichael et al., 2014).

Cancers primarily repress tumor suppressor genes through deletions, loss of function mutations, or increasing epigenetic silencing marks such as DNA methylation, H3K27me3, and H3K9me3 at the promoter regions. DNA methyltransferase enzymes

DNMT1, DNMT3A, and DNMT3B are responsible for maintenance and de novo methylation in the genome. Apart from DNMTs, UHRF1 is another crucial player in this process. UHRF1 facilitates the recruitment of DNMT1 to the newly synthesized DNA regions during replication (Figure 1.1) (Vaughan et al., 2018).

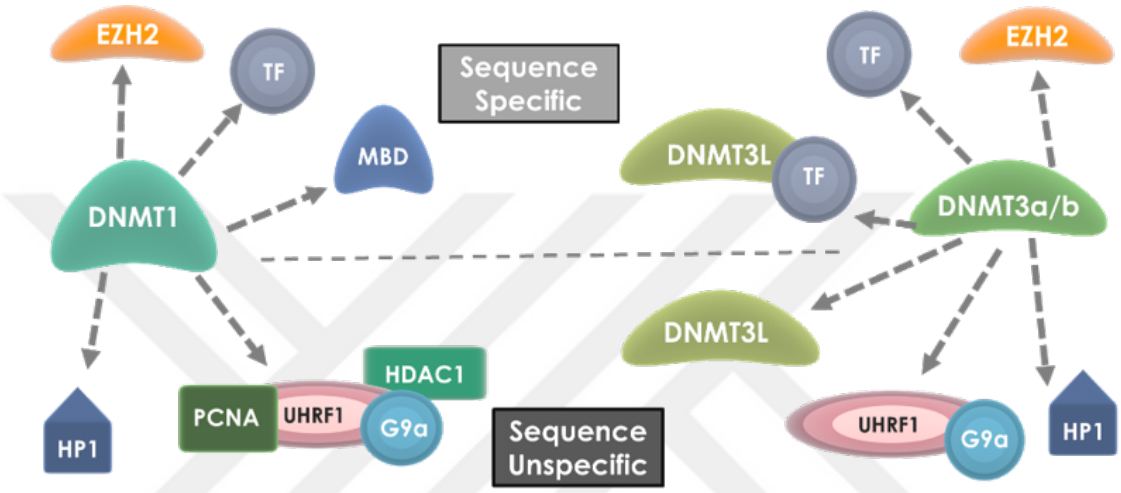

Figure 1.1. DNA methylation machinery and their partners based on sequence specificity (Based on Hervouet et al., 2018).

In BRAF/PTEN null melanoma mouse models, loss of DNMT3B leads to a significant decrease in tumor formation (Micevic et al., 2016). Also, patients with BRAFmt melanoma exhibit extensive DNA methylation by upregulation of DNMTs (Hou et al., 2012). In melanoma, hypermethylated genes include MGMT (a DNA repair enzyme), PTEN, RASSF1A (function in microtubule stability and regulation of growth), CDKN2A (p16INK4a and p14ARF), and CDKN2B (p15, cell cycle checkpoint kinase inhibitor). All these genes play critical roles in the regulation of various biological processes such as cell cycle, DNA repair, proliferation, cellular homeostasis, and survival (Fu et al., 2017; Güvenç et al., 2021). The TCGA study categorized cutaneous melanoma patients into four methylation groups: hypermethylated, hypomethylated, normal-like, and CpG island methylated. The CpG island methylated group is similar to the hypermethylated signature but with a more targeted focus on selected regions (Akbani et al., 2015). In stage III melanoma, hypomethylation is a prognostic

biomarker that predicts improved overall survival (Sigalotti et al., 2012). As one of the therapeutic agents in cancer treatment, the DNMT inhibitors 5-Azacytidine (5-Aza, azacitidine) and 5-aza-2'-deoxycytidine (Decitabine) have only been approved for the treatment of acute myeloid leukemia (AML). For several cancers, there are ongoing clinical trials (Stresemann et al., 2008; Stomper et al., 2021). Depending on cancer cell lines, 5-Aza can have higher cytotoxic activity than Decitabine. This can be due to the integration 5-Aza, a ribose cytosine analogue, into RNA and the inhibition of RNA transcription and its downstream processes (Shaefer et al., 2009; Diesch et al., 2016).

Histone modifications and their regulators are responsible for shaping the chromatin landscape in cells. The most common histone modification is lysine methylation which occurs when histone methyltransferases (writers) add one to three methyl groups to their target lysine. Depending on the lysine, the addition of methylation can contribute to silencing or activating signatures. H3K9me3 and H3K27me3 are the major contributors to establishing and maintaining silencing signatures in the genome. The writer for H3K27me3 is EZH2, which is the catalytic part of the polycomb repressive complex 2 (PRC2). During the last decade, many studies have shown increased EZH2 activity either through mutations or elevated expression levels in various cancer types (Gan et al., 2018). In melanoma, 3% of the tumors harbor mutations in EZH2 (Tiffen et al., 2014). In melanoma tumors, wild-type EZH2 activity can be modulated by different mechanisms. The BRAFV600E tumors increase EZH2 expression through the MAPK pathway (Hou et al., 2012). The in vivo experiments have further elucidated the crucial role of EZH2 in metastasis. In EZH2-conditional knockout mice, compared to control mice, there was a significant decrease in the number of metastatic tumors in lymph nodes and lungs (Zingg et al., 2015). The same group has shown that EZH2 activity regulates cell proliferation and tumor growth by silencing tumor-suppressing genes (Zingg et al., 2015). Additionally, one of the implications of high EZH2 expression in melanoma is increased WNT/β-Catenin activity through suppression of cilia-related genes and diminishing ciliogenesis (Zingg et al., 2018). Melanoma patients with increased EZH2 expression also exhibit a lower survival rate (Tiffen et al., 2015).

Studies indicate a major role for EZH2 as a mediator of immune response in tumors. Zingg et al. showed that EZH2 contributes to acquired resistance to anti-CTLA-4 and IL-2 immunotherapies (Figure 1.2) (Zingg et al., 2017). Due to the prominent role of EZH2 in tumor progression, several EZH2 inhibitors have been designed and used in studies in the last 15 years. The first FDA-approved EZH2 inhibitor was EPZ-6438. This drug is being actively used for the treatment of rhabdoid tumors and lymphomas (Knutson et al., 2012; Straining et al., 2022).

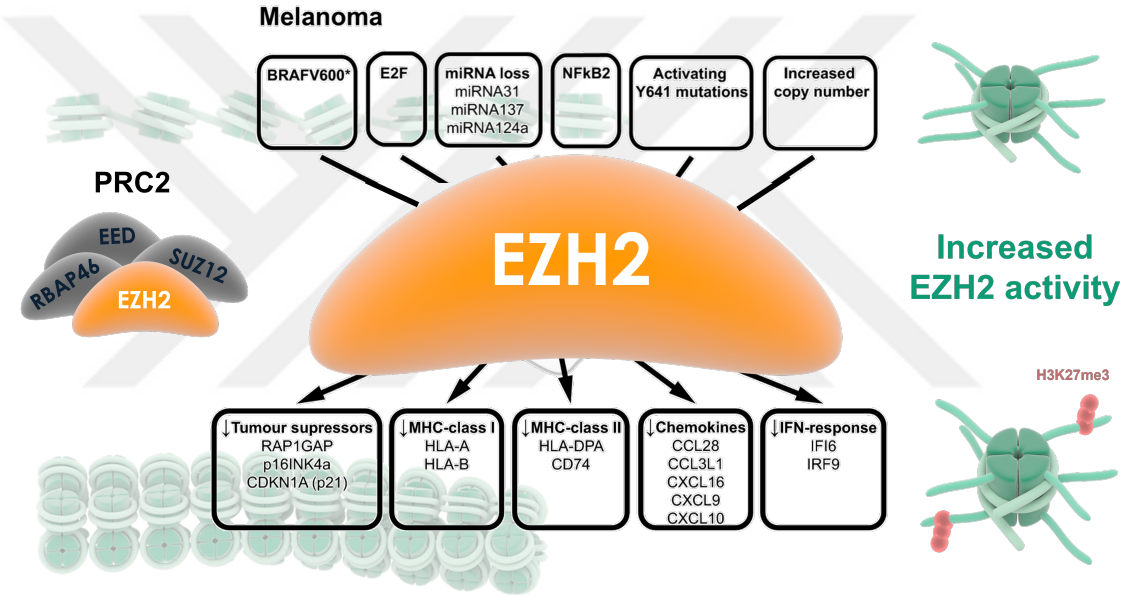

Figure 1.2. EZH2 in melanoma (Based on Tiffen et al., 2016).

To sum up, previous studies suggest that due to the alterations of two key components of epigenetic silencing, the DNA methylation machinery and the EZH2 activity, a subset of melanoma tumors possibly have sensitivity to either DNMT or EZH2 inhibitors.

1.1.4. Cell Plasticity in Melanoma

Melanoma initiation happens with increased proliferation of melanocytes and formation of a benign nevus in the basal layer of the skin, followed by dysplastic nevi with

irregular borders due to unusual growth. Malignant melanoma progresses through radial and vertical growth phases, with cells proliferating horizontally within the epidermal layer and potentially in the superficial dermal layer. At the vertical growth phase, melanoma cells, through phenotype switching, transform from proliferative phenotype to invasive phenotype. Therefore, they can metastasize first to regional lymph nodes and then to the brain, liver, and lungs (Laga et al., 2010; Mobley et al., 2012; Rambow et al., 2019).

Phenotype switching in melanoma is an indicator of cell plasticity and one of the fundamental reasons for cell heterogeneity in melanoma tumors. Initially, the phenotype switching in melanoma was defined by changing between two distinct transcriptional programs. The proliferative phenotype is orchestrated by high MITF and low AXL expression-guided transcriptional program. MITF as the master regulator in melanocyte development drives the proliferative melanocytic transcriptional landscape in cells (Falletta et al., 2017). Therefore, apart from MITF, the signature genes of the proliferative phenotype are from melanocytic lineages, such as premelanosome protein (PMEL), Tyrosinase (TYR), and melan-A (MLANA) (Rambow et al., 2015). In contrast, the invasive phenotype is driven by low MITF and high AXL expression. Invasive phenotype is governed by a less-differentiated more neural-crest-cell-like transcriptional program. The significant genes of the invasive phenotype are zinc finger E-box binding homeobox 1 (ZEB1), BRN2, and SOX9 (Goodall et al., 2008; Fane et al., 2019; Comandante-Lou et al., 2022).

However, more recent studies have shown that the switch between these two significant phenotypes is more gradual. Therefore, the model was revised to 4 different phenotypes based on the interplay between the driving transcriptional program and response to therapy in melanoma cells: melanocytic, transitory, undifferentiated, and neural crest-like (Tsoi et al., 2018). This new terminology for observed phenotypes in melanoma cells provides an improved explanation and understanding of many features of melanomagenesis and its response to therapy (Rambow et al., 2018; Tsio et al., 2018).

Overall, several players of cell plasticity in melanoma have been identified and studied. Nevertheless, due to the complexity of each phenotype, the identification of novel regulators and players is still important and needs to be done.

1.2. Interferon Regulatory Factor 4 (IRF4)

1.2.1. IRF4 in Hematopoietic Cells and Their Malignancies

The transcription factor IRF4 (also known as MUM1, Pip, LSIRF, ICSAT) is a member of the Interferon regulatory factor (IRF) family. IRF4 was first studied in B cells as a transcriptional modulator in immunoglobulin production and B-cell development. It was discovered that unlike most of its family members, the expression of IRF4 is mainly induced by mitogenic stimuli in immune cells. These stimuli activate the NF-κB pathway, leading to the binding of NF-κB heterodimers to the IRF4 promoter in B-Cells (Mittrucker et al., 1996; Gupta et al., 1999). Later, IRF4 expression was detected in other hematopoietic cells, such as macrophages and dendritic cells (Marecki et al., 1999; Gauzzi et al., 2005). Interestingly, cofactors and functions of IRF4 vary in each of these cell types. Studies have shown that IRF4 is pivotal for the differentiation, maintenance, and activity of cells from the myeloid and lymphoid lineage (Da Silva et al., 2012; Man et al., 2013; Fuji et al., 2020). Considering the crucial role of IRF4 in immune cells, dysregulated IRF4 levels can result in hematopoietic cancers. Depending on the cancer type, IRF4 can act as an oncogene or a tumor suppressor. HTLV-1-derived adult T cell leukemia/lymphoma (ATLL) has a constitutive expression of IRF4. In ATLL, activation of IRF4 leads to repression of a set of genes from distinct cellular pathways such as cell cycle, proliferation, DNA repair, and immune recognition (Tsuboi et al., 2000; Kataoka et al., 2015; Nakagawa et al., 2018; Wong et al., 2020). Similarly, multiple myeloma (MM) patients display elevated levels of IRF4 expression. MM patients with high IRF4 have a poorer prognosis and lower survival rate (Heintel et al., 2008). For their proliferation and survival, multiple myeloma cells are highly dependent on IRF4 (Shaffer et al., 2008; Huang et al., 2012; Lamy et al., 2013). Another type of hematopoietic cancer dependent on IRF4 for proliferation and

survival is the activated B-cell subtype of diffuse large B cell lymphoma (ABC-DLBCL) (Yang et al., 2012; Wang et al., 2014). Compared to germinal center B (GC-B) DLBCL patients with low IRF4 expression, ABCL-DLBCL patients with high IRF4 levels have a lower overall survival rate (Muris et al., 2006). In ABC-DLBCL cells, upon lenalidomide treatment, IRF4 is downregulated; following a decline in NF-κB activity, the drug treatment leads to cancer cell death.

For the most part, mature lymphoid cell malignancies such as multiple myeloma, ABC-DLBCL, Hodgkin's lymphoma, and anaplastic large cell lymphoma demonstrate IRF4 upregulation and dependency. Therefore, high IRF4 in these cancers is also an indicator of poor prognosis (Aldinucci et al., 2011; Xerri et al., 2014; Weilemann et al., 2015; Boddicker et al., 2015; Bandini et al., 2018). In contrast, in hematopoietic cancers originating from early lymphoid progenitors, IRF4 has a tumor suppressor role such as BCR/ABL-induced and pre-B-cell acute lymphoblastic leukemia (ALL) (Jo et al., 2012; Pathak et al., 2011; Pang et al., 2016). Additionally, in myeloid-origin cancers, IRF4 can suppress tumorigenesis, such as acute and chronic myeloid leukemias (Schmidt et al., 2000; Jo et al., 2010; Mangiavacchi et al., 2016). Hence, increased IRF4 expression indicates a good prognosis in these cancers.

1.2.2. IRF4 in cells of non-hematopoietic origin

Several studies have detected IRF4 expression in cells from the non-hematopoietic lineage, such as adipocytes, cardiac muscle cells, neurons, and melanocytes (Grossman et al., 1996; Eguchi et al., 2008; Jiang et al., 2013; Guo et al., 2014). Furthermore, in non-hematopoietic cancers, there are studies regarding the alteration in IRF4 expression with potential value as a prognostic biomarker, such as non-small cell lung cancer, gastrointestinal malignancies, and breast cancers (Pirini et al., 2017; Heimas et al., 2017; Qian et al., 2017; Zhang et al., 2018;).

For example, in melanocytes, a single nucleotide polymorphism (SNP, rs12203592) at the 4th intron of IRF4 demonstrates a strong association with various pigment-

related traits. This SNP creates a melanocyte-specific enhancer regulating the IRF4 expression. The occurrence of the C allele at the SNP generates a TFAP2A binding site which leads to TFAP2A and MITF, together with some other transcriptional activators, form a new chromatin loop leading to the activation of IRF4 (Praetorius et al., 2013; Visser et al., 2015). In response, IRF4 and MITF cooperatively upregulate melanin-pathway-related genes such as tyrosinase (Praetorius et al., 2013).

Regarding the significance of the presence of C or T nucleotide at rs12293592 SNP locus, different GWAS studies have reported various features. The T-allele is associated with fair skin color, blue eyes, more freckles, and high photosensitivity (Han et al., 2008; Praetorius et al., 2013; Norton et al., 2016; Hernando et al., 2018). In an age-dependent context, the presence of C or T-allele affects the nevus count differently. In adults, C-allele is linked to a higher nevus count, mainly localized in the torso, while the T-allele is connected to an increased nevus count during adolescence (Duffy et al., 2010; Orlow et al., 2015; Duffy et al., 2018). Furthermore, individuals with T-allele are predisposed to melanoma in regions of the skin that are frequently exposed to UV, such as the head and neck, while the same allele has a protective role in the torso with less UV exposure. On the other hand, C-allele is associated with the development of melanoma in the torso region (Duffy et al., 2010; Kvaskoff et al., 2011; Pena-Chilet et al., 2013). This disparity is related to the development of melanoma from two different paths. The first one, induced by intermittent exposure to UV, is more common in people with light skin. The second path is related to the nevus count. Regardless of the UV exposure factor, the risk of melanoma is higher in people with a high nevus count (Duffy et al., 2010; Kvaskoff et al., 2011).

Immunohistochemical studies in melanoma patients have reported elevated levels of IRF4 protein in tumor tissue (Natkunam et al., 2001; Sundram et al., 2003). A recent study has identified SOX10 as a transcriptional regulator of IRF4 with the role of a modulator of immunogenicity in melanoma. Furthermore, they report that SOX10-IRF4 negatively regulates IRF1 and PD-L1, therefore decreasing the efficacy of anti-PD-1 treatment (Yokoyama et al., 2021). Another recent study has reported

elevated IRF4 expression in 3% of melanoma samples due to copy number variance. They suggest that in these cells, the amplification of IRF4 copy numbers leads to an increase in IRF4 expression (Birkeälv et al., 2023). However, our knowledge of the potential role of IRF4 in non-hematopoietic cells and cancers is still limited.

1.3. CRISPR/Cas9 Pooled Library Genetic Screening

To study genome-wide scaled gene perturbations, pooled screens have been a popular technique to evaluate gene function in bacteria, yeast, and mammalian cells. Pooled screens are also among scalable methods which can be performed either for all genes or more targeted gene sets either in cell lines or in vivo animal models such as mice. For large-scale evaluation of gene perturbations, RNA interference-based pooled screens and, more recently, CRISPR/Cas9-based genetic screens have been vastly used in research. CRISPR/Cas9 pooled screens have broadly diversified the pooled-screening experiments. Unlike RNAi interference, which is used through gene suppression, CRISPR toolkit enables us to perform various screens, gene knockout, inhibition, and activation (Gilbert et al., 2014; Konermann et al., 2015; Sanson et al., 2018).

1.3.1. Brief Overview of CRISPR/Cas9 Screens

CRISPR/Cas9 screening methods are part of forward genetic screens, which means the phenotype is already known and selected, but the contributing genes are unknown and need to be identified (Carpenter et al., 2004; Boehm et al., 2011). In CRISPR/Cas9-based inhibition and activation pooled screening methods, modified versions of Cas9 are used. The nuclease-dead Cas9 (dCas9) is bound with either a transcriptional repressor, such as KRAB (CRISPRi), or a transcriptional activator, such as VPR64 (CRISPRa), to modify the expression of target genes (Gilbert et al., 2014; Konermann et al., 2015). CRISPRi screening is employed to study gene dosage effects, and it is more similar to RNAi pooled screens. CRISPRa advantage over using ORF (open reading frame) libraries is the modulation of endogenous expression, which

is more comparable to gene expression changes in biological conditions (Konermann et al., 2015; Zlatan et al., 2015). Similar to other CRISPR/Cas9 pooled screening techniques, CRISPR/Cas9 loss-of-function pooled screening starts with implementing genetic perturbations into a cell population through lentiviral transduction in a manner so each cell would have a single integrated gRNA. Library elements integrated subpopulations of cells are selected either using a fluorescence marker or antibiotic-selection protocols.

At the end of the screening, depending on the phenotype of interest, the next-generation sequencing libraries for samples from different time points are prepared and then sequenced. The results will uncover which genes have been positively selected (favored) or negatively selected in the phenotype of interest (McDade et al., 2016; Joung et al., 2017).

Currently, the CRISPR-based screening toolbox is still expanding. Among the more recently established and optimized methods, the most noteworthy techniques are CRISPR/Cas9-based screening coupled with single-cell sequencings methods such as CROP-seq, PERTURB-seq, and CRISP-seq which enable to obtain readouts from perturbation-modulated transcriptome changes (Jaitin et al, 2016; Dixit et al., 2016; Adamson et al., 2016). These methods provide a unique opportunity for CRISPR/Cas9 pooled screens in vivo.

1.3.2. CRISPR/Cas9 Screening in Cancer

In pursuit of novel therapeutic targets, CRISPR/Cas9-based screens have become a robust functional genomics tool. With CRISPR/Cas9 screen, we can discover vulnerabilities in a genotype-specific manner. Furthermore, we can discover the essential genes, which means their ablation results in diminishing cell viability. Also, the essential genes are potent drug targets. To characterize essential genes across cancers, large-scale genome-wide CRISPR/Cas9 screens have been carried out in numerous cancer cell lines (Hart et al., 2015; Aquirre et al., 2016; Munoz et al., 2016). The es-

sentiality of a gene can be defined either as core essentiality, which means that the gene is necessary for most of the cell lines, or context-dependent essentiality, which can be defined as the gene is essential based on the cancer type or only with the specific genetic background of the cell lines (Cowley et al., 2014; Meyers et al., 2017). The identification of context-dependent essential genes can guide us toward finding better targets for specific cancer. A recent study aimed at the discovery of genetic dependencies specific to melanoma and not present in other cancer types. They report a list of 33 genes whose depletion only affects the viability of melanoma cells. Some were previously identified genes, such as BRAF, MITF, and SOX10. They also identified several genes which were either regulating or components of MAPK signaling, such as MAPK1 and DUSP4 (Christodoulou et al., 2020).

1.4. Identification of Gene-Gene Synthetic Lethality in Cancer

Context-dependent essentiality at the gene-specific level depicts that a gene's importance depends on the presence of other genes. In cancer, this can be seen in the case of oncogene addiction and synthetic lethality. For example, in oncogene addiction, cells with an altered oncogene would lose their fitness if the oncogene was depleted. Whereas cells with wild-type oncogene can compensate for the loss of that oncogene. For example, inhibition of BRAF in BRAFmt or KRAS in KRASmt melanoma cells. On the other hand, in synthetic lethality, the loss of gene X or gene Y separately would not affect cell viability because the cells, in the event of perturbation in one, would compensate with the other one. However, simultaneous perturbations and alterations of both genes would kill the cells. In the context of cancer, this can be described as due to oncogene activation or tumor suppressor loss, a non-essential gene can transform into an essential status (Zhan et al., 2015; Huang et al., 2020). In a study, data indicate that in cells that harbor ARID1 loss-of-function mutation, treatment with GSK126, an EZH2 inhibitor, led to a significant reduction in the proliferation and growth of the cells. Whereas the same treatment in ARID1A wildtype cell lines did not cause any notable effect. Therefore, they have reported a synthetic lethal relationship between ARID1A and EZH2 in cancer cells (Bitler et al., 2015).

By implementing the CRISPR/Cas9 genetic screen alone or in the presence of a drug, we can unveil and widen the genetic interaction networks in different cancers. Large-scale CRISPR/Cas9 loss-of-function screenings across various genetic and epigenetic contexts are utilized to expand our knowledge of synthetic lethal pairs in human cancer cells. One of the first CRISPR/Cas9 screening studies was carried out to identify genes contributing to the BRAF inhibitor, Vemurafenib resistance in melanoma cells. Results showed that loss of NF1 would activate NRAS, which is vital for the vemurafenib-resistant cells (Nissan et al., 2014; Shalem et al., 2014). This type of screening, which is based on drug resistance, can also refer to genes and pathways with a possible synthetic lethal relationship (Huang et al., 2019; Zhang et al., 2021).

1.5. Brief Synopsis of previous studies in the group

Related to the topic of this thesis, here is a brief overview of the results from some of the previous studies from our group. With GFP competition assay, we have shown IRF4 knockdown reduces cell fitness in IRF4-expressing melanoma cells (Figure 1.3) (Ayhan M., 2014; Yildiz-Ayhan, 2023).

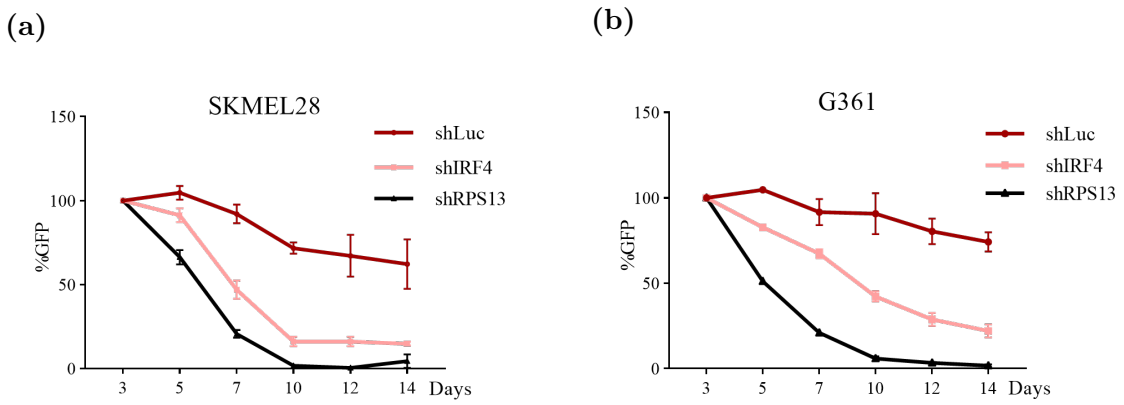

Figure 1.3. GFP competition assay in IRF4-depleted melanoma cell lines with shLuc and shRPS13 as negative non-targeting and the positive controls, respectively (n=3).

Furthermore, GFP competition assay for CRISPR/Cas9-based IRF4 knockout studies also demonstrated IRF4-dependency in melanoma cells (Yerinde, 2016). The colony formation data also indicated impaired growth in SKMEL28 and G361 cancer cell lines upon IRF4 depletion, whereas IRF4 knockdown in MELST (with no detected IRF4 expression) does not affect colony formation (Figure 1.4) (Yildiz-Ayhan, 2023).

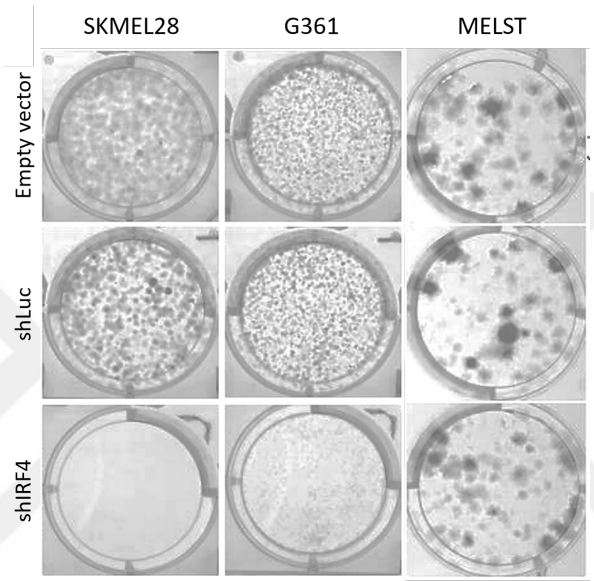

Figure 1.4. Colony formation assay in IRF4-depleted melanoma cell lines with MELST, IRF4 negative immortalized melanocyte cell line as negative control.

In the transcriptomics study of IRF4 depletion in melanoma cells, differentially expressed genes were defined by comparing shIRF4 transduced with shLuc, the non-targeting control transduced cells. The RNA-seq data have identified IRF4-regulated genes in SKMEL28 and SKMEL5 melanoma cell lines. In the RNA-seq study, the primary focus was the characterization of key transcription factors and critical survival pathways modulated by IRF4. Additionally, this study also demonstrated that IRF4 expression contributes to proliferative phenotype in melanoma cells (Yilmaz, 2014). To characterize IRF4 transcriptional target genes, for my master thesis work, we performed ChIP-seq in melanoma cells. Combined results from RNA-seq and ChIP-seq have led to the identification of IRF4 target genes such as MITF, TYR, and EZH2. Gene Ontology (GO) analysis of the intersection of RNA-seq and ChIP-seq data showed

that IRF4 transcriptional regulator genes are enriched for chromatin-associated factors, pigmentation, and regulation of proliferation (Figure 1.5) (Sobhiafshar, 2015).

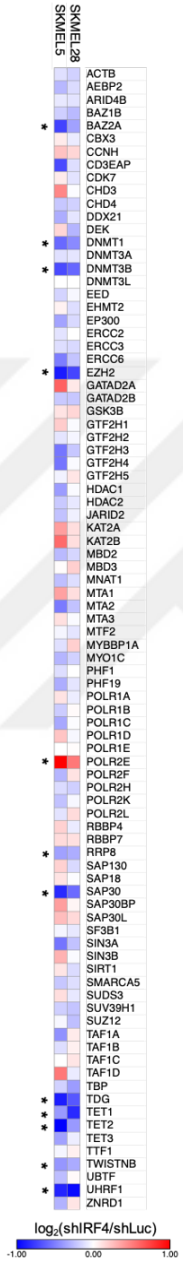

Figure 1.5. The Heatmap of IRF4 knockdown RNA-seq results, showing expression changes in chromatin-associated factors. The gene list from the REACTOME database (R-HSA-212165, except genes encoding histones). "*" genes whose expression significantly altered ($q < 0.001$) in both cell lines.

2. PURPOSE

IRF4 protein has been shown to play an important role in certain hematopoietic cancers. Recent studies have established IRF4's role in pigmentation in melanocytes. Studies from our group have found that IRF4 depletion in melanoma cell lines has negative implications on the proliferation and fitness of the cells.

In this thesis, we aim to explore the impact of IRF4 on epigenetic machinery in melanoma cells through a variety of molecular and cellular approaches. In this study, we set out to investigate global and target-gene-specific changes mediated by IRF4 through candidate chromatin-modifying enzymes in melanoma cells. The outcome will lead to gaining a better understanding of the phenotypic implications of the interplay between IRF4 and epigenetic machinery in melanoma. In the second part of this study, I aim to identify synthetic lethality partners of IRF4 in melanoma using CRISPR/Cas9 loss-of-function screening. With this study, we can provide a basis for the discovery of potential new drug combinations that have higher therapeutic efficacy in IRF4-expressing melanoma tumors.

3. MATERIALS

3.1. Equipment and Disposable Labwares

Here are the lists of equipment, disposable and non-disposable labware.

Table 3.1 Equipment and non-disposable labware.

Equipment	**Model and Supplier**
Beakers, 100 and 600 ml	VWR
Erlenmeyers, 250 and 500 ml	VWR
Bottles, 100, 300, 500, 1000 and 2000 ml	VWR
Forceps,	Isolab
Scalpel,	Isolab
Magnetic Stirrer	DragonLab
Magnetic Stirring Bar	VMS-C7, VWR
Cryobox	Mr. Frosty, VWR
Autoclave Indicator Tape	VWR
Measuring Cylinders, 100, 250, 500 and 1000 ml	VWR
pH Meter	Hanna Instruments
Microtube Racks	VWR
Electronic Balance	Sartorius
Microcentrifuge	VWR, USA CT15RE
Horizontal Electrophoresis	Cleaver
Micropipettes	Axygen
Multichannel pipette	Axygen
Heat Block	VWR,
Pipettor	Greiner
Vortex	VWR

Table 3.1 Equipment and non-disposable labware. (cont.).

Equipment	**Model and Supplier**
Centrifuges	Allegra X-22 Beckman
Cell culture hood	Safe Fast Classic, FASTER S.r.l.
Cell Culture Incubator	C-150, Binder
Documentation System	Gel Doc XR System, Bio-Doc Syngene
Ovens	KD200 and FN055, NÜVE
+4 Refrigerator	Arçelik
-20 Freezer	Ugur, UFR 370 SD
-80 Freezer	ULT deep freezer Thermo
-150 Freezer	MDF-1156, Sanyo
Confocal microscope system	DMi8, Leica
Inverted Microscope	Nikon Eclipse TS100
Fluorescence Microscope	Z1 Axio Observer Zeiss
Thermal Cycler	Bio-Rad
Power Supply	VWR
Real-time PCR Machine	PikoReal Thermo Scientific
NanoDrop	Thermo Scientific
Microplate reader	VersaMax™, Molecular Devices
Rotator	Isolab
Shaker	VWR
Carbon dioxide Tank	Genç Karbon
Ice Maker	Brema
Autoclave	UK ASB260T, Astell
Dishwasher	Mielie

Table 3.1 Equipment and non-disposable labware. (cont.).

Equipment	**Model and Supplier**
Heat block	VWR
Sonicators, bath and probe	Q800R, QSonica
Water bath	Memmerty
Automated cell counter	Countess™ , Invitrogen
Hemocytometer	Isolab
Accuri™ C6 flow cytometer	BD Biosciences
Western blot equipment	Bio-Rad
UV transilluminator	Bio-Rad
Magnetic stand	MERK millipore
Programmable mixer-rotator	Grant Instruments

Table 3.2 Disposable labwares.

Labware	**Supplier**
Protein LoBind 2.0ml Tubes	Eppendorf
Parafilm	VWR
Centrifuge Tubes, 15 ml	VWR
Centrifuge Tubes, 50 ml	VWR
Serological pipette, 5ml	Tpp
Serological pipette, 10ml	Tpp
Serological pipette, 25ml	Tpp
Pipette Tips, filtered	Biopointe
Pipette Tips, bulk	Biopointe
Microcentrifuge tubes	Axygen
PCR Tubes, 0.2 ml	Axygen
Round bottom tubes	BD Biosciences
Medical Gloves	VWR

Table 3.2. Disposable labware (cont.).

Labware	**Supplier**
Syringes, 1 and 10 ml	SET Medikal
Syringe Filters	Sartorius
Cryovial	TPP
Cell Culture Plates 6, 10 and 15 cm	TPP
Cell Culture Plates 6-, 12- and 24- well	Sarstedt
Cell Culture Flasks, 25 and 75cm2	TPP, Sarstedt
96 well Piko PCR plates	Thermo Scientific
Petri Dishes	Fıratmed
PVDF membrane	Merck Millipore
Whatman paper	Thermo Scientific
Kimwipes	Kimberly-Clark Professional
Coverslips, 12mm and 18mm	Marienfeld

3.2. Chemical Consumables

All the kits, enzymes, reagents, chemicals, and buffers are listed here.

Table 3.3 Kits, enzymes and reagents.

Name	**Supplier**
DMEM	Gibco, ThermoScientific
DMEM	Hyclone, Cytiva
Phenol-free DMEM	Gibco, ThermoScientific
FBS	Gibco, ThermoScientific
FBS	Hyclone, Cytiva
Non Essential Amino Acids	Hyclone, Cytiva
Penicillin / Streptomycin	Hyclone, Cytiva

Table 3.3. Kits, enzymes and reagents (cont.).

Name	**Supplier**
Trypan Blue	Gibco, ThermoScientific
Trypsin-EDTA (0.05%)	Gibco, ThermoScientific
HEPES-buffered saline, pH 7.0	Alfa Aesar
Proteinase K	Invitrogen,ThermoScientific
RNase A	Sigma-Aldrich
Dynabeads Protein G	ThermoScientific
Plasmid Miniprep Purification Kit	GeneMark
ZymoPURE Plasmid Midiprep Kit	ZymoResearch
ZymoPURE Plasmid Midiprep Kit	ZymoResearch
XbaI	New England Biolabs (NEB)
XmaI	New England Biolabs (NEB)
BsmBI	New England Biolabs (NEB)
T4 DNA Ligase	New England Biolabs (NEB)
T4 PNK	New England Biolabs (NEB)
AciI	New England Biolabs (NEB)
HpaII	New England Biolabs (NEB)
HinP1I	New England Biolabs (NEB)
HpyCH4IV	New England Biolabs (NEB)
FastAP	Thermo
MyTaq DNA polymerase	Bioline
Gateway^{TM} LR Clonase II kit	Thermo Scientific
10X NEB 3.1 buffer	New England Biolabs (NEB)
10X T4 DNA ligase buffer	New England Biolabs (NEB)
10X CutSmart buffer	New England Biolabs (NEB)
5X MyTaq reaction buffer	Bioline
DNA ladders	New England Biolabs (NEB)
6X DNA Gel Loading Dye	New England Biolabs (NEB)

Table 3.3. Kits, enzymes and reagents (cont.).

Name	**Supplier**
Protease Inhibitor Cocktail Tablets	Roche
Pierce^{TM} BCA Protein Assay Kit	ThermoScientific
NucleoSpin Gel and PCR Clean-up kit	Macherey-Nagel
WesternBright ECL	Advansta
Western Sirius	Advansta
PageRuler Prestained Protein Ladder	Thermo Scientific, Biolegend
NucleoZOL	MACHEREY-NAGEL
MaxiPrep Plasmid kit	Qiagen
Q5	New England Biolabs (NEB)
Phusion HF	New England Biolabs (NEB)
dNTP Reagent	Thermo Scientific
phosphatase inhibitor	PhosSTOP Roche
iScriptTM cDNA synthesis kit	BioRad
RealQ plus master mix SYBR green	Ampliqon
XTT Assay Kit	Roche

Table 3.4 Chemicals.

Chemical	**Supplier**
Ethidium Bromide	Merck
EDTA	Merck
Hydrochloric Acid	Merck
Sodium Chloride	Merck
Potassium Chloride	Merck
Calcium Chloride	Merck
Formaldehyde	Sigma-Aldrich
Sodium hypochlorite solution (15%)	Sigma-Aldrich

Table 3.4. Chemicals (cont.).

Chemical	**Supplier**
Tween 20	Merck
Triton x-100	Merck
Glycine	Sigma-Aldrich
DMSO	Merck
Nonidet NP40 substitute	Sigma-Aldrich
Sodium Dodecyl Sulfate (SDS)	AppliChem
Sodium Deoxycholate	Sigma-Aldrich
Acrylamide xtra solution (40%)	BioFroxx
DEPC-treated water	Fisher Scientifi
Agarose	Sigma-Aldrich
Tris-Cl	Merck
Tris-Base	Sigma-Aldrich
HEPES	Gibco Invitrogen
Bromophenol Blue	Merck
Calcium chloride dehydrate	Merck
Chloroquine	Merck
DAPI	AppliChem
LB Broth	Caisson Laboratories
Glycerol	Merck
Ethanol	Merck
Methanol	Merck
Isopropanol	Merck
Phenol-chloroform-Isoamyl	Sigma-Aldrich
β-mercaptoethanol	Merck
Sodium Acetate	Sigma-Aldrich
Tazmetostat	SelleckChem
Decitabine	SelleckChem

Table 3.4. Chemicals (cont.).

Chemical	**Supplier**
Azacitidine	SelleckChem
DTT	Sigma-Aldrich
Bovine serum albumin (BSA)	Bioshop
Tween 20	BioFroxx
PIPES	Merck
Glycine	AppliChem
Di-Sodium Hydrogen Phosphate	Merck
BS3 cross-linker	Thermo Scientific
TEMED	Bioshop
Ammonium Persulfate (APS)	AppliChem
Agar Bacteriology Grade	AppliChem
Polybrene (hexadimethrine bromide)	Sigma-Aldrich
doxycycline, hyclate	Merck
Carbenicillin	NeoFroxx
Ampicillin Sodium Salt	AppliChem
Puromycin dihydrochloride	Santa Cruz
Neomycin (Genticin sulfate, G418)	Chem Cruz
Paraformaldehyde (PFA)	Sigma-Aldrich

Table 3.5 Buffers and other solutions.

Solution/Buffer	**Composition**
PBS buffer	1 mM Tris pH8, 0.1 mM EDTA pH8 8 mM Na_2PO_4, 150 mM NaCl 2 mM KH_2PO_4, 3mM KCl
PBS-T buffer	0.01% Tween 20 in PBS
10X Tris buffered saline (TBS)	500 mM Tris-HCl pH7.4, 1.5 M NaCl

Table 3.5. Buffers and Other Solutions (cont.).

Solution/Buffer	**Composition**
1X TBS with Tween-20 (TBS-T)	50 mM TrisHCl pH 7.4 150 mM NaCl, %0.05 Tween-20
TE buffer	10 mM Tris pH8, 1 mM EDTA pH8
50X TAE buffer	2 M Tris, 50 mM EDTA pH8, 1 M acetic acid
Cytoplasmic extraction buffer (ChIP)	85 mM KCl, 0.5% NP40 5 mM PIPES pH 8
Nuclear extraction buffer (ChIP)	50 mM Tris pH8, 10 mM EDTA pH8, 1% SDS
IP buffer (ChIP)	16.7 mM Tris pH 8, 1.2 mM EDTA pH8, 167 mM NaCl 0.01% SDS, 1.1% Triton X100
High salt buffer	50mM HEPES, 500mM NaCl, 1% TritonX 100 0.1% Na-deoxycholate, 1mM EDTA
RIPA buffer	150 mM NaCl, 1% NP40 0.5% Sodiumdeoxycolate 0.1% SDS, 50 mM Tris pH 7.4
5X Protein loading dye (Laemmli)	300mM Tris-HCl pH 6.8, 10% SDS 50% Glycerol, 25% β-mercaptoethanol, 0.05% Bromophenol Blue
10% Resolving gel	375 mM Tris-HCl pH 8.8, 0.1% SDS 10% Acrylamide 0.1% APS, 0.1% TEMED
15% Resolving gel	375 mM Tris-HCl pH 8.8, 0.1% SDS 15% Acrylamide 0.1% APS, 0.1% TEMED
6% Stacking gel	125 mM Tris-HCl pH 6.8, 0.1% SDS 6 %Acrylamide 0.1% APS, 0.1% TEMED

Table 3.5. Buffers and Other Solutions (cont.).

Solution/Buffer	Composition
10X SDS running buffer	1% SDS, 1%Tris Base, 14.4% Glycine
Semidry transfer buffer	48 mM Tris-base, 39 mM Glycine, 20% methanol
Western blot blocking solution	5% BSA in TBS-T
Agarose gels	x%Agarose in TAE
Ethidium bromide solution	0.00005% ethidium bromide
4% PFA solution	4%PFA in PBS pH 7.4
Permeabilization solution	0.5% Triton X-100 in PBS
1%BSA IF blocking solution	1% BSA, 0.05% Triton X-100 in PBS
Mounting medium	20 mM Tris-HCl pH 8, 80% Glycerol

3.3. Biological Materials

3.3.1. Cell Lines.

The cell lines used in this study are SKMEL28 (gift from Dr. Eiríkur Steingrímsson, University of Iceland), G361, A375 (gift from Tolga Sütlü, Acibadem University), UACC62, MALME3M and MELST (gift from María S. Soengas, CNIO). HEK293FT cell line was used for lentiviral production (gift from Ferruh Özcan, Gebze Technical University).

3.3.2. Plasmids and Oligos.

Here are the lists of all the plasmids and oligos used in this thesis.

Table 3.6 Plasmids.

Name	ID/Catalog
psPAX2	Addgene N 12260
pCMV-VSV-G	Addgene N 8454
pKH1	Kindly provided by Maria Soengas
pInducer20	Addgene N 44012
pDONR221-IRF4	HsCD00040446 DNASU
pLKO5.sgRNA.EFS.GFP	Addgene N 57822
pCW-Cas9-Blast	Addgene N 83481
TOPFLASH (3X TCF/LEF)	Kindly provided by Necla Birgül
pRL-SV40-Renilla	Kindly provided by Necla Birgül

Table 3.7 Oligos.

Oligo ID	Sequence (5' to 3')	App.
DNMT1-IRF4-F	TAGCCACCAGGGAGCTACGG	ChIP
DNMT1-IRF4-R	ATGTCCGCAGGCGGTAGGTA	ChIP
DNMT3B-IRF4-F	TGCTTTGCCCCATCGAGACA	ChIP
DNMT3B-IRF4-R	TGGTTCCAGCGCCCAATAGC	ChIP
EZH2-IRF4-F	CAGCTGGGTGTGAAGTTGGC	ChIP
EZH2-IRF4-R	CAGGCACTGTCTATGCACCG	ChIP
ChIP-pTyr-F	GTGGGATACGAGCCAATTCGAAAGA	ChIP
ChIP-pTyr-R	CCCACCTCCAGCATCAAACACTTTT	ChIP
ChIP-neg-F	AATATGTACATCAGGCAATCGGCTCTTC	ChIP
ChIP-neg-R	CAACTGGAATCAGATCCACTTCATGGAAA	ChIP

Table 3.7. Oligos (cont.).

Oligo ID	**Sequence (5' to 3')**	**App.**
WDR19-K27me3-F	CTCCTCCCTTCTACCCCAGA	ChIP
WDR19-K27me3-R	GGAGGCAGGATGGGCTAAAT	ChIP
Bactin-K27me3-F	CTGGGTCATCTTCTCGCGGT	ChIP
Bactin-K27me3-R	TCCTTTCCTTCCCAGGGCGTG	ChIP
IRF4-exp-F	GAGAACGAGGAGAAGAGCATC	Exprs.
IRF4-exp-R	CTTTCCTTTAAACAGTGCCCAAG	Exprs.
DNMT1-exp-F	CAAACCCCTTTCCAAACCTC	Exprs.
DNMT1-exp-R	GCCTGGTGCTTTTCCTTGTA	Exprs.
DNMT3B-exp-F	AGGGAGGTGTCCAGTCTGCT	Exprs.
DNMT3B-exp-R	CTGTGTCGTCTGTGAGGTCG	Exprs.
UHRF1-exp-F	GCCATACCCTCTTCGACTACG	Exprs.
UHRF1-exp-R	GCCCCAATTCCGTCTCATCC	Exprs.
EZH2-exp-F	CCCTGACCTCTGTCTTACTTGTGGA	Exprs.
EZH2-exp-R	ACGTCAGATGGTGCCAGCAATA	Exprs.
p21-exp-F	TGTCCGTCAGAACCCATGC	Exprs.
p21-exp-R	AAAGTCGAAGTTCCATCGCTC	Exprs.
p27-exp-F	AACGTGCGAGTGTCTAACGG	Exprs.
p27-exp-R	CCCTCTAGGGGTTTGTGATTCT	Exprs.
PTEN-exp-F	TGGATTCGACTTAGACTTGACCT	Exprs.
PTEN-exp-R	GGTGGGTTATGGTCTTCAAAAGG	Exprs.
WDR19-exp-F	TGATGAGGCCTGAATACCGC	Exprs.
WDR19-exp-R	AATGGACATGGAGTCGTGGC	Exprs.
AXIN2-exp-F	AGCCAAAGCGATCTACAAAAGG	Exprs.
AXIN2-exp-R	AAGTCAAAAACATCTGGTAGGCA	Exprs.
MET-exp-F	AGCAATGGGGAGTGTAAAGAGG	Exprs.
MET-exp-R	CCCAGTCTTGTACTCAGCAAC	Exprs.
RPS28-exp-F	GACACGAGCCGATCCATCATC	Exprs.

Table 3.7. Oligos (cont.).

Oligo ID	Sequence (5' to 3')	App.
RPS28-exp-R	TGACTCCAAAAGGGTGAGCAC	Exprs.
PTENp-met-F	GTCCCTGCATTTCCCTCTACACT	MSRE
PTENp-met-R	GGGGTGGAGGACTGATGATGAAA	MSRE
p21p-met-F	CTCACTCGTCAAATCCTCCCCTT	MSRE
p21p-met-R	CACCCTACACTCACCTGAACAGA	MSRE
p27p-met-1F	AATACATCGCGGTCCCTCTCACTA	MSRE
p27p-met-1R	GGGGATGAAAAACCCACTACCTCC	MSRE
p27p-met-2F	CCAGAGCAGCTACTTGTAACCCAG	MSRE
p27p-met-2R	CCTAGTTCTTGTTCGGATGGGCAA	MSRE

3.3.3. Antibodies.

The antibodies which have been used for western blot, ChIP and immunofluorescence staining are listed here.

Table 3.8 Antibodies.

Antibody	Catalog	Supplier	Dilutions
IRF4	4964	Cell Signaling	IF: 1:1000
IRF4	*	Proteogenix	ChIP: 5ug/IP , WB: 1:1000
IRF4(M-17)	sc-6059	Santa Cruz	ChIP: 5ug/IP
GAPDH	sc-25778	Santa Cruz	WB: 1:1000
H3	4499S	Cell Signaling	WB:1:2000

Table 3.8 continued from previous page

Antibody	Catalog	Supplier	Dilutions
H3K27me3	9733S	Cell Signaling	WB: 1:1000 ChIP: 1:100
H3K4me1	5326P	Cell Signaling	WB: 1:1000
DNMT1	5032S	Cell Signaling	WB: 1:1000
DNMT3B	57868S	Cell Signaling	WB: 1:1000
UHRF1	sc-373750	Santa Cruz	WB: 1:750
B-tubulin	2146S	Cell Signaling	WB: 1:1000
EZH2	5246S	Cell Signaling	WB: 1:1000
B-actin	sc-47778	Santa Cruz	WB: 1:1000
Normal Goat IgG	sc-2028	Santa Cruz	ChIP: 5μgr/IP
Normal Rabbit IgG	2729	Cell Signaling	ChIP: 3 μgr/IP
p27	2552p	Cell Signaling	WB: 1:1000
p21	2946p	Cell signaling	WB: 1:1000
PTEN	sc-7974	Santa Cruz	WB: 1:1000
WDR19	13647-1-AP	Proteintech	WB: 1:1000
AF488 goat anti-mouse	ab150113	Abcam	IF: 1:1000
AF647 goat anti-Rabbit	A-21244	Invitrogen	IF:1:1000
AKT	9272S	Cell Signaling	WB: 1:1000
pSer473 AKT	9271S	Cell Signaling	WB: 1:1000
S6	2217	Cell Signaling	WB: 1:1000
pS6	4858	Cell Signaling	WB: 1:1000
FOXO1	2880	Cell Signaling	WB: 1:1000
pSer265 FOXO1	9461	Cell Signaling	WB: 1:1000
ARL13b	17711-1-AP	Proteintech	IF: 1:500
AcTub	T6793	Sigma-Aldrich	IF: 1:10000

4. METHODS

4.1. Cell Culture

4.1.1. Cell Maintenance and Storage

All cell lines were grown in high-glucose (4500 mg/L) DMEM supplemented with 10% FBS, 1% Penicillin-Streptomycin, and 1% Nonessential amino acids solution (Complete medium). Cells were maintained in T75 flasks and passaged every 3-4 days as they reached 80-90% confluency. The medium was aspirated for passaging, and cells were washed with PBS. After aspirating the PBS, 2 ml of 0.05% trypsin was added to the cells and incubated for 3 min inside the cell culture incubator. After checking that the cells were fully detached under the microscope, 3ml of the medium was added to stop trypsin activity. Cells were diluted in a 1:5-1:10 manner, and finally, the cells were resuspended in 10-12 ml of medium. Until the next passage, cells were kept at 37°C and 5% CO2 incubator.

To prepare for long-term stock of the cells at -150°C, during the passaging process, they were transferred to 15ml tubes and centrifuged at 700 g for 2 minutes. The medium was discarded, and the cell pellet was resuspended in the freezing medium (DMEM, 20% FBS, 10% DMSO). The cell suspension was aliquoted as 3 x 10^6 per ml in each cryovial. Cryotubes are first kept in MrFrosty at -80°C and then stored at -150°C for long-term storage.

To thaw the cells, the cryovials were defrosted at a 37°C water bath for 1 min. Immediately the defrosted cells were mixed with 3 ml of complete medium and centrifuged at 700 g for 2 min. After discarding the medium, the cells were resuspended in the complete medium again and seeded in T75 or T25 flasks.

4.1.2. Cell Count with Trypan Blue

For counting cells, the homogenous cell suspension was made in a 15 ml tube. 40 μl of cell suspension were mixed with an equal amount of trypan blue in a 0.2 ml PCR tube. After mixing well, 10 μl of the mixture was pipetted into each chamber of the hemacytometer. The number of live and dead cells was counted and recorded with Countess II automated cell counter.

4.1.3. Lentivirus Production

4.1.3.1. Transfection with calcium phosphate method. $6x10^6$ HEK293FT cells were seeded in a 10 cm plate supplemented with a 10 ml complete medium for lentivirus production. The next day, the medium was refreshed and complemented with 25 μl of 10 mM chloroquine (25μM final concentration). 4 μg of the envelope plasmid pCMV-VSV-G, 7.5 μg of packaging plasmid psPAX2, and 10 μg of the lentiviral vector of interest were mixed in a total volume of 437.5μl. Then, 62.5 μl of 2 M of CaCl2 was added and mixed well. 500μl of cold, sterile HEPES buffer Saline (HBS) was added to the tube slowly dropwise. The solution was mixed by passing the tube on a tube rack for several seconds until the mixture was full of bubbles. After 5-7 minutes of rest at RT, the mixture was added to the plate drop by drop and with a circular motion to cover the surface of the plates. After 6 hours, the medium was changed.

4.1.3.2. Virus Collection. The media were collected 48 hours post-transfection and filtered through a 0.45 μm filter. The virus-containing media were aliquoted and stored at -80°C freezer.

4.1.4. Lentivirus Transduction

Cells were seeded at 20-25% confluency. The following day, room-temperature lentivirus-containing medium was added to the complete medium supplemented with 8 μg/ml polybrene. After 8 hours of incubation, the medium was changed.

4.1.5. Virus Titration and Analysis of Transduction Efficiency by Flow Cytometry

Different dilutions of GFP-Lentivirus-containing media were titrated via transduction on each cell type. 72 hours post-transduction, the cells were analyzed with the BD Accuri^{TM} C6 flow cytometer to measure the percentage of GFP+ cells and the mean fluorescence intensity (MFI) value for each sample.

4.1.6. Generation of IRF4, and EZH2 Overexpressing Stable Cell Lines

For the generation of overexpression cell lines, 48 hours post-transduction, cells were passaged and seeded at 30% confluency. On day 3 after transduction, G418 (Neomycin) was added to transduced cells and untransduced cells as control at a 1 mg/ml concentration. G418 was renewed every 2-3 days until all the untransduced cells died. Then cells were expanded while still being treated with G418. When almost confluent, they were frozen and added to long-term cell stock.

4.1.7. Generation of CRISPR/Cas9 and IRF4 Knockout Cell Lines

To generate IRF4 knockout cells, as of the first step, cells were transduced with pCW-Cas9-puro or pCW-Cas9-blast. The generation of stable cell lines is similar to 4.1.6, except that 2 μg/ml of puromycin or 5 μg/ml of blasticidin was used during the selection process. After selection and expansion of the stable cells, daily doxycycline (dox) treatment of cells started at 750 ng/μl concentration for 2 days.

With no-dox as the control, Cas9 expression was verified with Cas9 and Flag-tag antibodies in western blot. Then, Cas9-stable cells, which were not treated with dox previously, were seeded for transduction with sgRNA lentiviruses of interest. Day 3 post-transduction, daily dox treatment of Cas9-sgRNA expressing stable cells was started and continued until the collection time point.

4.1.8. Drug Treatments

For certain assays, cells were treated with Azacytidine (5-Aza), Decitabine (Dac), and Tazmetostat (EPZ-6438). Treatments were started the day after seeding the cells unless it has been stated otherwise in the results chapter. All three drugs are dissolved in DMSO. In all experiments, the stock solution was 750x-1000x of the final concentration needed in the assay. Cells were treated daily with 5-Aza and Dac for 3-5 days in the 0.062-1 μM concentration range. EPZ-6438 treatment was applied every other day for 6-8 days in the 0.5-8 μM range.

4.2. Bacterial Cell Culture

4.2.1. Bacterial Culture Growth

E. coli cells were cultured in LB supplied with required antibiotics and incubated at 30°C or 37°C, depending on the addgene-advised growth condition, while shaking at 220 RPM. To select a single colony, cells were spread on Petri dishes containing the necessary antibiotics with a spreader and incubated overnight at 37°C without shaking. For long-term storage of bacteria, overnight-grown single colonies in liquid culture were diluted 1:1 with glycerol at a final concentration of 10% w/v and preserved in cryotubes at -80°C.

4.2.2. Preparation of Competent Bacteria

E. coli competent cells from the stbl3 strain from the previous batch were incubated with 50 ml antibiotic-free LB in a 250 ml flask overnight for 16 hours at 37°C with shaking at 220 RPM. The next day, 4ml of the overnight grown culture was added to 200ml of antibiotic-free LB in a 1 L flask, incubated at 37°C, and shaken at 220 RPM until the OD at 590 nm was 0.375. After aliquoting the culture in four 50-ml tubes and 5-10 minutes of incubation on ice, cells were centrifuged at 1600 g for 10 minutes at 4°C. The supernatant was discarded, and each aliquoted pellet was resus-

pended in 10 ml of ice-cold CaCl2 solution. After another 30-minute incubation on ice, all aliquots were combined in one tube, divided into 200 μl aliquots, and flash-frozen in liquid nitrogen and ready for storage at -80°C.

4.2.3. Competent Bacteria Transformation

4.2.3.1. Transformation with Heat Shock. For every transformation, an aliquot of the competent *E. coli*, the stbl3 strain, was thawed on ice for 10-20 min. Plasmid DNA of interest was added to competent cells (not more than 200 ng) and incubated together for 20-30 minutes. Heat shock of the cells was carried out in a heat block at 42°C for 45 seconds. Then cells were immediately transferred on ice for 3-5 minutes, 800 μl of antibiotic-free LB was added, and the competent cells were incubated at 37°C shaking for 1 hour. After one-hour incubation, cells were centrifuged at 10,000 g for 1 min, and the supernatant was discarded afterward. Pellet was resuspended in 100 μl of LB and added to ampicillin-LB agar plates. Using a sterile glass spreader to distribute the bacterial cell suspension equally on the surface of the plate. Plates were incubated overnight at 37°C.

4.2.3.2. Transformation with Electroporation for the Pooled Library. For this transformation method, the Lucigen Endura electrocompetent cells were thawed on ice for 15 minutes. Also, 0.1 cm electroporation cuvettes were pre-chilled on ice. 50 μl of Lucigen cells were mixed with 1 μl (25ng) of pooled DNA. After flicking to mix, it was incubated for another 30 minutes on ice. The mixture was transferred to a pre-chilled cuvette while avoiding generating any bubbles. Electroporation was carried out using Bio-Rad Gene Pulser Xcell at 1.8kV, 600 Ω, 10 μF in the 0.1 cm cuvette. Then immediately, 2 ml (1 ml at a time) Lucigen recovery media was added to electroporated cells. The suspension was transferred into a 14ml round bottom culture tube, which was incubated for 2 hours at 37°C shaking at 225 rpm. After the two-hour incubation, 3-4 dilutions (5000X, 10,000X, 50,000X, and 100,000X) of the bacterial suspension were prepared and spread on 15 cm LB-Carbenicillin agar plates to check transformation efficiency and used the rest of the recovery suspension was added to 0.5 L of

LB-carbenicillin media in a 2 L flask. Cultures were incubated for 16 hours at 37°C, shaking at 225 rpm for the liquid culture. The following day, colonies were counted to estimate the transformation efficiency. Maxi Prep can be carried out if coverage is at least 30x (the optimal being 100x). Coverage is calculated by multiplying the number of colonies by the dilution factor and dividing by the number of elements in pooled screening. For example, a library of 10,000 elements must have at least 6 colonies in a 50,000X dilution plate. Although sometimes 100+ colonies can be counted in 50,000X dilution plates. After centrifugation at 6084 g for 20 min at 4°C, maxiprep was carried out using Qiagen HiSpeed Plasmid Maxi Kit.

4.2.4. Plasmid DNA Isolation

Plasmid to be used for transfection or sequencing was extracted using the mini-prep or midi-prep kit by ZymoResearch, and for the Maxi-prep kit, Qiagen HiSpeed Maxi kit. All the procedure was carried out according to the manufacturer's instruction and later measured by NanoDrop and stored at -20°C.

4.3. Western Blotting

4.3.1. Lysate Preparation

Protein lysates were prepared either before or after trypsinization. In both instances, after aspirating the medium, the cells were washed with PBS twice. To prepare whole cell lysates, RIPA buffer supplemented with protease inhibitor and phosphatase inhibitor cocktails was added to the trypsinized samples or directly on the plates. The lysed cells were collected from plates after at least 1 hour of incubation at -20°C with a scraper and then transferred into a 1.5 ml tube. After 30-minute incubation on ice, with a brief vortex in between, the samples were sonicated with the water-bath sonicator at 40% power with a 15s ON/ 45s OFF pulse for 3 minutes. After sonication, samples were centrifuged at 14,000 g for 10 min at 4°C. The supernatant was transferred to a new tube and either used immediately or stored at -20°C.

4.3.2. BCA Assay: Quantification of Protein in Lysates

Total protein concentration in the lysates was determined with Pierce BCA assay according to the manufacturer's protocol with minor modifications. First, a 1:2 dilution of each unknown sample was prepared. Then, 7.5 μl of each unknown sample or standard solution was mixed with 150 μl of master mix (1:20 ratio). The 150 μl master mix consists of a 50:1 ratio of solution A and solution B respectively (150 μl of Solution A with 3 μl of solution B). After determining the concentration of each sample based on the standard curve, the value was multiplied by the dilution factor to obtain protein concentration in each lysate.

4.3.3. SDS Gel Preparation & PAGE

According to BCA-measured concentrations, the volume of 20-30 μgr total protein per well was calculated. Then, depending on how many gels will be used, multiply the volume per well for each sample. Next, the final volume for each sample was transferred into one tube in which 5X loading dye (Laemmle buffer) and RIPA (to equalize the final volume among different samples) were added. Each mixture was boiled at 95°C for 10 minutes and cooled on ice. SDS polyacrylamide gels were prepared according to the recipe in table 3.5, 6% for stacking, and based on the interested protein sizes, 8%, 10%, 12%, or 15% resolving gels were prepared. All the gels were prepared in a 1.5 mm cast. Based on the experiment, a 10 or 15-well comb was used in each gel. The gels can be prepared beforehand and stored at 4°C for several days. For 10-well gels, up to 60 μl and for 15-well gels, up to 30 μl were used. The samples were first run at 80 V until the samples passed stacking gel and protein ladder bands started separating. Then, the voltage could be raised to 120 V. The run was completed when the dye reached the end of the gel.

4.3.4. Transfer and Blotting

Approximately 10-15 min before completion of the run, PVDF membrane and thick Whatman filter papers were cut into 5.8 x 8.4 cm sizes. Next, the PVDF membrane was activated with 20-sec incubation in methanol on a shaker. Then, after 30-sec was in distilled water, it was transferred into the transfer buffer. Depending on the transfer method, the buffer composition changes. For semi-dry transfer with turbo trans-blot, Bjerrum Schafer-Nielsen buffer and for wet transfer, Towbin buffer was used. And For semi-dry turbo trans-blot transfer, the setting was 25V for 30 min, and wet transfer at 100 V for 3 hours.

After completion of the transfer, the membrane was incubated with blocking buffer, and 5% skim milk in TBS-T for 1 hour at RT or overnight at 4°C.

4.3.5. Primary and Secondary Antibody Incubations

After blocking, membranes were washed with TBS-T twice for 3 minutes. Following the brief wash, the membrane was cut across the width, separating different ladder sizes. Each part of the membrane was incubated overnight with a 5ml solution containing the primary antibody on interest at 4°C inside a 50 ml tube on a roller. The following day, membranes were washed 3 times (5 minutes each) with TBS-T and afterward incubated with the corresponding secondary antibody for 1 hour at RT in a 50 ml tube on a roller. Post-secondary antibody incubation, membranes were washed with TBS-T 4 times (5 minutes each). After completion of the wash steps, the membranes were kept in TBS until visualization with SynGene.

A noteworthy point, NaN_3, at a final concentration of 0.025%, was added to primary antibody solutions for long-term storage at -20°C since they can be reused several times. Secondary antibodies can be kept at 4°C for up to a week.

Moreover, primary antibodies were mainly prepared in 5% BSA in TBS-T. However, secondary antibodies, if they were to be used to detect the phosphorylated form of a protein, they should be prepared in 5% BSA-TBST, whereas for the rest, 5% skim milk in TBS-T was used.

4.3.6. Visualization

Based on the antibody efficiency and signal strength, WesternBright ECL or Sirius were used for visualizations. In each kit, after mixing equal volumes of peroxide chemiluminescent detection reagent and luminol enhancer solution, the mix was added on top of the membranes. With some orbital movements, the mixture was distributed across the membrane surface. Then, the membranes were visualized in the SynGene system using Genesys software. Further image analysis was carried out using Image J.

4.4. Investigation of RNA Expression

4.4.1. RNA Isolation and cDNA Synthesis

Total RNA isolation was performed using Nucleozol and per the manufacturer's protocol. After elution of RNA samples in nuclease-free water, they were vortexed briefly and kept at -80°C.

RNA sample concentrations were assessed with the NanoDrop machine. Complementary DNA (cDNA) was synthesized with iScript™ cDNA synthesis kit according to the manufacturer's protocol. For cDNA synthesis, 500-750 ng of RNA samples were used, and the final products were stored at -20°C.

4.4.2. RT-qPCR & Analysis

For qPCR, each forward and reverse primer was diluted as 2.2μl from the stock with 62.5 μl of nuclease-free water. Also, each cDNA sample was diluted 1:25 with

nuclease-free water. 2.5μl of each sample was added to each well. For the oligo-enzyme master mix, per each well, 0.25 μl of each primer together with 5 μl of Enzyme master mix and 2 μl of nuclease-free were calculated and based on the number of wells for each primer set plus one well for possible pipetting errors, the oligo-enzyme master mix was prepared. 7.5 μl of the final master mix was added to each well. During this process, the plate and samples were kept on ice. Then Piko PCR plate was sealed with the adhesive sheet, vortexed briefly, and centrifuged at 2000 rpm for 2 min. The qPCR program used is 15 min at 95°C (this can differ based on the brand of SYBR enzyme mix used) for hot-start activation of the enzyme and followed by 40 cycles of 30 sec at 95°C, 1 min at 63°C and completion after melting curve analysis between 60-95°C. After setting up the qRT-PCR program and putting the plate in the PikoReal machine, the run was started.

For analysis of technical triplicates in each plate, after confirming no amplification at no-template-control samples. Relative expression values were calculated using the $\Delta\Delta$Ct method (Bustin et al., 2009) and normalized to corresponding signals from a housekeeping gene (RPS28 or PGK1).

4.5. Chromatin Immunoprecipitation coupled with qPCR

4.5.1. Preparation of Lysate for Immunoprecipitation

Adherent melanoma cells were grown in 10 cm or 15 cm petri-dish plates. At least 2 plates were seeded, one for counting and the other for the ChIP procedure. Cells were grown up to 80-90% confluency, then after calculating the number of cells per plate, crosslinking of protein-DNAs was carried out with formaldehyde at a final concentration of 1% for 10 min at RT with shaking at 200 RPM and then quenching of the reaction with glycine at a final concentration of 0.125 M incubated at RT for 5 minutes while shaking. Immediately after, the plates were put on ice until scraping started. Scraped and collected cells were transferred into a 50-ml tube, washed with ice-cold PBS twice, and kept on ice the entire time. At each step after collection, samples

were centrifuged at 2000 rpm for 2 min at 4°C. The supernatant was discarded, and the cell pellet was resuspended in cellular lysis buffer (CLB) supplied with a protease inhibitor cocktail. For every 10 million cells, 1 ml of CLB buffer was used. After 5 min incubation on ice, samples were centrifuged at 1200 g for 2 min at 4°C. The supernatant containing cytoplasmic material was discarded, and the nuclei pellet was resuspended in protease-inhibitor-cocktail added nuclear lysis buffer (NLB). 300μl of NLB was added per 10 million cells, and if the volume was more than 300 μl, the samples were aliquoted into 300μl sonication tubes. The water-bath sonication was done with the following setting: 70% power, 15 sec: 45 sec ON/OFF cycle, and timer of total sonication set at 15 min. Post-sonication, samples were centrifuged at 14000 rpm for 10 min at 4°C. The supernatant was transferred into a 1.5 ml tube and either used immediately or was snap-frozen with liquid nitrogen and kept at -80°C. Before starting immunoprecipitation (IP), a small amount (30 μl) of samples were boiled at 95°C for 10 min and then run on 2% agarose gel to verify that the majority of DNA fragments were at 200-700 bp size.

4.5.2. Immunoprecipitation of Chromatin

Following washing and equilibrating protein G and A magnetic beads with PBS-T, the beads were suspended in 150 μl of PBS-T per IP reaction. For histones, 2 μg, and transcription factors, 5 μ of antibody per IP was combined with resuspended beads and incubated for 40-60 min at RT on an orbital shaker/rotator. While incubating beads with antibodies, 60-150 μl of sonicated nuclear lysate per IP was mixed with 540-1350 μl of IP buffer supplemented with the protease inhibitor cocktail in a 2 ml protein low-bind Eppendorf tubes. Upon antibody and magnetic beads conjugation, the mix was washed with 500 μl of PBS-T followed by 500 μl of IP buffer. Washed antibody-conjugated beads resuspended in IP buffer (25 μl per IP). The antibody-conjugated beads were combined with diluted nuclear lysates and incubated for 1 hour at RT or overnight at 4°C. After the beads-chromatin complex incubation, samples were washed once with 1ml of each of the following buffers - IP buffer, High salt Buffer, LiCl buffer, and TE buffer for 5 minutes on the orbital shaker. Post-wash step, samples are

resuspended in 100 μl of TE buffer and boiled for 10 min, followed by a brief cool-down on ice. Then, proteinase K was added to each tube, incubated for 30 min at 55°C, and boiled for 10 min to inactivate the enzyme. As of the final step, beads were discarded, and DNA was cleaned with a ZymoResearch ChIP DNA clean-up kit according to the manufacturer's protocol.

The preparation of the input DNA was carried out using 50 μl of sonicated lysate, combined with 50 μl of TE buffer and 1 μl of RNase A, and incubation at 38°C for 45 min. After RNase A treatment, similar to ChIP DNA, the input sample was gone through the cycle of boiling-proteinase K treatment -boiling. After cooling down on the ice, a cleanup with an MN PCR cleanup kit was carried out for input DNA.

4.5.3. qPCR

ChIP and input samples were diluted for qPCR at 1:15 and 1:50, respectively. The volumes of each reaction and the amplification program are as mentioned in 4.4.2, with the only difference being the annealing time of 45 sec instead of 1 min at 63°C.

4.6. Immunofluorescence Staining (IF)

Cells were seeded on 12mm coverslips in 24-well plates. At the time point of interest, cells were washed with 1ml of PBS twice and fixed with 500 μl of methanol, which was added in a dropwise manner and incubated at -20°C for 10 min. Following the incubation with methanol, fixed cells were washed gently with 1 ml of ice-cold PBS three times. Coverslips were blocked using 3% BSA containing 0.1% Triton-X for 1 hour at RT, followed by incubation with primary antibody for 1 hour at RT or overnight at 4°C. Before secondary antibody incubation, coverslips were washed with PBS-T twice. Then samples were incubated with the fluorescence-tagged secondary antibodies of interest and 1μg/ml of DAPI for 1 hour at RT.

Following three times wash with PBS, coverslips were mounted on the glass slide using 5μl per coverslip of VectaShield and sealed with nail polish. The coverslip of cells was imaged in Leica SP8 with LAS X software with 40X water-enhanced objective. Further image processing was carried out LAS X and Image J.

4.6.1. Immunofluorescence Staining (IF) of Cilia

Cells were seeded on 12mm coverslip in 24-well plates at 40% confluency. The following day, cells were washed with PBS twice, and the starvation protocol was started by adding DMEM supplied with 0.2% FBS and Pen-strep. The starvation continued for 48 hours. After 48 hours, IF staining was performed, as mentioned in the previous section. Coverslips were stained with AcTub and Arl13b primary antibodies, followed by incubation with Alexa fluor 488 anti-mouse and Alexa fluor 647 anti-rabbit secondary antibodies, respectively. Quantitative analysis of cilia was performed on cells first by counting DAPI-stained nuclei representing the number of cells, followed by counting cilia structures based on the partially overlapping signal from AcTub and Arl13b from 4 different regions of each coverslip using identical gain and exposure settings in between samples. All data acquisition was carried out with a blinded approach.

4.7. gDNA Isolation

gDNA isolation was carried out using the ZymoResearch gDNA purification kit according to the manufacturer's protocol. gDNA samples were eluted in 50-100μl of TE buffer and stored at -20°C for later.

4.8. 5-mC ELISA

Genome-wide 5-mC levels were performed as described in the manufacturer's ZymoResearch 5-mC ELISA kit protocol. For this assay, 100 ng of denatured gDNA was prepared and coated the wells in a 96-well plate in duplicates. ELISA assay results

were read with the plate reader at 430nm, at three different time points of 15, 35, and 55 min. The values with the best standard curve were used for further analysis in MS Excel. Graphs were generated with GraphPad 8.

4.9. Methylation Sensitive Restriction Enzyme Digestion coupled with qPCR (MSRE-qPCR)

To measure locus-specific DNA methylation levels at promoters of genes of interest, MSRE-qPCR was carried out according to Beikircher et al. protocol (Beikircher et al., 2018). In summary, 500 ng of DNA was incubated with a combination of 4 different methylation-restriction enzymes – AciI, HpaII, HinP1I, and HpyCH4IV. After heat-inactivation of enzymes, digested DNA and control DNA is diluted 1:10–1:20. Similar to the conditions described in Section 4.4.2, qPCR was conducted with a change in annealing temperature from 63 to 60°C (Figure 4.1.).

The primer design for MSRE-qPCR was based on two criteria: 1. Reverse correlation between CpG methylation and gene expression from the TCGA and CCLE databases for the promoter of each target gene 2. A minimum of 3 out of 4 restriction enzyme sites are present in the candidate regions.

4.10. Luciferase Reporter Assay for β-Catenin Targets

4.10.1. Preparation of Conditioned Medium

L929 cells were seeded in 6-wells at 30% confluency, and the next day, they were transfected with an LNCX-wnt3a vector or pIRES-GFP vector as control using a K2 transfection reagent as described by the manufacturer. 48 hours and 72 hours after transfection, conditioned medium (CM) was collected and filtered through a 0.45 μm filter. The conditioned media from two collection times were mixed, aliquoted, and kept at -20°C.

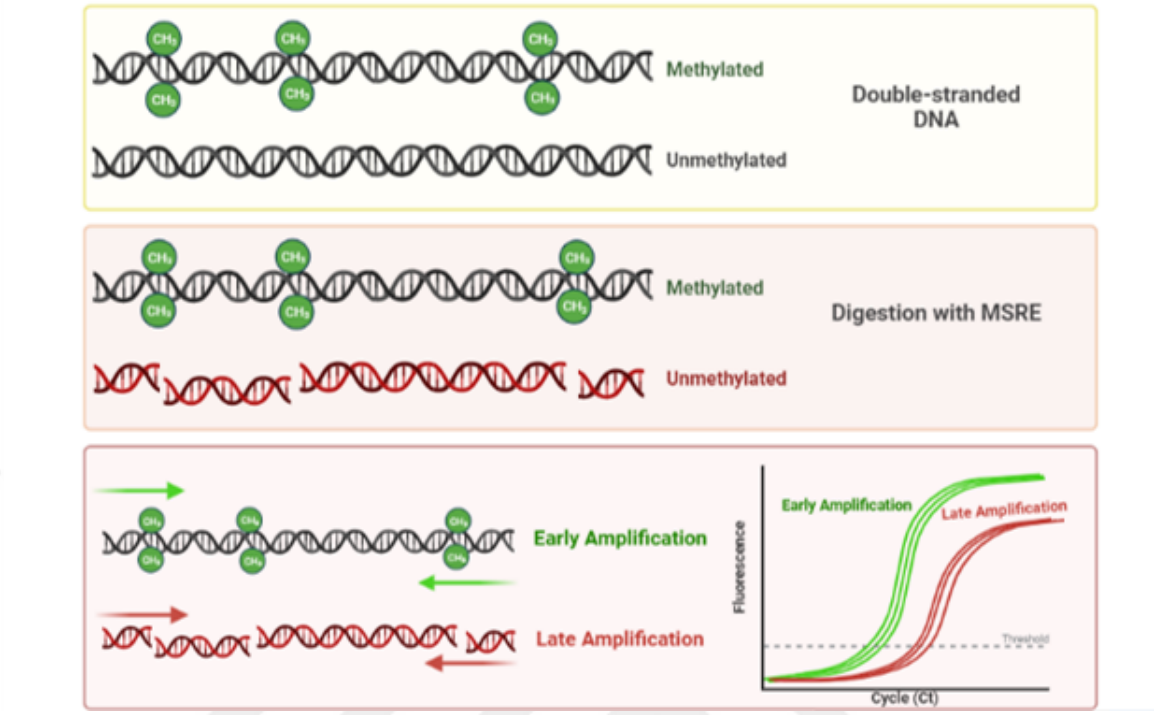

Figure 4.1. How MSRE-qPCR works. Prepared in BioRender

4.10.2. Canonical WNT β-Catenin Pathway Activation

To activate the canonical WNT pathway, cells were treated either with 10 mM of LiCl or 1:1 mixed WNT3a-CM or Ctrl-CM with Complete DMEM for 24 hours.

4.10.3. Luciferase Reporter Assay

Melanoma cells were co-transfected with TOPFLASH plasmid and pGL3-SV40-Renilla in a 12-well plate with K2 transfection reagent according to the manufacturer's instructions. At the time of collection, cells are trypsinized, transferred to a tube, and washed with PBS twice. The lysis and subsequent luciferase assay were performed with Luc-Pair™ duo-luciferase assay kit according to the manufacturer's protocol. For analysis, firefly luciferase readings were normalized to Renilla luciferase readings. Plots are generated with GraphPad.

4.11. TCGA RNA-Seq Analysis

IRF4 mRNA expression and survival data in SKCM TCGA patients were downloaded from the Xena browser (Goldman et al., 2020). Data for pan-cancer expression of the IRF4 gene was acquired from FireBowse (Deng et al., 2017). The data from FireBrowse were replotted using GraphPad 8.

For Kaplan-Meier overall survival analysis, SKCM patients were ranked based on IRF4 mRNA levels from high to low. The top and bottom quartiles of patients were selected based on IRF4 levels, and overall survival analysis was performed with GraphPad 8. The Log-Rank Mantel-Cox test was used to calculate the p-value for the Kaplan-Meier survival analysis.

To analyze the relation between IRF4 expression DNA methylation signature, the IRF4 expression data for the 333 patients for the 2015 article from the TCGA network was downloaded from Xena Browser. Anti-log IRF4 expression was calculated, and patients were grouped based on DNA-methylation signatures. For statistical analysis between each of the two groups, Mann-Whitney statistical test was applied.

4.12. Phenotypic Assays

4.12.1. XTT Assay

In a 96-well plate, 5000-7500 cells per well were seeded in triplicates. The next day, treatment with 5-Aza or decitabine was started. For the XTT assay of EPZ-6438, in the first 48 hours, cells were treated in a 24-well plate and transferred to a 96-well for the rest of the treatment. On the day of the XTT assay, to avoid color interference and false OD read, the medium was changed to 100 μl phenol-red-free DMEM. The XTT reagents were prepared according to the manufacturer's instructions. 50 μl of XTT reagent mix was added to each well. Then, 1.5-2 hours of incubation in the dark at 37°C, and 5% CO2, wrapped in an aluminium foil. At the end of the incubation,

the absorbance (OD) was measured at 492 and 650 nm, which was used to calculate the final OD values as described by the manufacturer's protocol in MS Excel.

4.13. Measuring Cell Death with Trypan Blue Exclusion Assay

In parallel with the XTT assay, cells were seeded in 12-wells in technical duplicates. At the end of treatments and on the day of assay, the medium of each well and the PBS used for subsequent wash were collected in a tube. Post-trypsinization cells were also added to the corresponding tubes. The collected suspension was mixed well with pipetting, and 50 μl was transferred into a PCR tube, where it was mixed with 50 μl Trypan blue. The remaining steps of the protocol are similar to the 4.1.2 section. Finally, Countess II was used to determine live/dead cell percentages.

4.14. Cell Cycle Analysis

For cell cycle assay, approximately 1x10^6 cells are needed. Since the cells also need to be in the sub-confluent state, for this assay, the cells were seeded in 6-cm plates. On the day of the assay, medium and trypsinized cells were all collected into a tube. After counting the cells with the Countess cell counter, 1-1.5 million cells per sample were collected into round-bottom tubes. After initial 2-min centrifugation at 2000 rpm, cells were washed with ice-cold PBS twice. After the final centrifugation, the supernatant was discarded. While slowly vortexing the sample tubes, 750 μl freshly prepared ice-cold 70% Ethanol was added to samples dropwise. At this step, cells are fixed after 30 min incubation on ice, and they can either be processed immediately or stored in 70% Ethanol solution at -20°C for several weeks.

On the day of flow cytometry analysis, fixed samples were briefly thawed on ice and then centrifuged at 600 g for 5 min at 4°C. Ethanol was carefully removed with micropipettes and washed with ice-cold PBS twice. After the final wash-centrifuge cycle, pellets were resuspended in 500 μl of filtered PBS with freshly added propidium iodide (PI) and RNase A at final concentrations of 50 μg/ml and 100 μg/ml, respec-

tively. Samples were incubated for 1.5-2.5 hours at 37°C in the dark, depending on the cell type. SKMEL28 and MALME3M were incubated for 2.5 hours, whereas A375 and UACC62 cells were stained only with 1.5 hours of incubation.

Immediately before analysis with FACS Calibur, 500 μl extra PBS was added to each sample to decrease the risk of blockage by PI while passing through the FACS machine. Notable details while running the samples in FACS Calibur, vortex well immediately before positioning the tube in the FACS machine to avoid cell clumping. Inadequate RNase A digestion can cause broaden the peak distribution (high CV value). While setting up the FACS Calibur software, always view the values associated with the PI channel (FL-2) on a linear scale. Finally, to gate single-cell population gate the cells either FL-2 area vs. width or FL-2 area vs height. For analysis of the cell cycle phases, FLOWJO 10.8 was used.

4.14.1. Real-time Cell Analysis and XCELLigence

For real-time impedance-based cell analysis with XCELLigence, 5000-10,000 cells were seeded in RTCA 16-well E-plates. Software and plates were set up as recommended by the XCELLigence manufacturer. Real-time proliferation and growth were detected based on the impedance measurements of the adherent cells every 30 min, which continued for 80-90 hours until cells became confluent, and the growth curve reached the plateau.

4.15. CRISPR/Cas9 loss-of-function Screening Assay

For CRISPR knockout screening assay, two pooled lentiviral sgRNA plasmid libraries, one targeting genes related to gene expression machinery (GEEX) and the other one targeting genes with crucial roles in apoptosis and cancer (ACOC), were acquired from Addgene and Bassik group from Stanford university (a gift from Michael Bassik, Addgene 101926, & 101928).

4.15.1. Efficiency of Transformation and Estimation of Diversity of sgRNA Elements

4.15.1.1. Counting Colonies. The plasmid libraries were transformed into electrocompetent *E. coli* as described in section 4.2.4.2. After the estimation and verification of efficiency by counting the number of colonies in the dilution plating assay, transformation efficiency (coverage) was calculated by multiplying the counted colonies with a dilution factor and then dividing by the number of elements in the library. After confirmation of optimal transformation efficiency and preserved diversity in the libraries, maxiprep was carried out for liquid cultures of libraries.

4.15.1.2. Analysis of sgRNA Representation and Diversity with NGS. Apart from the presence of abundant colonies in dilution plating assay, in order to determine the sgRNA distribution and representation quantitatively, 5 μg from GEEX and ACOC pooled libraries were used in a two-step PCR to connect adaptors and generate NGS libraries to be sequenced in Illumina NovaSeq machine at Company of Gen-Era.

The oligos for each PCR step were modified and ordered based on the requirements of the NGS lab at Gen-Era. The first PCR was carried out with forward and reverse oligos partially annealed to U6 elements and BlpI-XhoI cut sites amplifying the gRNA cassette in the plasmid. The non-annealed part of these oligos is the sequence used in the tagmentation process, which is adapted from 2nd generation of NGS library preparation, Nextera protocol which fragmentation and tagging are done in a single step. In the first PCR reaction, 5 μg from the maxiprep product of each library was mixed with 1 μl of 100 μM stock of U6 and BlpI-XhoI primers, 20 μl of 5x Q5 buffer, 20 μl of High GC enhancer, 1 μl of 10mM dNTPs, 2 μl of Q5 enzyme. And nuclease-free water to adjust the final volume to 100μl. The conditions for PCR reactions are 2 min at 98°C, 18 cycles of 30 sec at 98°C, 30 sec at 59.1°C, 45 sec at 72°C] followed by 3 min at 72°C. 5 μl of the first PCR was run on 2% agarose gel to verify the efficient amplification of targets. The second PCR was carried out with Illumina adaptor primers i7 and i5, which annealed to the tagmentation sequence from the first PCR product

for amplification. For the second PCR reaction, 5 μl from the first PCR reaction was combined with 0.8 μl of i7 and i5 Illumina adaptors, 20 μl of 5X Q5 buffer, 20 μl of 5X CG enhancer, 2 μl of 10mM stock from dNTP, 2 μl of Q5 polymerase were mixed with 49.4 μl of nuclease-free water. PCR conditions were the same as the first one, with the minor change of 20 cycles instead of 18, which was the case at first PCR.

Analysis of the NGS results was done with Galaxy Online (The Galaxy Community, 2022). After trimming the adapters with the Trimmomatic package, reads were aligned and counted to sgRNA sequences in the pooled libraries using MAGeCK counts. The output was manipulated with Excel, where the read counts of individual gRNA in each library were normalized by the total number of read counts assigned to the respective library.

Since the dispersion of read counts is equal to the coefficient of variation (CV), then, for the assessment of the homogeneousness and gRNA representation of each library, data were analyzed with the Lorenz curve. In the Lorenz curve, gRNAs are ranked by abundance, which is scaled to 1 and exhibit the ratio of total sequencing reads, which are exemplified by the sum of gRNA read counts. If the area under the curve (AUC) in the Lorenz curve was between 0.5-0.7. it was confidently interpreted as a high-quality amplification with good dispersion among gRNAs in the library (Figure 4.2).

4.15.2. Virus Production and Titration

$14x10^6$ HEK293FT cells were seeded with complete DMEM in 15-cm plates. The following day cells were transfected with 20 μg of a pooled library, 15 μg psPAX2, and 7 μg of pCMV-VSV-G. The rest of the transfection process is described in section 4.1.3.

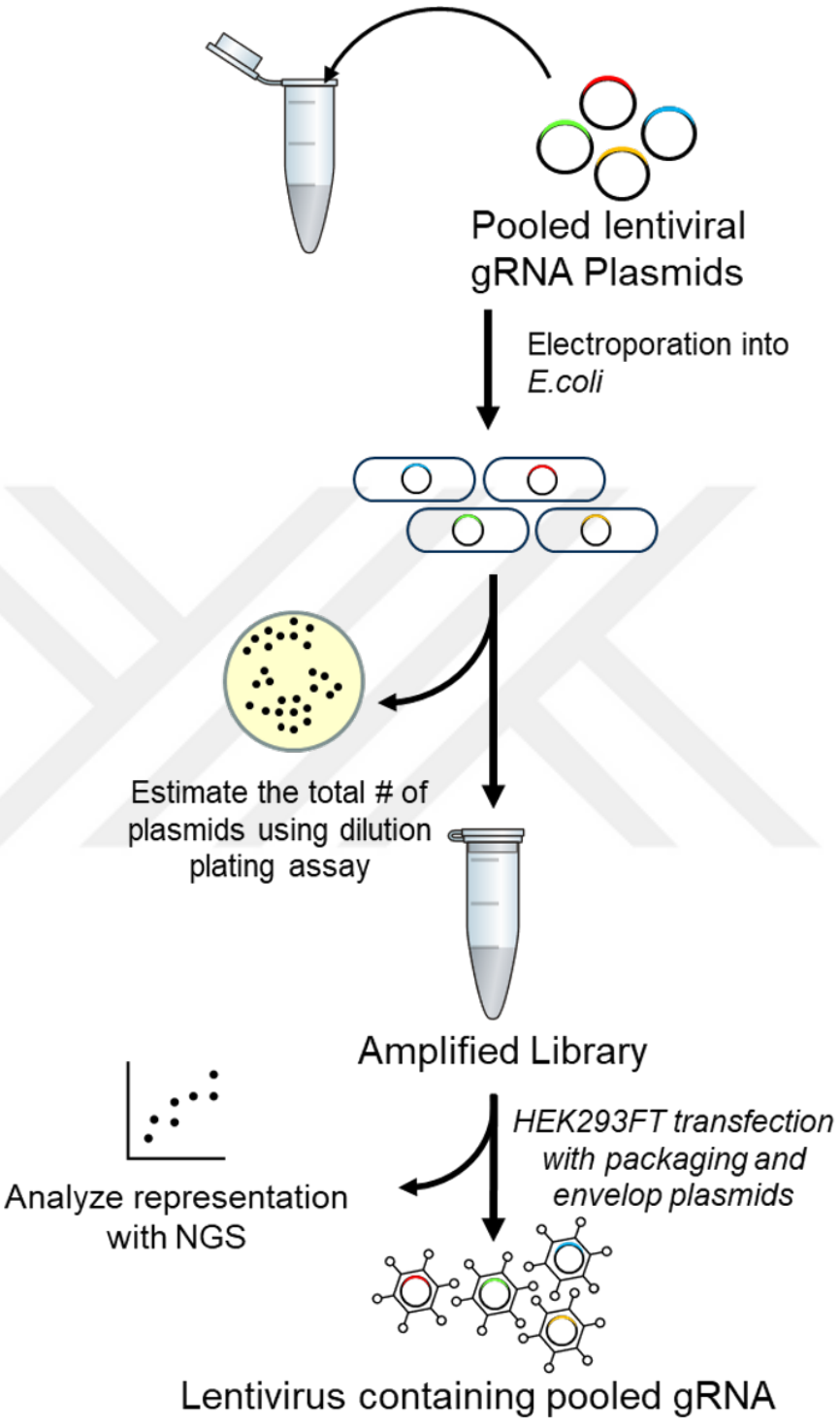

Figure 4.2. CRISPR/Cas9 loss-of-function steps until virus production (Based on McDade et al., 2016).

4.15.3. Generation of Single-Clones of SKMEL28-Cas9 for Screening

SKMEL28 was transduced with the pCW-Cas9-Blast lentiviral vector. Following antibiotic selection with blasticidin, cells were expanded for a few days. On the day of passage, cells were counted and diluted in the medium to achieve a final concentration of 1000 cells per ml. Subsequently, the cell suspension was serially diluted in a 10x manner and seeded into multiple 96-well plates. The next day, wells containing a single cell were marked and monitored for several days until they reached 80% confluency. Single-cell clones from each well were then transferred to a 24-well plate and further seeded into 25 cm^2 flasks upon reaching 80% confluence.

To assess dox-related leakage, single-clone cells were treated with doxycycline (dox) or left untreated. After 12 hours of dox treatment, protein lysates were prepared, and a western blot with Cas9 and Flag antibodies was performed to identify and separate single clones with no dox leakage.

4.15.4. Transduction of Pooled Libraries

The protocol is as mentioned in 4.1.4 and 4.1.5, with slight modifications. The multiplicity of infection (MOI) for pooled screening should be set between 0.2 and 0.3 (Joung et al., 2017). After determining the virus titration using flow cytometry, the number of cells to be transduced was calculated to achieve 500X coverage.

On the day of transduction, cells were seeded into several 75 cm^2 flasks based on the size of the pooled library and transduced with the appropriate amount of virus mixed with a complete medium. Eight hours after transduction, the medium was changed. After 48 hours of transduction, cells were transferred to 175 cm2 flasks, and puromycin selection was initiated. Upon completion of antibiotic selection, the viability of transduced cells was assessed using the trypan blue exclusion assay, aiming for a live/death ratio of approximately 30%.

The screening process was launched via dox treatment after the cell number reached 15 x 10^6, and throughout the screening, at each passage, cells were counted and seeded in the same quantity.

4.15.5. Sample Collection and NGS Library Preparation

The screen was completed on day 21 of dox-induction. The same number of cells were collected, and gDNA extraction was carried out with the phenol-chloroform method (Sambrook J et al., 2001) and later concentrated and desalted using the ZymoResearch gDNA concentrator kit according to the manufacturer's protocol. To prepare NGS libraries, The first PCR need to scale up since all the isolated gDNA would be amplified. Both PCR conditions are the same as 4.13.1.2. For each sample, all the reactions from the first PCR were mixed in a single tube, and for the second PCR with illumine index primer, which will generate NGS-ready libraries, 5 μl from the first PCR was used as the template (Figure 4.3).

4.15.6. Analysis of NGS Results

For preliminary analysis of NGS results, using Galaxy. Sequencing quality control was done with FASTQC 0.12.1 (Andrews S., 2010). Then with Cutadapt 4.4 (Martin M., 2011), 3'and 5'adaptors were trimmed for each sample using default values of Cutadapt. After trimming, with packages in MAGeCK suite 0.5.9.2, the analysis continued. With MAGeCK count, sgRNAs were aligned and each sgRNA count was determined for each sample pair. Then MAGeCK test calculated and generated a ranked gene list, based on fold-change and significance. Further gene ontology and pathway enrichment analysis using the ranked gene list were done in EnrichR (Xie et al., 2021; Kuleshov et al., 2016).

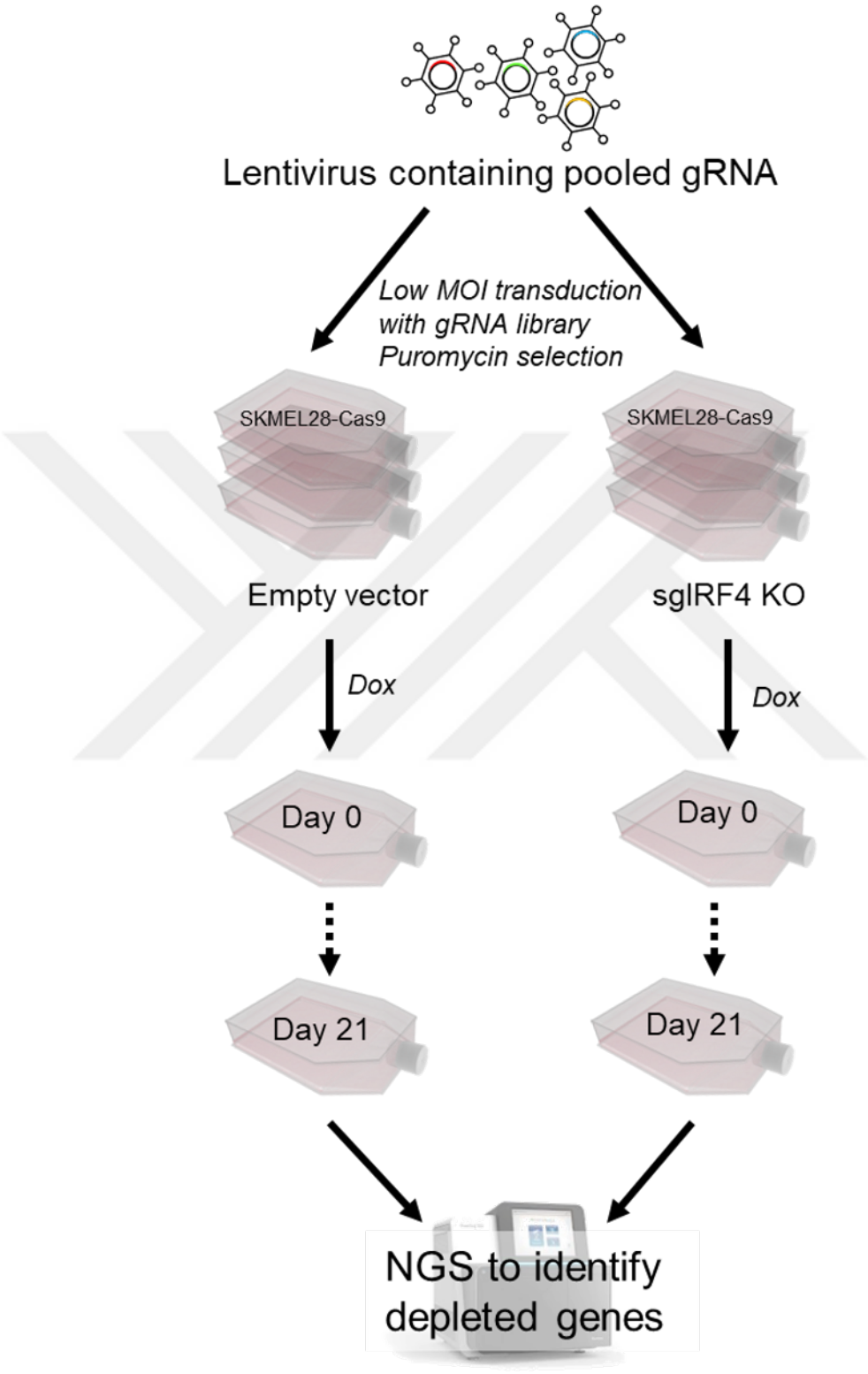

Figure 4.3. CRISPR/Cas9 Loss-of-function: From virus production to next-generation sequencing. Adapted from (McDade et al., 2016)

5. RESULTS

5.1. Investigation of IRF4 Expression in Melanoma Cells and Tumors

5.1.1. IRF4 Expression and Dependency in Cancer Cell Lines

In the last decade, public databases related to the characteristics of cancer cell lines and cancer patients have been rapidly developing. The Cancer Genome Atlas (TCGA) has the most comprehensive multi-omics patient data in various cancers. and the Dependency Map (DepMap) portal for cell lines have become two of the most comprehensive and pivotal databases in cancer studies (Grossman et al., 2016; Tsherniak et al., 2017).

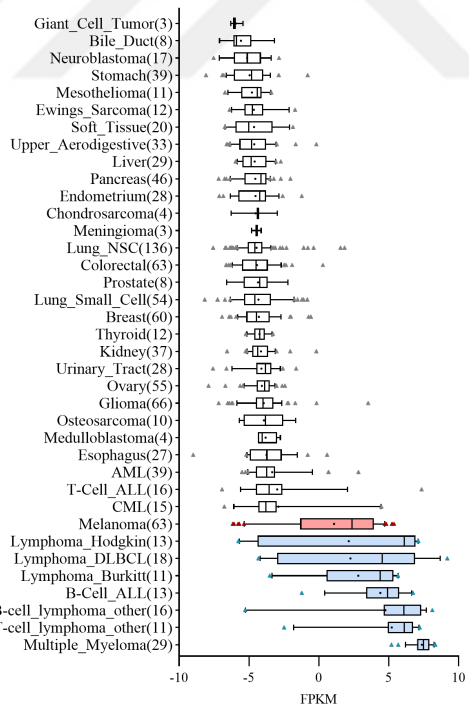

Figure 5.1. IRF4 levels in RNA-seq data from Cancer Cell Line Encyclopaedia (CCLE). Blue: Lymphoid cancers, Red: Melanoma cell lines.

As a part of this thesis, in parallel with IRF4-related experiments in the laboratory, the IRF4 expression and its potential implications have been investigated in TCGA and DepMap samples. IRF4 expression and dependency were analyzed in data from the DepMap portal. Besides several hematopoietic malignancies, melanoma cells have the highest IRF4 expression (Figure 5.1). Consistent with the mRNA data from DepMap, IRF4 expression was verified in a subset of melanoma cell lines, particularly MALME3M, G361, SKMEL28, and SKMEL5 (Appendix Figure D.1).

Furthermore, the data from the CRISPR studies indicate an IRF4-dependency in a subset of melanoma cells with elevated IRF4 levels (Figure 5.2). Analyzed data from the DepMap suggests IRF4-dependency in a subset of melanoma cells.

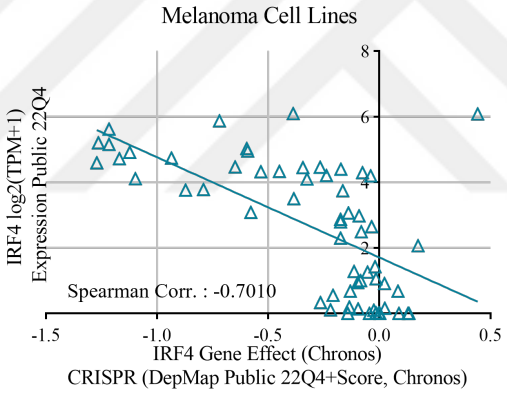

Figure 5.2. Correlation between IRF4 expression levels vs dependency across melanoma cells (blue triangles).

5.1.2. Assessing IRF4 Expression Correlation With Prognostic Markers in TCGA

A 2015 study based on the TCGA data in cutaneous melanoma patients (SKCM) has described a genomic classification based on the mutational landscape of tumor samples and various prognostic features in these patients (Akbani et al., 2015). IRF4 expression and survival data of SKCM patients in TCGA were obtained from Xena Browser (Goldman et al., 2020) and used to assess IRF4 expression and its potential

impact on melanoma patient survival. According to TCGA pan-cancer data, uveal melanoma (UVM) and cutaneous melanoma (SKCM) have higher IRF4 expressions than most cancers (Figure 5.3). The survival analysis was performed for the top and bottom quartiles of patients ranked based on IRF4 expression levels. Kaplan-Meier survival analysis showed that patients with the higher IRF4 expression (top quartile) have a lower survival rate than patients with the lower IRF4 expression (bottom quartile) (Figure 5.4).

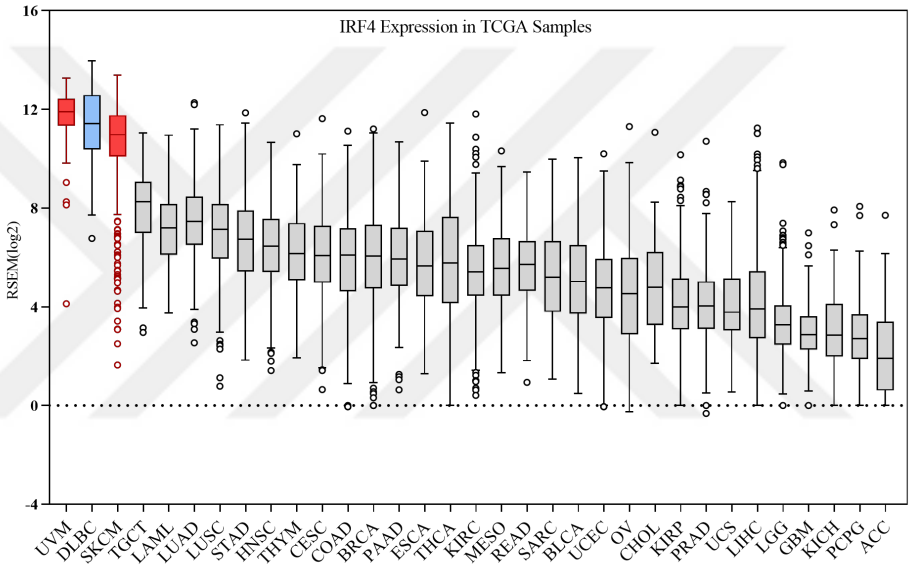

Figure 5.3. IRF4 mRNA expression from TCGA pan-cancer data. Red: melanoma cancers, Blue: Lymphoma cancer

Further assessment of TCGA data with regard to IRF4 expression in cutaneous melanoma and its correlation with prognosis and diagnosis markers were carried out. The results from TCGA melanoma patients demonstrate elevated IRF4 expression is more prominent in primary tumor samples than metastatic samples (Figure 5.5a). Further analysis of the genome-wide methylation signature in SKCM patients concerning IRF4 expression signifies that patients with higher IRF4 expression levels are predominantly in the hypermethylated group (Figure 5.5b).

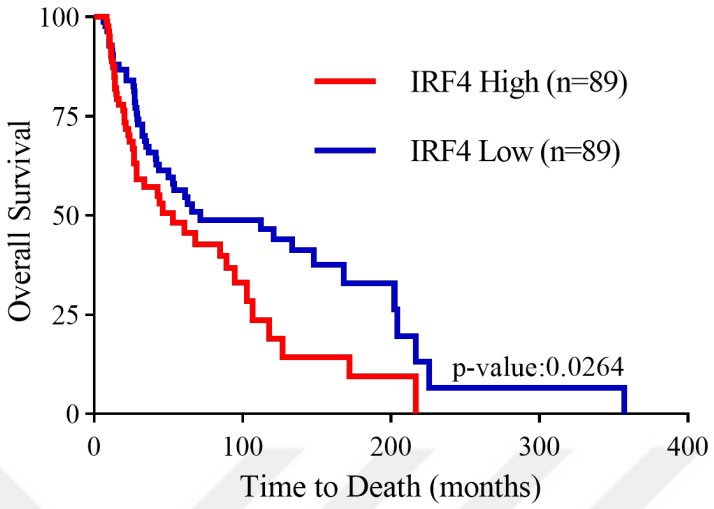

Figure 5.4. Kaplan-Meier overall survival analysis based on IRF4 expression for SKCM patients in TCGA.

The TCGA results suggest IRF4 expression has a prognostic effect in melanoma patients. Furthermore, the correlation between methylation signature and IRF4 expression data implies a possible link between IRF4 and DNA methylation machinery in melanomagenesis.

5.2. IRF4 is Essential for Growth and Survival of Melanoma Cells

To investigate the role of IRF4 in melanoma cells, IRF4 expression was interfered with either by constitutively expressed shRNAs (Figure 5.6a) or via inducible CRISPR/Cas9 system targeting genomic IRF4 loci (Figure 5.6c). IRF4 was overexpressed via an inducible system in melanoma cells (Figure 5.6b).

To elucidate the phenotypic consequences of loss of IRF4 expression, shIRF4 and shLuc transduced SKMEL28 and MALME3M cells were seeded in the XCELLigence plates 48 hr. post-transduction. Real-time cell analyses were carried out for $\sim$ 4

days, during which impedance-based measurements were recorded every 30 min by the XCELLigence machine. Results indicated that IRF4 depletion in melanoma cells impairs cell growth significantly (Figure 5.7).

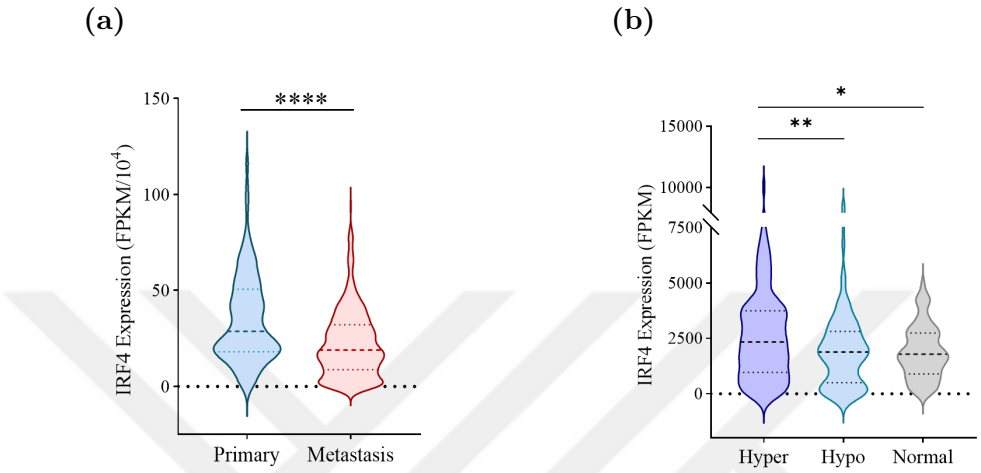

Figure 5.5. In TCGA cutaneous melanoma data. (a) IRF4 expression in primary vs metastasis $p < 0.0001$. (b) Correlation of IRF4 levels and patient methylation signature. $^{**}p < 0.01$, $^{*}p < 0.05$ (Mann-Whitney test). Hyper: hypermethylated, Hypo: hypomethylated.

On the other hand, IRF4 overexpression in A375, UACC62, and SKMEL28 showed decreased proliferation rate (Figure 5.8, Appendix Figure E.1). In addition, XTT assay exhibited that while IRF4 knockdown and knockout cells have lower viability than the controls (Figure 5.9), IRF4 overexpression had no significant effect on cell viability (Appendix Figure E.2).

Consistent with previous results from our group, IRF4 expression is shown to be crucial for the proliferation and maintenance of the subset of melanoma cells with high endogenous IRF4 levels. Interestingly IRF4 overexpression in melanoma cells has no implications on cell viability, although the XCELLigence data suggests the proliferation process is deregulated in the IRF4-overexpressing cells. Taken together, it seems IRF4 levels in a subset of melanoma cells have a vital role in maintaining the proliferation and growth in melanomagenesis.

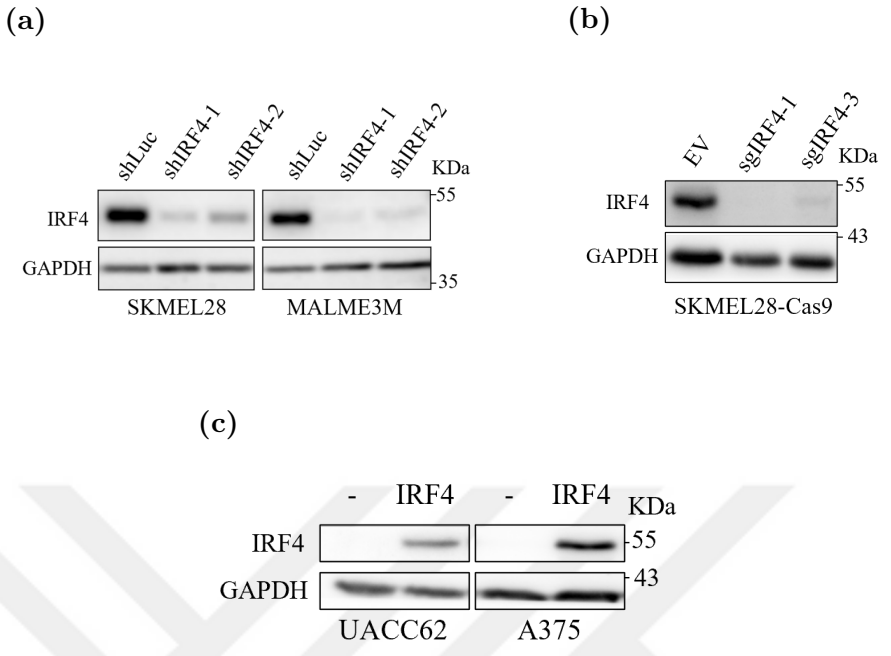

Figure 5.6. Depletion of IRF4 protein with (a) constitutively expressed shRNA or (b) dox-inducible IRF4 overexpression in UACC62 and A375 and (c) dox-inducible CRISPR/Cas9 coupled with gRNAs targeting IRF4 exon1 (n=3).

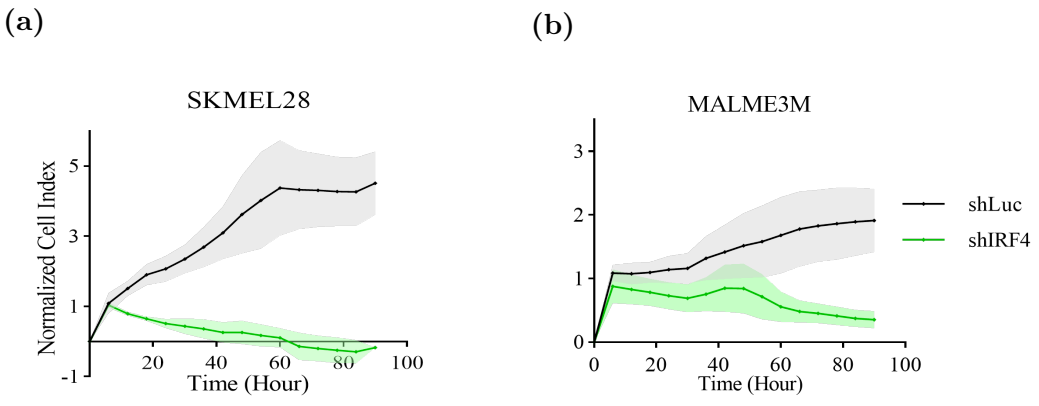

Figure 5.7. Real-time cell analysis with XCELLigence in IRF4 knocked down (a) SKMEL28 and (b) MALME3M (n=3).

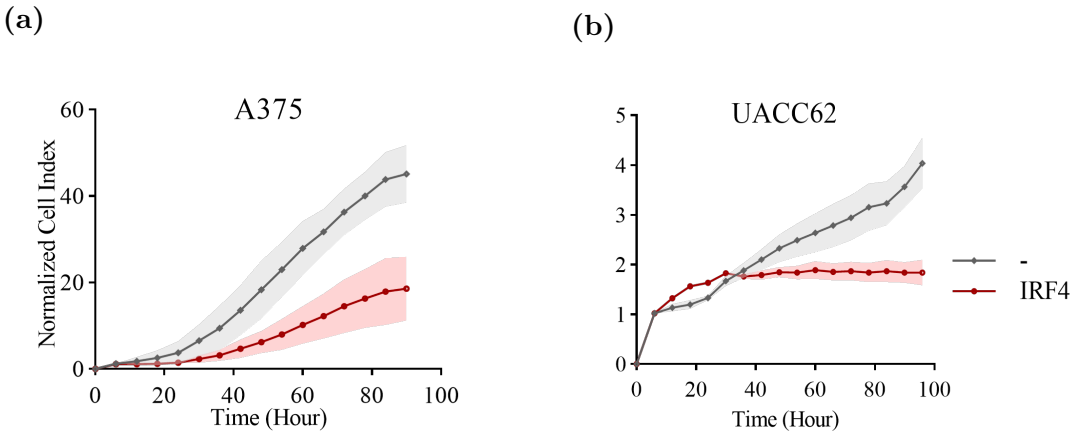

Figure 5.8. Real-time cell analysis with XCELLigence in IRF4 overexpressing (OE) cells a) A375 and b) UACC62 (n=2).

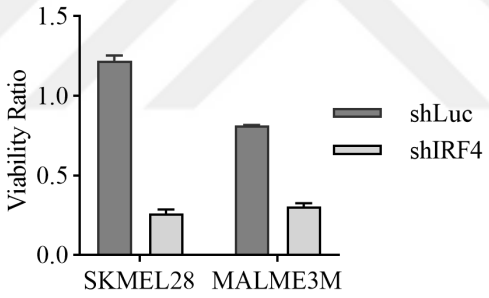

Figure 5.9. XTT results in IRF4 depleted a) shRNA transduced SKMEL28 and MALME3M b) dox-induced IRF4 knockout SKMEL28-Cas9. n=2

5.3. IRF4 Regulates Key Components of Epigenetic Silencing Machinery.

An in-depth analysis of previous RNA-seq data from our group suggests IRF4 as a potential regulator of chromatin-modifying enzyme (Yilmaz, 2014). Among differentially expressed chromatin modifier genes, in this thesis, we focused on key elements of transcriptional silencing, DNA methylation enzymes, and EZH2 from polycomb repressive complex 2 (PRC2). The genes related to DNA methylation machinery were

DNMT1, DNMT3B, and UHRF1. DNMT1, DNA methyltransferase 1, is mainly responsible for the maintenance of DNA methylation, and one of its key partners in this process is UHRF1 (Liu et al., 2013). On the other hand, DNMT3B controls de novo methylation in the genome (Okano et al., 1999).

Another key player in marking the genes for silencing is the polycomb repressive complex (PRC) family. EZH2 methyltransferase enzyme is the essential member of PRC2 and the writer of the H3K27me3 mark (Cao et al., 2004). Increased EZH2 and deregulation of H3K27me3 have already been implicated in several cancers, such as melanoma and lymphoma (Kim et al., 2016). According to RNA-seq data, IRF4 depletion in SKMEL28 and SKMEL5 cells led to an almost 2-fold decrease in EZH2 mRNA levels (Yilmaz, 2014).

Thus RNA-seq results suggested that IRF4 manipulation on DNA methylation machinery and PRC2-related gene silencing possibly have follow-up impacts on the chromatin landscape and cell phenotype.

5.3.1. IRF4 regulates DNMT1, DNMT3B and UHRF1 expression

Consistent with RNA-seq data, the qRT-PCR and western blot data indicate that depletion of IRF4 in melanoma cell lines is followed by a decrease in DNMT1, DNMT3B, and UHRF1 levels (Figure 5.10, Figure 5.11a, and Appendix Figure F.1). Similar results are achieved upon knocking out IRF4 with CRISPR/Cas9 system (Appendix Figure F.2). Furthermore, due to IRF4 overexpression in melanoma cell lines, mRNA levels of DNMT1, DNMT3B, and UHRF1 genes are increased which is followed by an increase in the protein levels (Figure 5.10, Figure 5.11b and c). Hence, the qPCR and immunoblot results confirm the RNA-seq results.

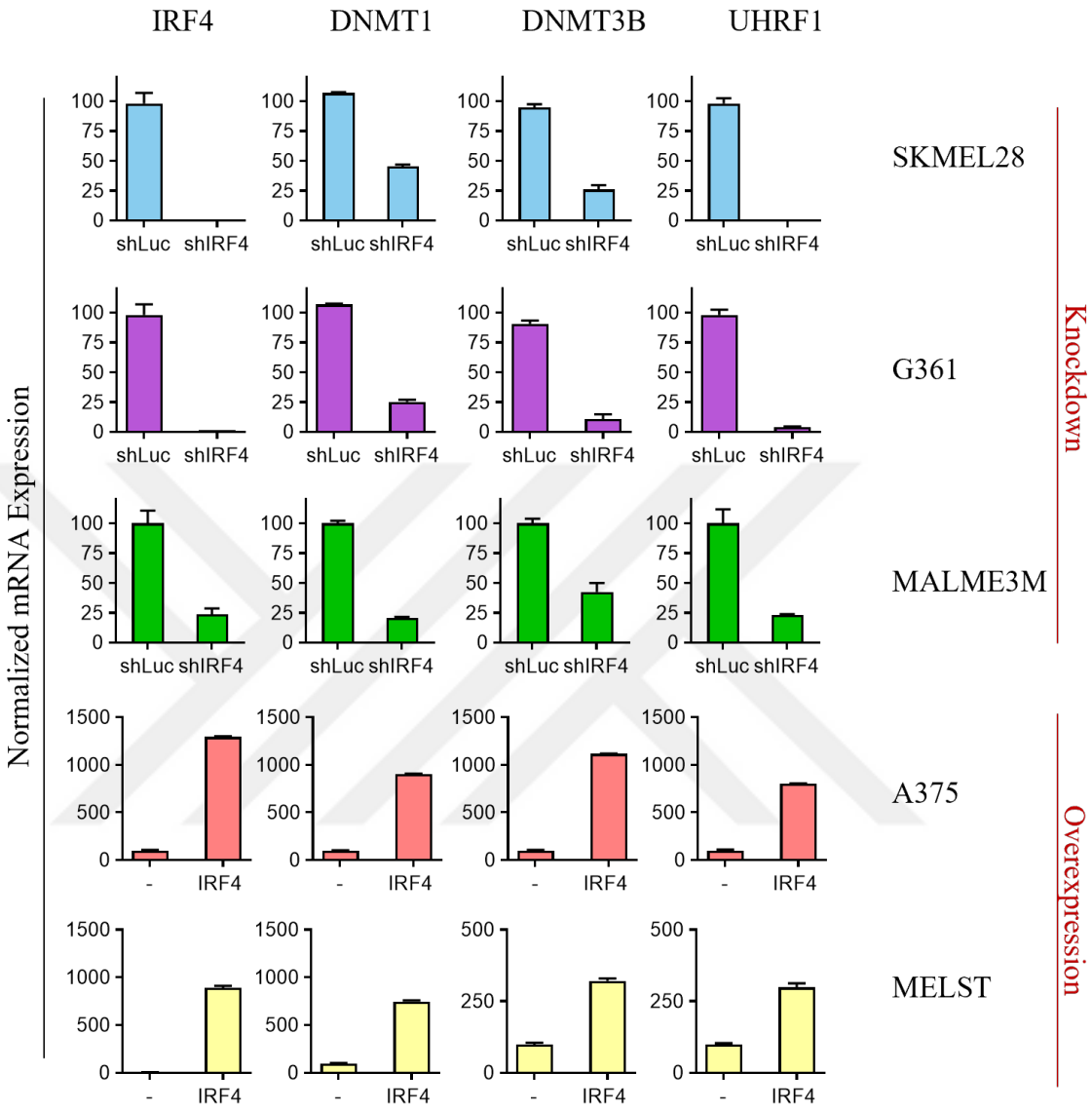

Figure 5.10. qRT-PCR results for DNMT1/3B and UHRF1. Top: IRF4 knockdown; Bottom:IRF4 overexpression. First, mRNA expression was normalized to RPS28, the housekeeping gene, and then it was normalized to the control in each set.

The changes in the expression of these three genes at early time points (e.g., 12–18 hours after dox-induction for IRF4 overexpression and day 3 after transduction with shIRF4) imply IRF4 as the transcriptional regulator for components of DNA methylation machinery. Therefore, the locus for each candidate gene was investigated in the

UCSC genome browser. To identify potential IRF4 binding regions, ENCODE DNase-seq tracks from several IRF4-expressing melanoma cell lines (SKMEL-5, COLO829, and MEL-2183) together with transcription factor ChIP-seq cluster from ENCODE 3 were loaded in the UCSC genome browser. At DNMT1 and DNMT3B loci, potential IRF4-binding regions were identified (Appendix Figure G.1). Chromatin immunoprecipitation combined with qPCR (ChIP-qPCR) using IRF4 antibody was carried out for these two candidate regions. The ChIP-qPCR results indicate IRF4 is binding to DNMT1 and DNMT3B genes and consequently transcriptionally regulating them in SKMEL28 and MALME3M cell lines (Figure 5.10, Figure 5.12).

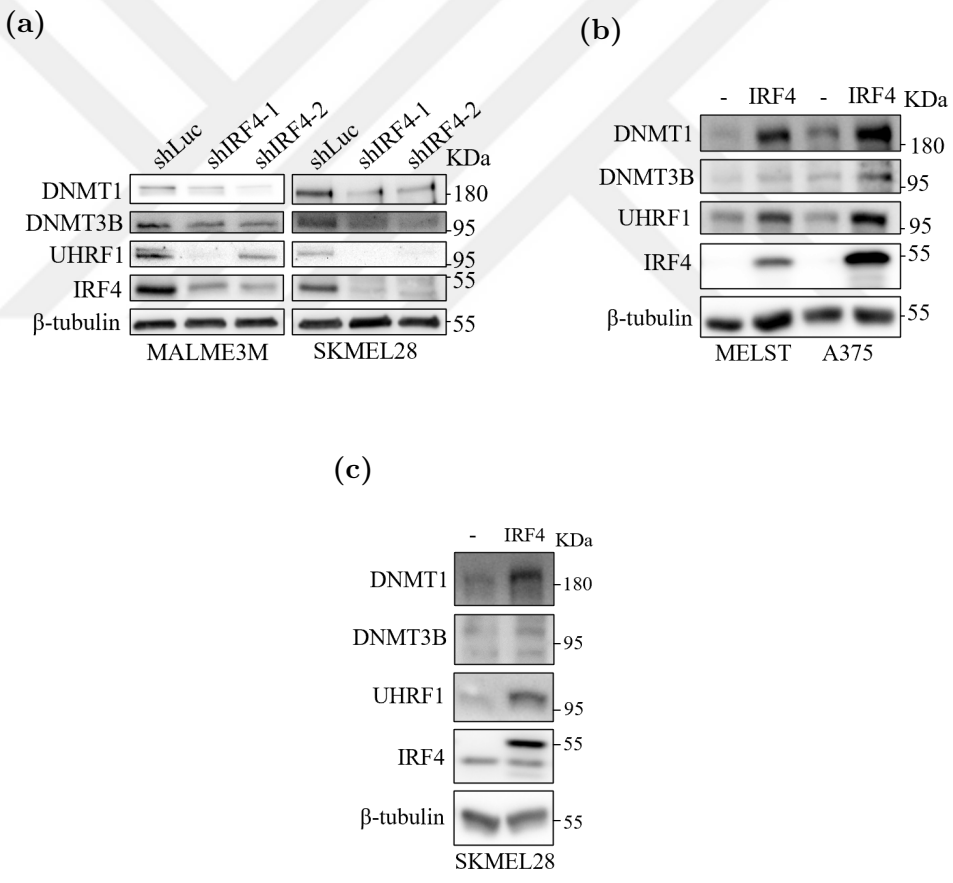

Figure 5.11. Western blot of (a) IRF4 downregulation by shRNA system (b-c) IRF4 overexpressing MELST, A375 and SKMEL28 on day 3 of dox-induction (n=3).

Taken together, the alteration of DNA methylation machinery has been an important prognostic feature in many cancers. Changes in the expression of both de novo and maintenance of DNA methylation enzymes suggest the possibility of IRF4-mediated progression in a subset of melanoma tumors.

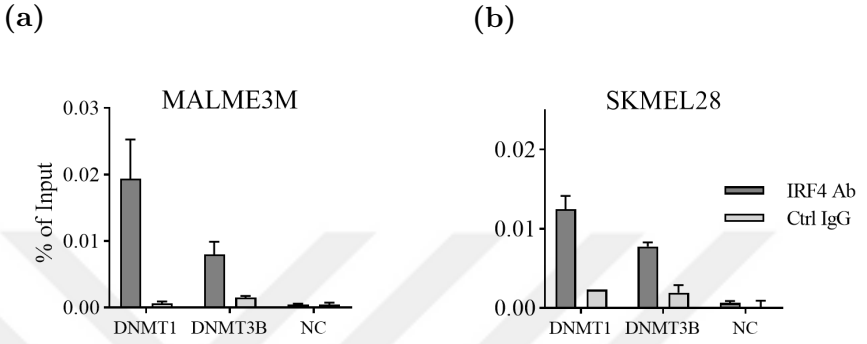

Figure 5.12. ChIP-qPCR with IRF4 antibody and control IgG in DNMT3B and DNMT1 regions in (a) MALME3M and (b) SKMEL28 cells (n=3).

5.3.2. IRF4 Manipulation Affects Global DNA Methylation Levels

The results from 5.3.1 and correlative data from TCGA SKCM patients suggest the possible effect of IRF4 manipulation on global DNA methylation levels. To investigate whether the modulation of DNMT1, DNMT3B, and UHRF1 genes by IRF4 have any implications on global DNA methylation, an indirect ELISA assay was carried out with the 5-mC antibody. The results from 5-mC ELISA demonstrate a decline over time in genome-wide DNA methylation levels upon knocking out IRF4 in SKMEL28 cells (Figure 5.13a). In comparison, overexpression of IRF4 increases global DNA methylation levels in melanoma cells (Figure 5.13b). Finally, our results demonstrated that IRF4 regulates key DNA methylation enzymes and global DNA methylation levels in melanoma cells. Taken together, the IRF4-DNA methylation axis potentially regulates the silencing of some key tumor suppressor genes and, moreover, vast parts of the non-coding genome, where transposons are hypermethylated and silenced.

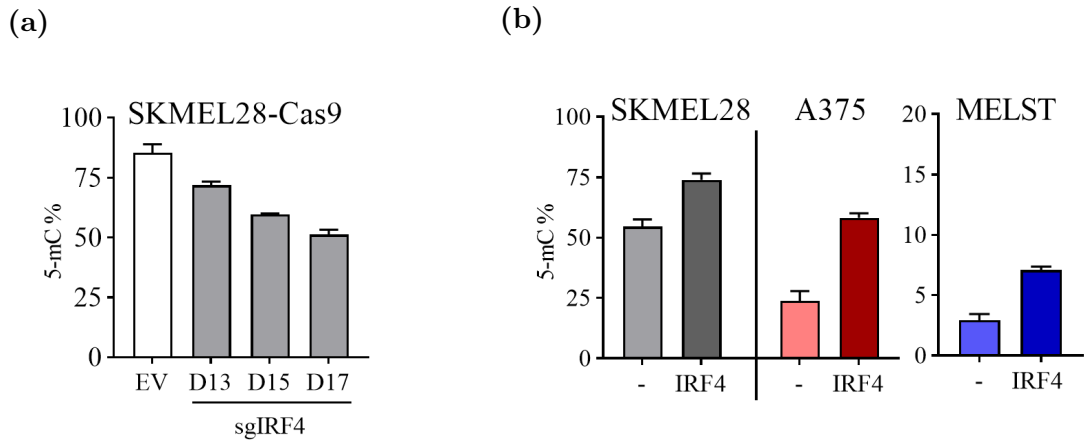

Figure 5.13. 5-mC ELISA in (a) CRISPR/Cas-9 IRF4 knockout in SKMEL28 and (b) IRF4 overexpressing SKMEL28, A375, MELST cells (n=3).

5.3.3. In Melanoma Cells IRF4 Regulates EZH2, Key Component of PRC2

To validate the RNA-seq data regarding changes in EZH2 expression (Appendix Figure R.1), IRF4 was depleted using the shRNA system in SKMEL28 and MALME3M cell lines. IRF4 deficiency in these cells resulted in a significant decrease in EZH2 expression both at mRNA and protein levels (Figure 5.14 top, Figure 5.15a and b). In contrast, IRF4 overexpression in 3 different cell lines exhibited slight elevation in EZH2 expression at the protein level only in 2 cell lines, MELST and SKMEL28 (Figure 5.14 bottom, Figure 5.15c and d).

Moreover, previous ChIP-seq data coupled with ENCODE DNase-seq data identified a few possible IRF4 binding sites at the EZH2 locus. The IRF4 binding for one of the EZH2 candidate regions in different melanoma cell lines was verified with ChIP-qPCR (Figure 5.16). The results indicate that IRF4 transcriptionally regulates EZH2.

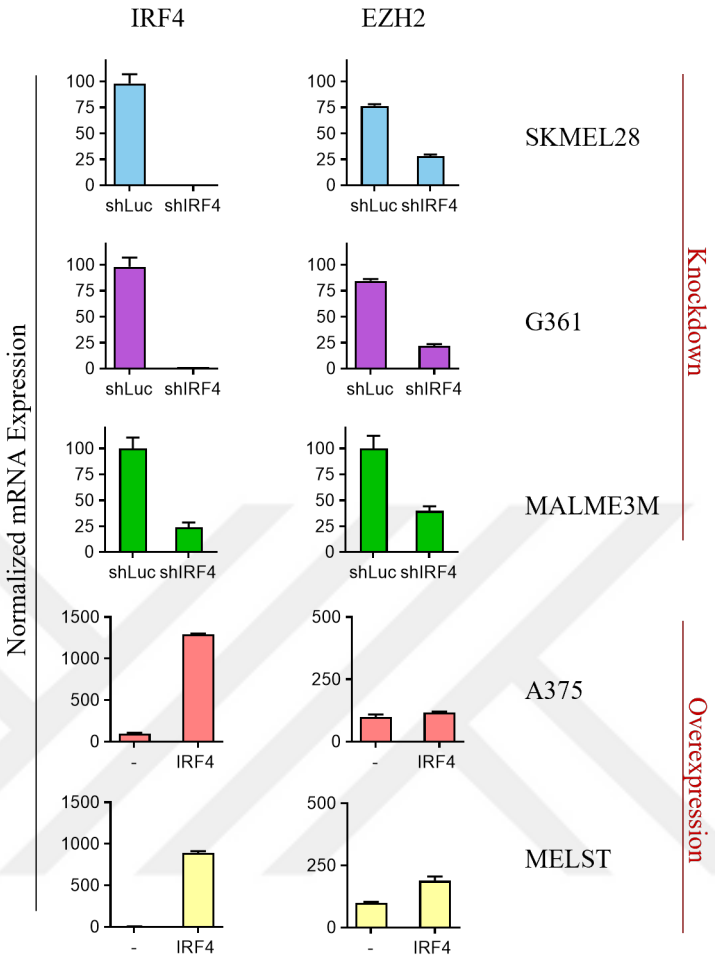

Figure 5.14. qRT-PCR results for EZH2 Top: IRF4 knockdown; Bottom:IRF4 overexpression. First, mRNA expression was normalized to RPS28, the housekeeping gene, and then it was normalized to the control in each set.

5.3.4. IRF4 Regulates Global H3K27me3 Levels in Melanoma Cells.

Diminishing IRF4 expression, either with CRISPR/Cas9 or shRNA method, decreases EZH2 expression, which results in a significant reduction in H3K27me3 levels genome-wide (Figure 5.17). However, IRF4 depletion did not lead to any change in an unrelated histone marker, H3K4me1 (Appendix Figure H.1).

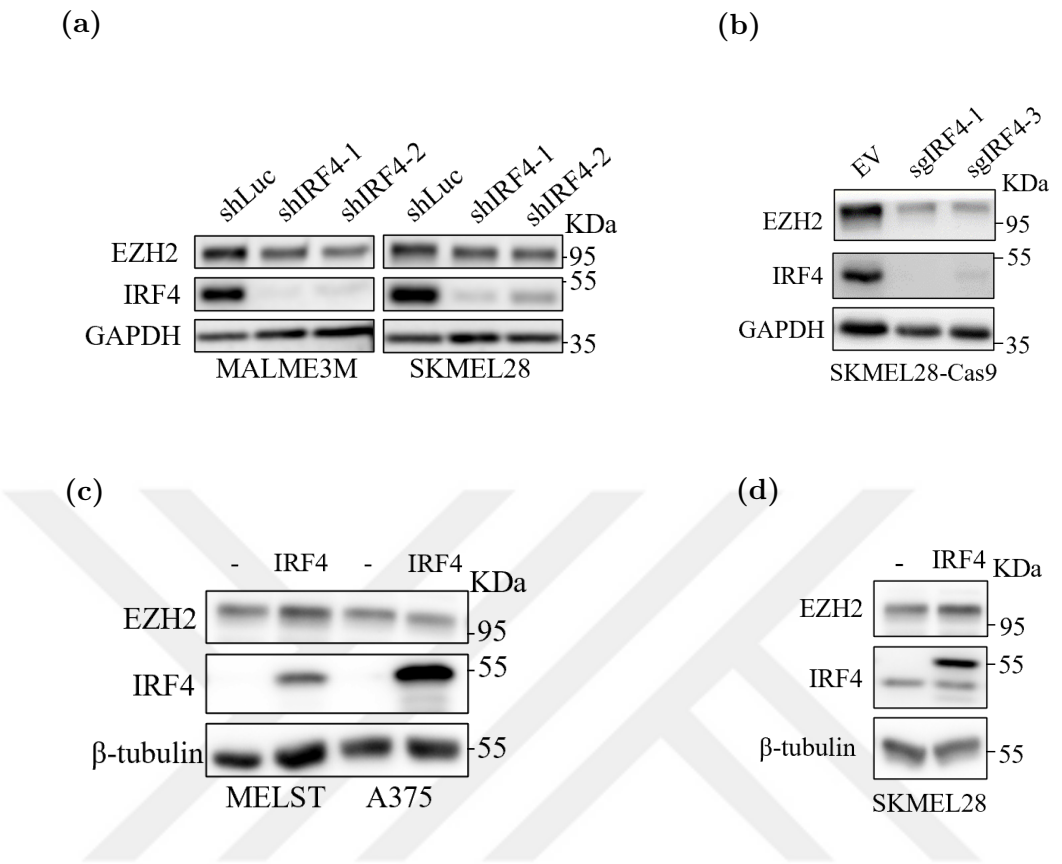

Figure 5.15. Immunoblot for EZH2 in (a) IRF4 knockdown MALME3M and SKMEL28 (b) CRISPR/Cas-9 IRF4 knockout in SKMEL28 (c) IRF4 overexpressing MELST, A375 and (d) SKMEL28 (n=3).

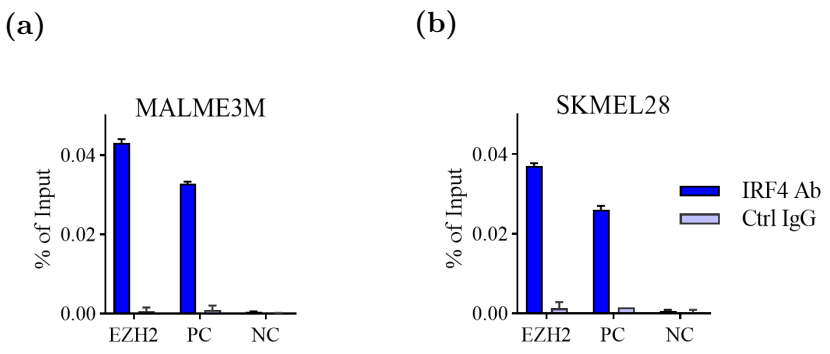

Figure 5.16. ChIP-qPCR with IRF4 antibody and control IgG in EZH2 locus in (a) MALME3M and (b) SKMEL28 cells. PC: positive control, tyrosine promoter. NC: negative control from the intergenic desert (n=3).

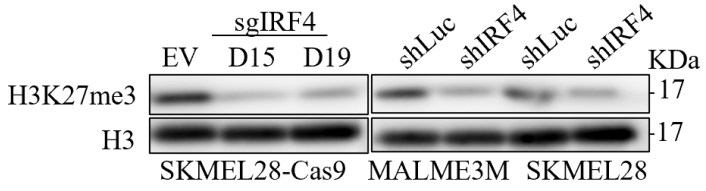

Figure 5.17. Immunoblot shows H3K27me3 levels in IRF4 depleted cell lines with shRNA or CRISPR/Cas9 systems (n=2).

Overall, results indicate a potentially pivotal role for IRF4 as a regulator of two main epigenetic suppressive mechanisms that affect vast parts of the genome and particularly tumor-suppressive genes. The activation of certain tumor suppressive genes can threaten melanoma progression.

5.4. IRF4-Mediated Epigenetic Silencing of Key Cell Cycle and Growth-Related Genes in Melanoma.

In the pan-cancer view, tumor suppressor genes (TSG) are either mutated, deleted or suppressed through an accumulation of silencing marks such as DNA methylation and H3K27me3 (Zob et al., 2022). To identify downstream targets of IRF4-mediated epigenetic silencing in melanoma cells, first, we selected TSGs that did not have any known IRF4 binding sites at their regulatory regions. The second filter for TSG selection was finding the genes with no/little change in expression at earlier time points. Yet, significant changes would be observed later, such as day 6-8 of IRF4 knockdown or Day 3-5 in IRF4 overexpressing cells. Following the strategies above, ten tumor suppressor genes implicated in melanoma as silenced genes were selected (Figure 5.18).

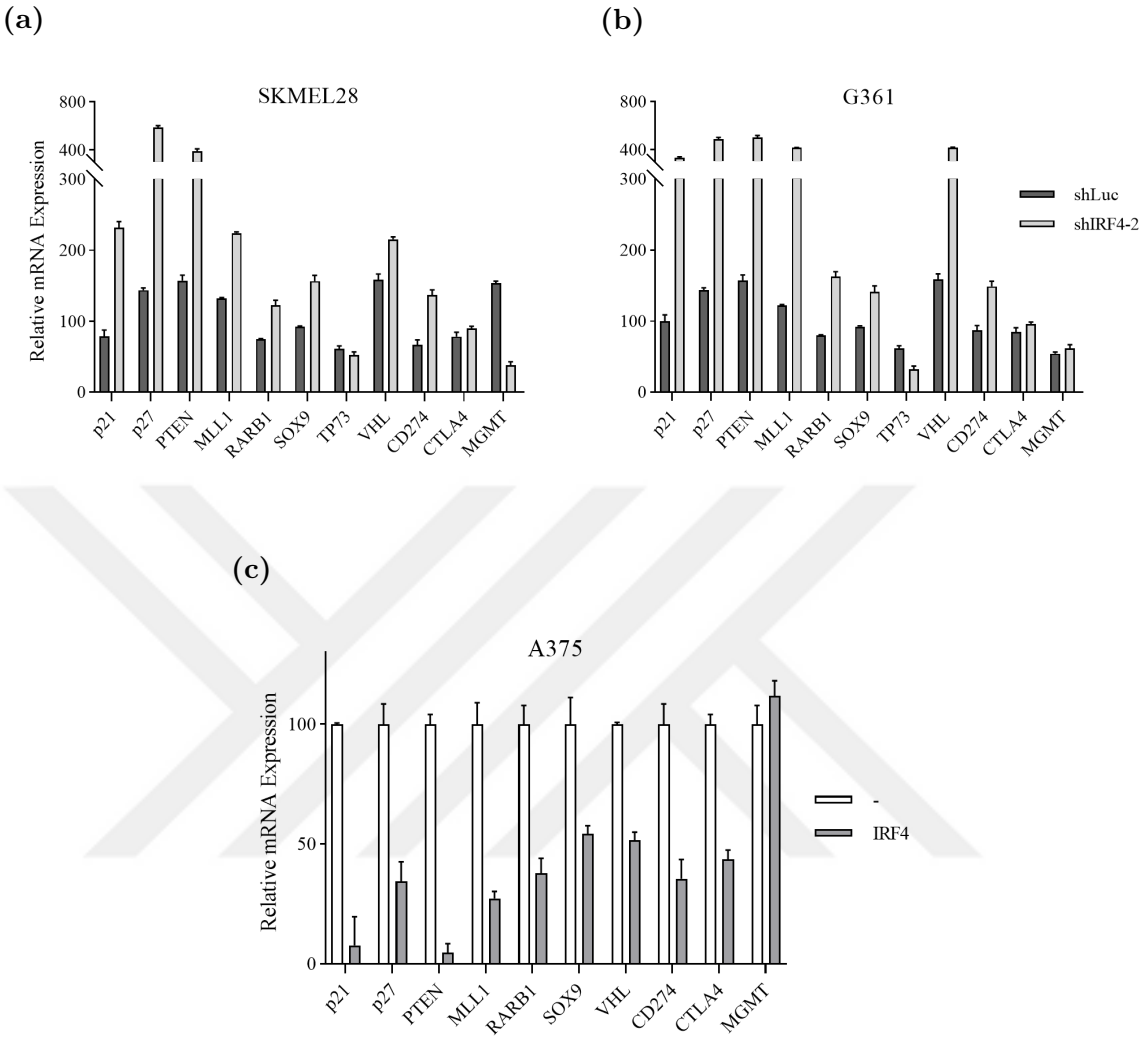

Figure 5.18. Screening of candidate TSGs with qRT-PCR. Day 7 of IRF4 KD with shRNA in (a) SKMEL28 (b) G361 (c) Day 3 of IRF4 OE in A375 (n=2).

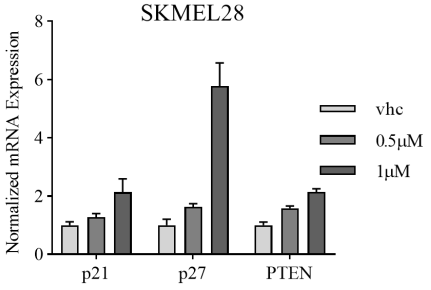

Figure 5.19. qRT-PCR for 3 TSGs in SKMEL28 on Day 3 of Decitabine treatment.

5.4.1. IRF4-DNMT Mediated Regulation of Cell Cycle Genes by Altering Promoter Methylation Levels

In melanoma, one of the mechanisms by which CDKN1A/p21, CDKN1B/p27, and PTEN genes are suppressed is through hypermethylation of their promoters (Alcazar et al., 2012). Therefore, we selected CDKN1A/p21 and CDKN1B/p27, the cell cycle regulators, and PTEN, the negative regulator of the PI3K-AKT pathway, for further study.

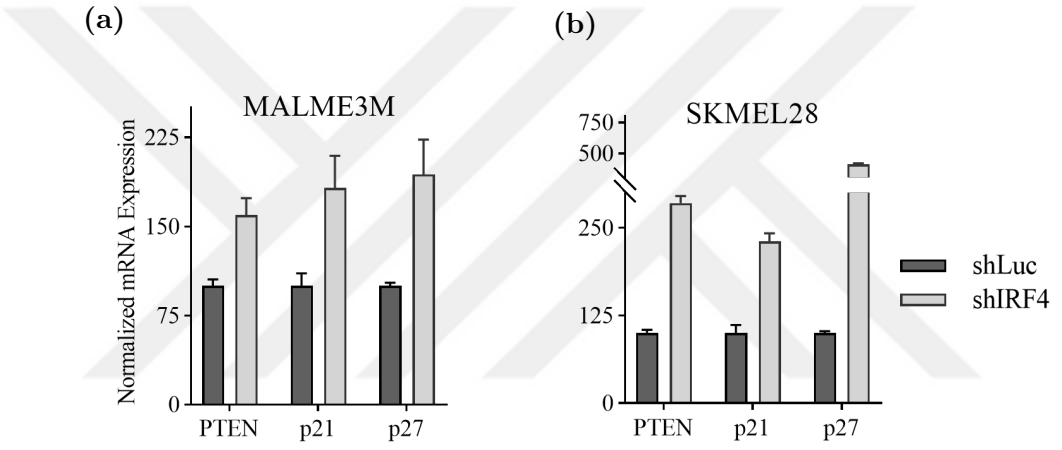

Figure 5.20. qRT-PCR for 3 selected tumor suppressor genes on day 7 post-transduction with shRNA in a) MALME3M and b) SKMEL28 (n=3).

SKMEL28 cells were treated with Decitabine, a DNMT inhibitor, for three days to see whether the 3 candidate genes were activated, which is also an indirect indicator of DNA-methylation-mediated expression for these 3 genes. The qRT-PCR of Decitabine-treated SKMEL28 samples demonstrates elevated expression of the three tumor suppressor genes, CDKN1A/p21, CDKN1B/p27, and PTEN (Figure 5.19). Therefore, qRT-PCR results indicate DNA-methylation controlled expression of these three genes in melanoma cells.

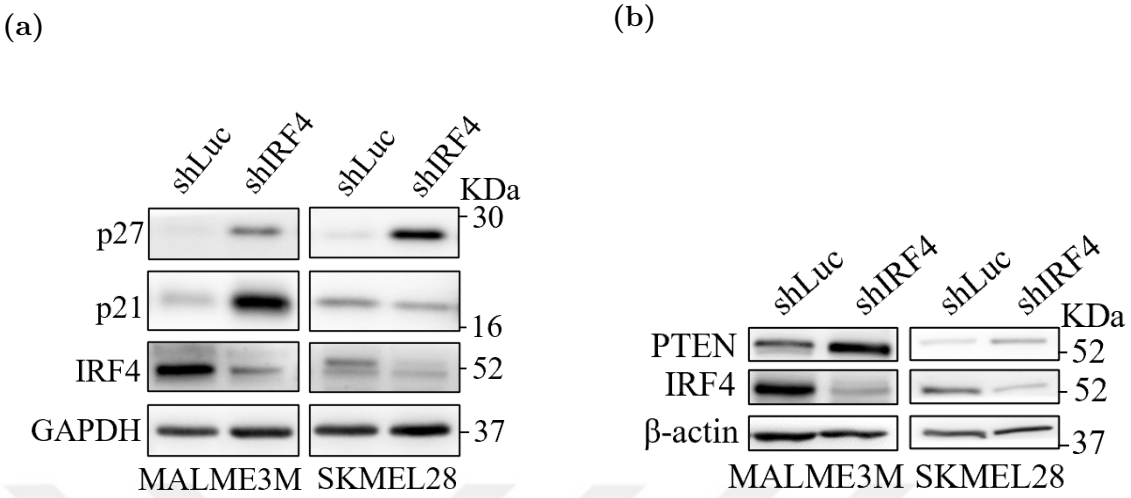

Figure 5.21. Immunoblot shows IRF4 depletion leads upregulation of (a) p21, p27 and (b) PTEN (n=3).

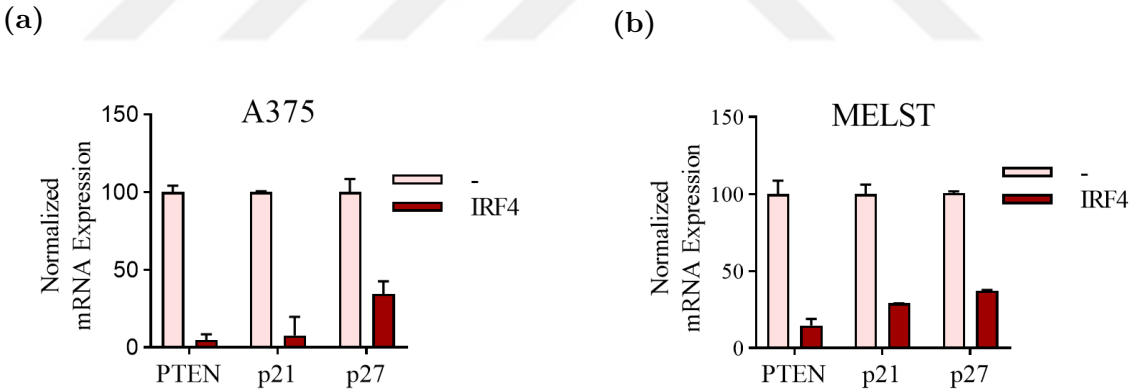

Figure 5.22. qRT-PCR for 3 selected tumor suppressor genes on day 5 of dox-inducible expression of IRF4 in a) A375 and b) MELST cell lines (n=3).

Downregulation of IRF4 with shRNA increased PTEN, p21, and p27 expression in melanoma cell lines, both mRNA (Figure 5.20) and protein levels (Figure 5.21, Appendix Figure I.1). Furthermore, overexpression of IRF4 led to the downregulation of p21, p27, and PTEN at mRNA (Figure 5.22) and protein level (Figure 5.23, Appendix Figure I.2). The western blot results for PTEN exhibit no significant change in

SKMEL28, which can be explained due to the presence of the heterozygous mutation in the PTEN gene. Due to the heterozygous nature of the mutation, the PTEN mRNA is transcribed from the wildtype allele in the SKMEL28 cell line (DepMap, 2022). A similar effect for p21 in SKMEL28 was observed. One of the key activators of p21 expression is p53 (Fan et al., 2011). The p53 null status of SKMEL28 suggests the non-significant change of p21 protein in the western blot (Figure 5.21a).

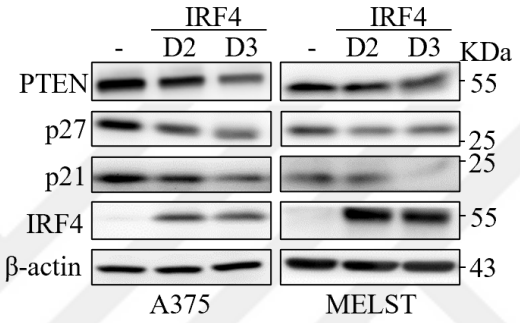

Figure 5.23. Immunoblot shows a, b) IRF4 overexpression leads decrease in PTEN, p21 and p27 levels (n=3).

To determine if these genes are suppressed through the IRF4-DNMT axis and whether IRF4 expression modulates the methylation of their promoters, methylation-sensitive restriction enzyme digestion followed by qPCR (MSRE-qPCR) was performed. In the MSRE-qPCR method, while MSRE digests the unmethylated region, the methylated region stays almost intact. During qPCR, the amplification of the unmethylated region will start in later cycles compared to the methylated region. The MSRE-qPCR results suggest IRF4 expression modulates methylation of p27, p21, and PTEN promoters in melanoma cell lines (Figure 5.24, Appendix Figure J.1 and J.2).

Hence, our results indicate IRF4-modulated alteration of p27, p21, and PTEN expression. The changes in expression of these 3 genes are due to IRF4-mediated changes in DNA methylation levels at their promoters.

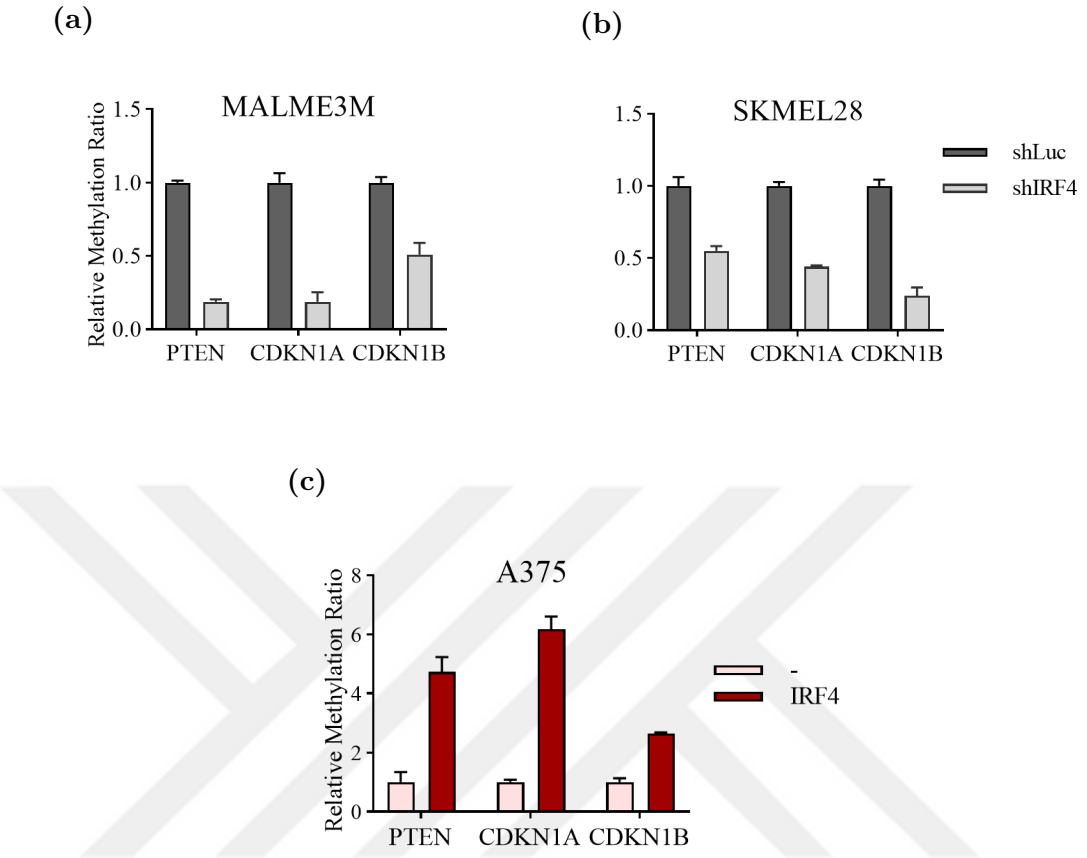

Figure 5.24. MSRE-qPCR results for PTEN, CDKN1A/p21 and CDKN1B/p27 promoter upon (a-b) IRF4 knockdown (c) IRF4 overexpression.

5.4.2. IRF4-DNMT Modulation of p21 And p27 Expression Affects Cell Cycle

To elucidate the phenotypic aspect of alteration in p21 and p27 expression levels, we performed the cell cycle assay via propidium iodide staining. IRF4 depletion resulted in an increase in the G1 cell population, leading to cell cycle arrest (Figure 5.25). On the other hand, IRF4 overexpression results in an increase in the S phase population (Figure 5.26). The increase in the S-phase population suggests the deregulation of cell cycle phases. Overall, data suggest that IRF4-mediated cell cycle changes are potentially affecting proliferation and growth.

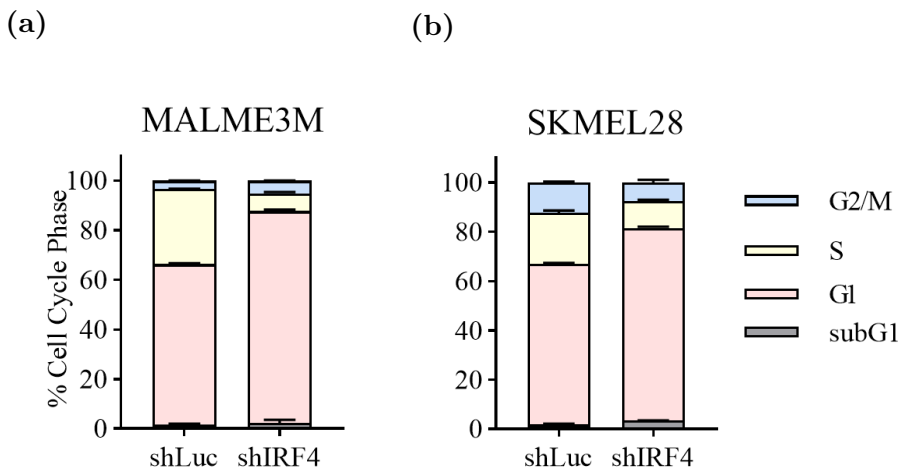

Figure 5.25. Cell cycle assay in IRF4 depleted (a) MALME3M and (b) SKMEL28.

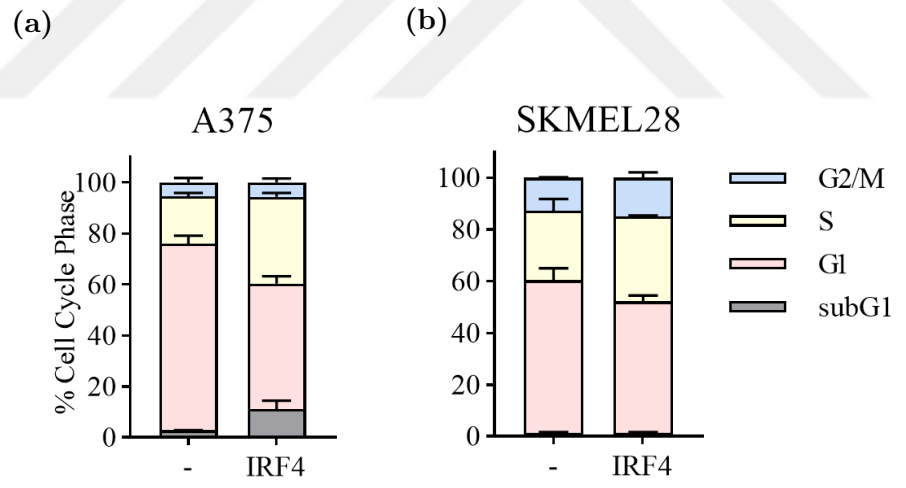

Figure 5.26. Cell cycle assay in IRF4 overexpressing (a) A375 and (b) SKMEL28.

5.4.3. IRF4-Related Changes in PTEN And the PI3K-AKT Pathway

One of the highly active oncogenic pathways in melanoma that can be modulated through suppressive marks is the PI3K-AKT pathway (Kwong et al., 2013). In Figure

5.24, we have shown alterations in DNA-methylation levels at the PTEN promoter and, consequently, the changes in its expression (Figure 5.21b, Figure 5.23, and Appendix Figure K.1). To investigate the downstream of PTEN expression as a negative regulator of the AKT pathway, pSer473AKT (pAKT) levels were checked as the indicator of AKT activity. The results demonstrate depletion of pAKT, the key modification for AKT activation, upon increased PTEN expression following IRF4 knockdown. The decrease in pAKT level is followed by a reduction in pSer235/236-S6 (pS6) in melanoma cells (Figure 5.27, Appendix Figure K.2), which suggests the potential deregulation of global mRNA translation and growth. Another AKT target is FOXO1, a pro-apoptotic protein negatively regulated by AKT. Phosphorylation of FOXO1 at Ser256 negatively affects protein stability. As expected, the IRF4-mediated decrease of pAKT leads to a reduction in pFOXO1 levels and, consequently, stabilization of FOXO1 levels in cells (Fig, 5.27b). Likewise, overexpression of IRF4 in MELST and A375 cells led to decreased PTEN and activation of the AKT pathway, which increased its downstream targets, such as S6 and pS6 ribosomal protein (Figure 5.28). The outcome of IRF4-dependent changes in the AKT pathway impacts proliferation and cell growth. At the phenotypic level, as shown with the real-time cell analysis assay with XCELLigence, IRF4 knockdown diminishes cell growth and proliferation in melanoma cells at later time points (Figure 5.7).

Interestingly, IRF4 overexpressing cells have a lower proliferation rate (Fig 5.8); whether this is because melanoma cells have switched to an invasive-like phenotype or the result of another event in the cells needs to be investigated. Therefore, our data indicates that IRF4 modulates proliferation and growth through various approaches, such as PI3K-AKT-promoted growth and p21/p27-mediated cell cycle control in IRF4-expressing melanoma cells.

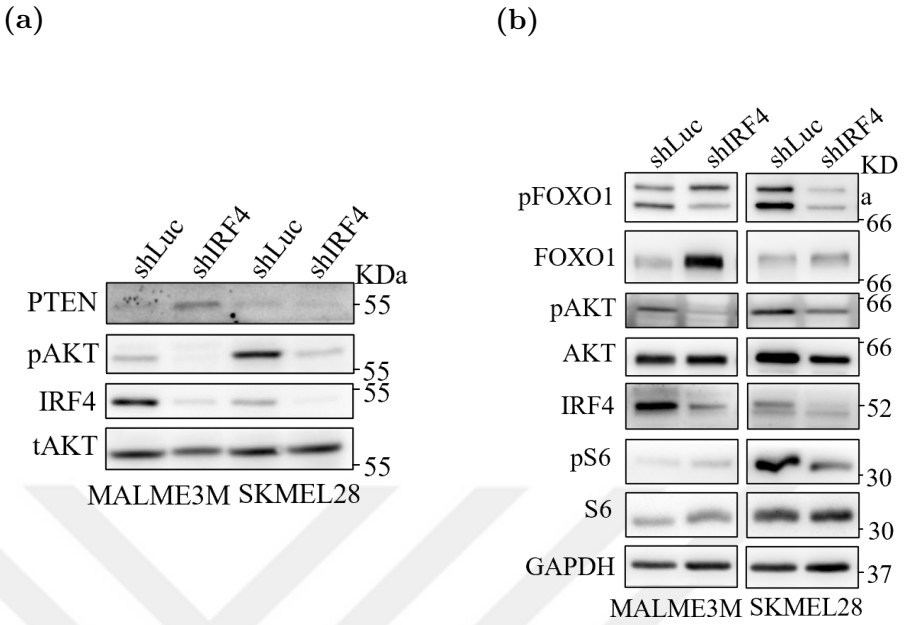

Figure 5.27. Western blot for the impact of IRF4 depletion on (a) PI3K-AKT pathway and (b) its downstream targets such as pS6 and pFOXO1.

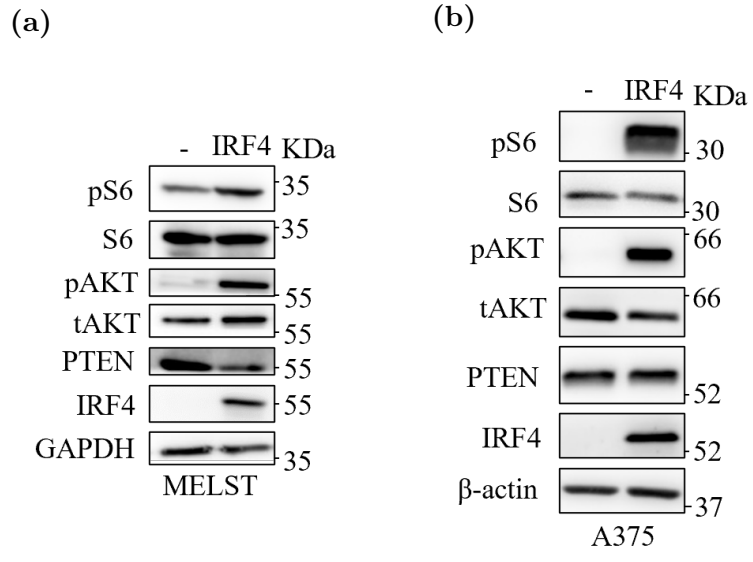

Figure 5.28. Western blot for effects of IRF4 overexpression on PI3K-AKT pathway and one of its downstream targets pS6 in (a) MELST and (b) A375.

5.4.4. IRF4-EZH2 Axis Controls WDR19 Levels And Cilia Formation

WDR19/IFT144, an essential gene for transport and maintenance in cilia and similar to several other ciliary genes, is regulated by EZH2 (Zingg et al., 2017). To understand whether IRF4 is the upstream regulator of the EZH2-WDR19 relationship, qRT-PCR, and Western blot were carried out in IRF4 overexpressing stable cell lines, A375 and UACC62. Upon IRF4 overexpression, WDR19 expression is diminished in both melanoma cell lines (Figure 5.29). Whereas results from experiments with IRF4-depleted cell lines show WDR19 expression is upregulated in both cell lines to varying degrees (Figure 5.30). To validate the IRF4-EZH2-WDR19 axis further, chromatin immunoprecipitation with H3K27me3 antibody at WDR19 promoter was performed in SKMEL28 and MALME3M. Results from this experiment confirm H3K27me3 enrichment at the WDR19 promoter (Figure 5.31a) (Zingg et al., 2015). Moreover, to determine that H3K27me3 occupancy at the WDR19 promoter is mediated by IRF4, H3K27me3 ChIP-qPCR was executed in IRF4-depleted samples. The H3K27me3 signal at the WDR19 promoter is diminished in both IRF4 knockdown and knockout cells (Figure 5.31b).

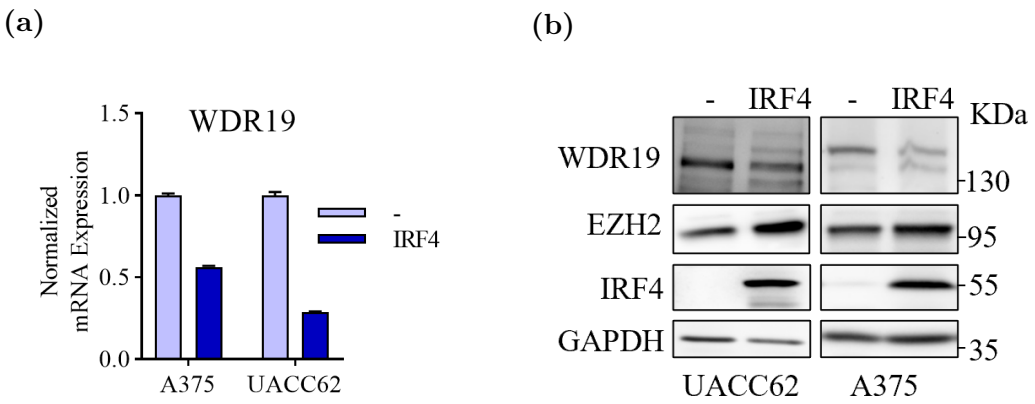

Figure 5.29. Western Blot and qRT-pCR for WDR19 in IRF4 overexpressing melanoma cells (n=3).

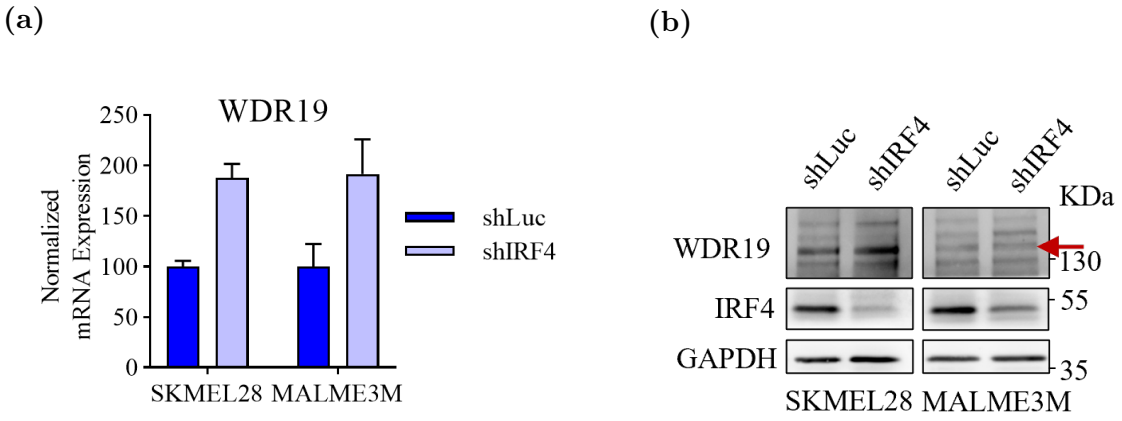

Figure 5.30. Western Blot and qRT-PCR for WDR19 in IRF4 knockdown melanoma cells (n=3).

To corroborate whether the changes in H3K27me3 occupancy and WDR19 expression affect cilia formation in the cells, Immunofluorescence (IF) staining with acetylated Tubulin and Arl13b, two cilia markers was performed in dox-inducible IRF4 overexpression A375 and UACC62 cells. IF results revealed that IRF4 overexpression significantly reduces ciliated cells in both cell lines (Figure 5.32).

To further elucidate whether the loss of cilia is the direct effect of IRF4-regulated EZH2 activity, we decided to investigate if depletion of H3K27me3 levels via treatment with EZHi (EZH2 inhibitor, EPZ-6438) will evoke ciliogenesis again. As it is shown in Figure 5.33, while IRF4-overexpression in DMSO-treated samples once again led to the loss of the ciliated cell population when treated with EZHi, the ciliogenesis is partially rescued in A375 cells (Figure 5.33).

A recent study has reported that ciliogenesis and cilia are present in melanocytes and lost during melanoma progression (Snedecor et al., 2015). Taken together, our data suggest suppression of cilia genes and ciliogenesis by the IRF4-EZH2 axis may contribute to melanoma progression toward a more invasive phenotype.

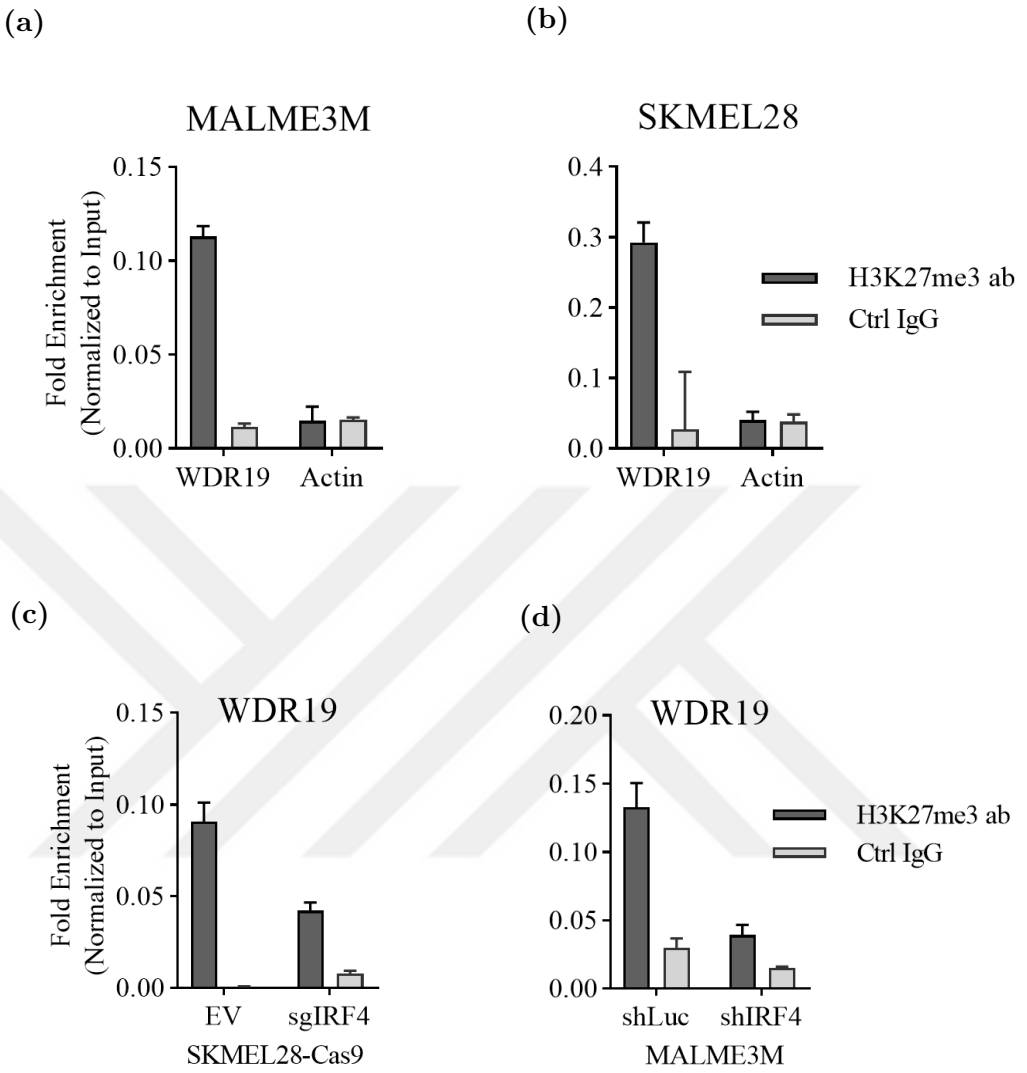

Figure 5.31. H3K27me3 occupancy at WDR19 shown by ChIP-qPCR. (a) in SKMEL28 and (b) MALME3M IRF4 depletion with (c) sgIRF4 in SKMEL28 and (d) shIRF4 in MALME3M.

5.4.5. IRF4-Mediated Ciliogenesis Is Regulating Canonical WNT Pathway

The activation of EZH2 in melanoma cells leads to the deregulation of multiple pathways, which promotes tumor growth (Emran et al., 2019; Zingg et al., 2018). One of the pathways that is deregulated by EZH2 activation is the canonical WNT

β-catenin pathway. One of the ways that EZH2 promotes the activation of the WNT pathway is by disrupting the structure and function of cilia (Zingg et al. 2018).

To investigate whether overexpression of IRF4 in melanoma cells after evoking cilia loss activates the WNT pathway, we performed a luciferase assay with TOPFLASH plasmid (3x wt TCF4 binding sites) and PGL3-empty plasmid as a positive control in A375 cell line. To enhance the WNT-pathway signal, in this assay, all samples were treated with WNT3a-conditioned medium (CM, L929 cells transfected with WNT3a), control CM (L929 cells were transfected with pIRES-EGFP as a control), or 20 mM of LiCl (GSK3β inhibitor) for 24 hours after transfection, and then Luciferase reporter assay was carried out with the samples. The results indicate that TOPFLASH luciferase activity is higher in IRF4 overexpressing samples, which can be interpreted as activation of β-Catenin and its downstream transcriptional targets (Figure 5.34).

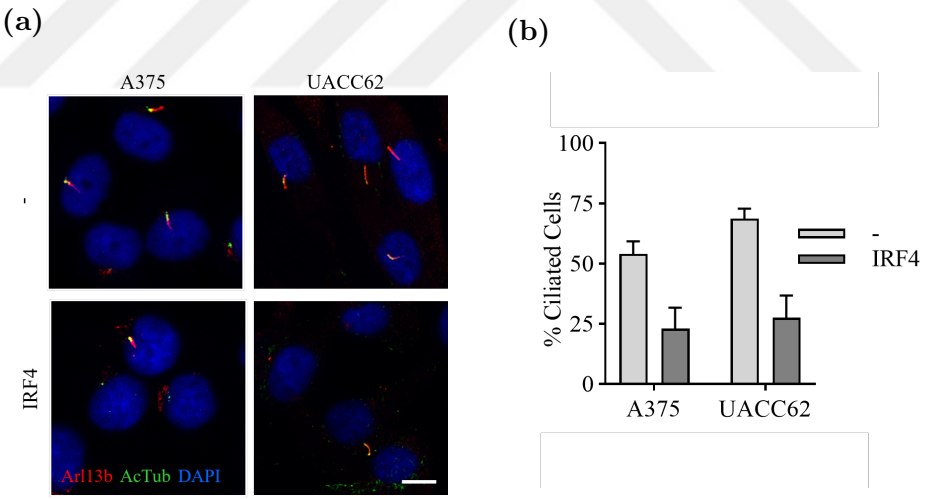

Figure 5.32. IF staining of cilia in A375 and UACC62; (a) Representative confocal microscopy images of 48-hour serum-starved cells. Percentage of ciliated cells defined by staining for Arl13b (red), acetylated tubulin (AcTub; green), and DAPI. Scale bar: 5 μM. (b) Quantification from at least 2 biological replicates.

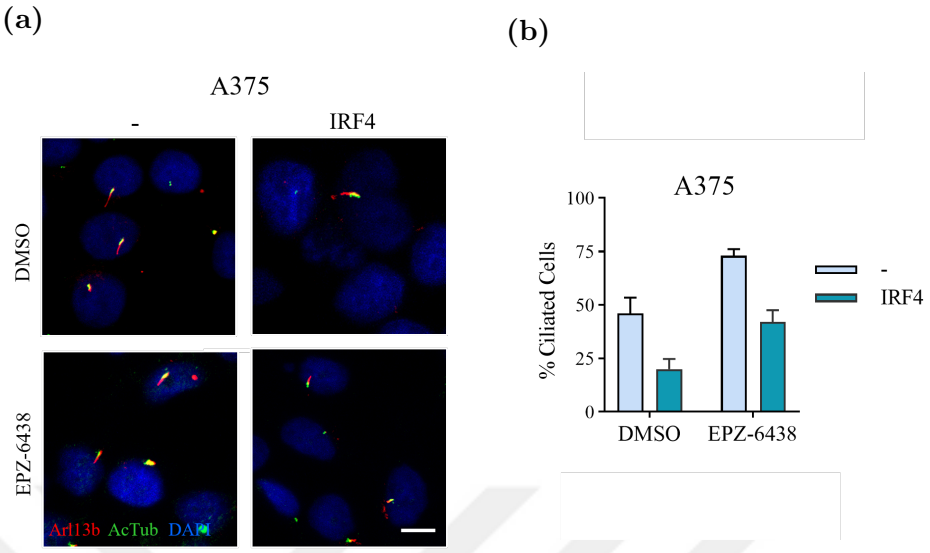

Figure 5.33. IF staining of cilia in A375 cell line treated with EPZ-6438 in both dox-treated (IRF4 overexpressing) and dox-untreated. Staining with Arl13b (red) and AcTub (green), treatment with EPZ-6438 for 6 days.

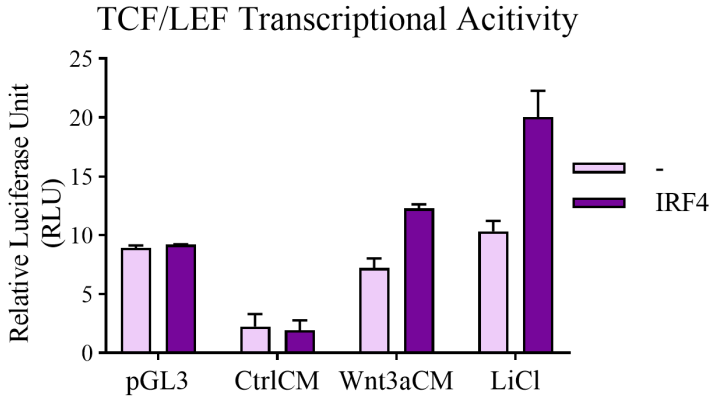

Figure 5.34. Luciferase reporter assay for measuring TCF/LEF transcriptional activity in A375 cell line. pGL3: positive control CtrlCM: L929 transfected with pIRES-GFP-conditioned medium (n=3).

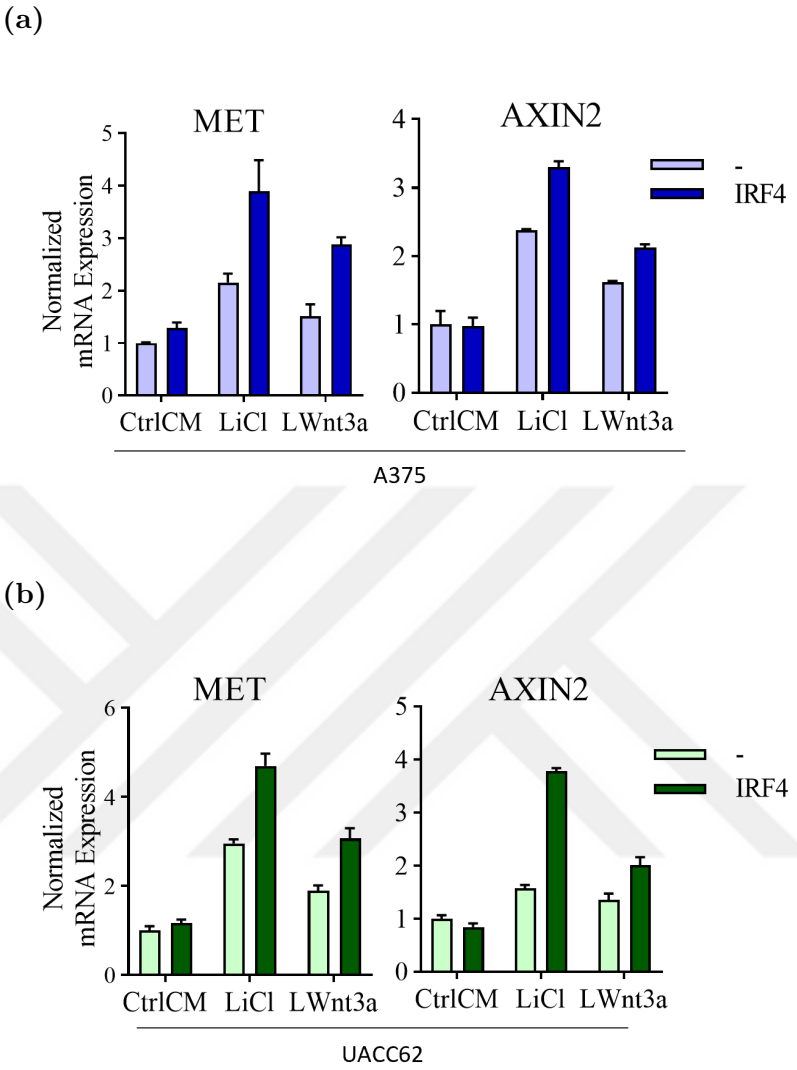

Figure 5.35. qRT-PCR for β-Catenin targets upon IRF4 overexpression and inducing the WNT pathway in IRF4 overexpressing (a) A375 and (b) UACC62 cell lines (n=2).

AXIN2 and MET are two well-known targets of βCatenin in melanoma and colon cancer (Chien et al., 2009). We validated the activation of β-Catenin with RT-qPCR for AXIN2 and MET genes (Figure 5.35). As the findings have shown, IRF4 plays a role in the regulation and activation of β-Catenin and its downstream targets, which play a critical role in melanoma progression.

5.5. IRF4 Regulates Melanoma Cell Response to Certain Epigenetic Drugs

Previous studies have shown that various chromatin-regulating factors are deregulated in different cancers, which causes the cancer epigenome landscape to differ from normal and creates a unique opportunity to explore novel inhibitors and therapeutic strategies. This section aims to zoom into a few selected inhibitors and their implications on IRF4-high melanoma cells. The selection of these drugs is based on the experimental data and correlative data about IRF4 expression vs. targeted drugs in melanoma in public databases.

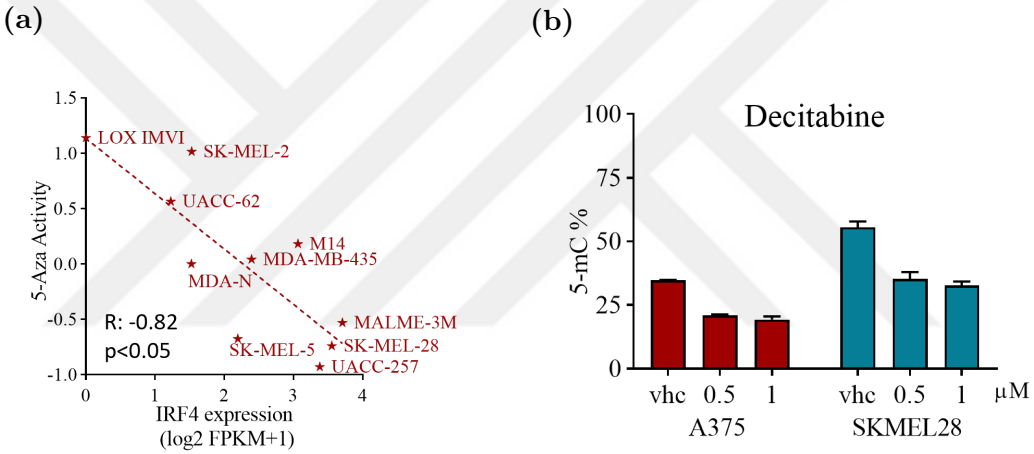

Figure 5.36. IRF4 expression and DNMT inhibitors. (a) NCI-60 data for IRF4 expression correlation with IRF4 in melanoma (b) 5-mC ELISA for A375 and SKMEL28 after 3 days treatment with decitabine.

5.5.1. IRF4 Expression Versus Cytostatic Activity of Epigenetic Inhibitors

NCI-60 database contains screening results for thousands of drugs and small molecules in 60 cancer cell lines (Luna et al., 2021). The database includes drug activity data for each cell line and molecular features such as transcriptomics, proteomics, and miRNA-seq data for all 60 cell lines. 10 melanoma cell lines are present among the 60 cancer cell lines. We investigated the most significant correlations between IRF4 and

the cytostatic activity index of all NCI-60 drugs. Reviewing the results, 5-Azacytidine is represented as the most promising epigenetic inhibitory molecule to investigate. 5-Azacytidine (5-Aza), a cytosine analogue, is the first discovered DNA methylation inhibitor and has a significant inverse correlation with IRF4 expression measured by RNA-seq. NCI-60 data suggest resistance to 5-Aza cytostatic activity in melanoma cell lines with high IRF4 expression (Figure 5.36a). Additionally, there is also comparable data on IRF4 versus Decitabine, the deoxyribose form of 5-Aza. It should be mentioned that the correlation is melanoma-specific, and there is no significant correlation between IRF4 and 5-Aza activity in data from all 60 cell lines (Appendix Figure L.1).

5.5.2. IRF4 Expression Modulates Cytotoxic Response to DNMT Inhibitors in Melanoma Cells

As the NCI-60 consists of promising yet only correlative data, we investigated the IRF4-DNMTs/UHRF1 axis's potential impact on melanoma cells when treated with 5-Aza or Decitabine. First, the drug's effect on DNA methylation was studied using a 5-mC ELISA kit. Treating SKMEL28 and A375 with 2 different doses of decitabine for 3 days resulted in lower global methylation levels in these cells (Figure 5.36b). IRF4-modified cells were treated with 5-Azacytidine, or Decitabine (5-Aza-2'-Deoxycytidine) for 5 days. The results from SKMEL28-Cas9 cells suggest that both KO1 gRNA and KO3 gRNA, which are IRF4 knocked-out samples, are more sensitive to 5-Aza than control samples (Figure 5.37a). In contrast, overexpression of IRF4 in SKMEL28 and A375 can rescue the cells from the cytotoxic effects of 5-Aza to some extent (Figure 5.37b and c). Since 5-Aza is the ribose analog of cytosine, it can interfere with transcription, and at high doses, it can cause DNA-methylation-independent cytotoxicity. Therefore, we also performed XTT assays with Decitabine, the deoxyribose form of 5-Aza, to validate the phenotypic results. Treatment of MALME3M and SKMEL28 with 0.5 μM decitabine coupled with shRNA-based IRF4 depletion also resulted in sensitization for IRF4-depleted cells compared to non-targeting shLuc controls (Figure 5.38a). Whereas in IRF4 overexpressing cells, the cells are partially rescued from the effects of Decitabine (Figure 5.38b and c, Appendix Figure L.2).

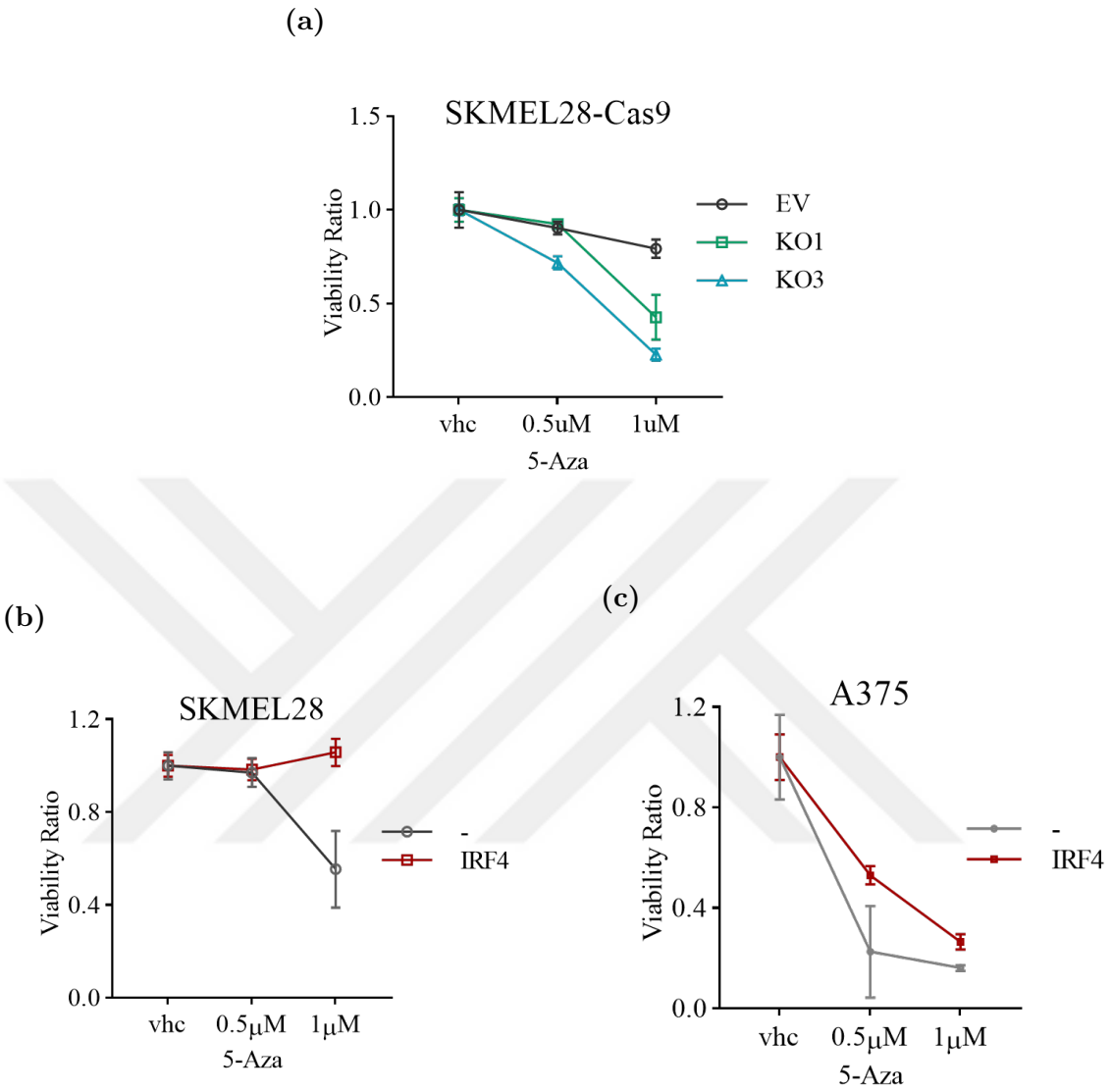

Figure 5.37. XTT assay for 5-Aza treatment in (a) SKMEL28-Cas9 IRF4 knockout cells (b-c) IRF4 overexpression in SKMEL28 and A375 respectively (n=3).

The outcome of phenotypic data for 5-Aza and decitabine treatment denotes a functional IRF4-DNA methylation link, where IRF4 modulates Aza and Decitabine activity. To sum up, this link between IRF4 and DNA methylation inhibitors sheds light on the possibility of lower drug response to 5-Aza and decitabine in IRF4-expressing melanoma tumors, which needs to be tested *in vivo*.

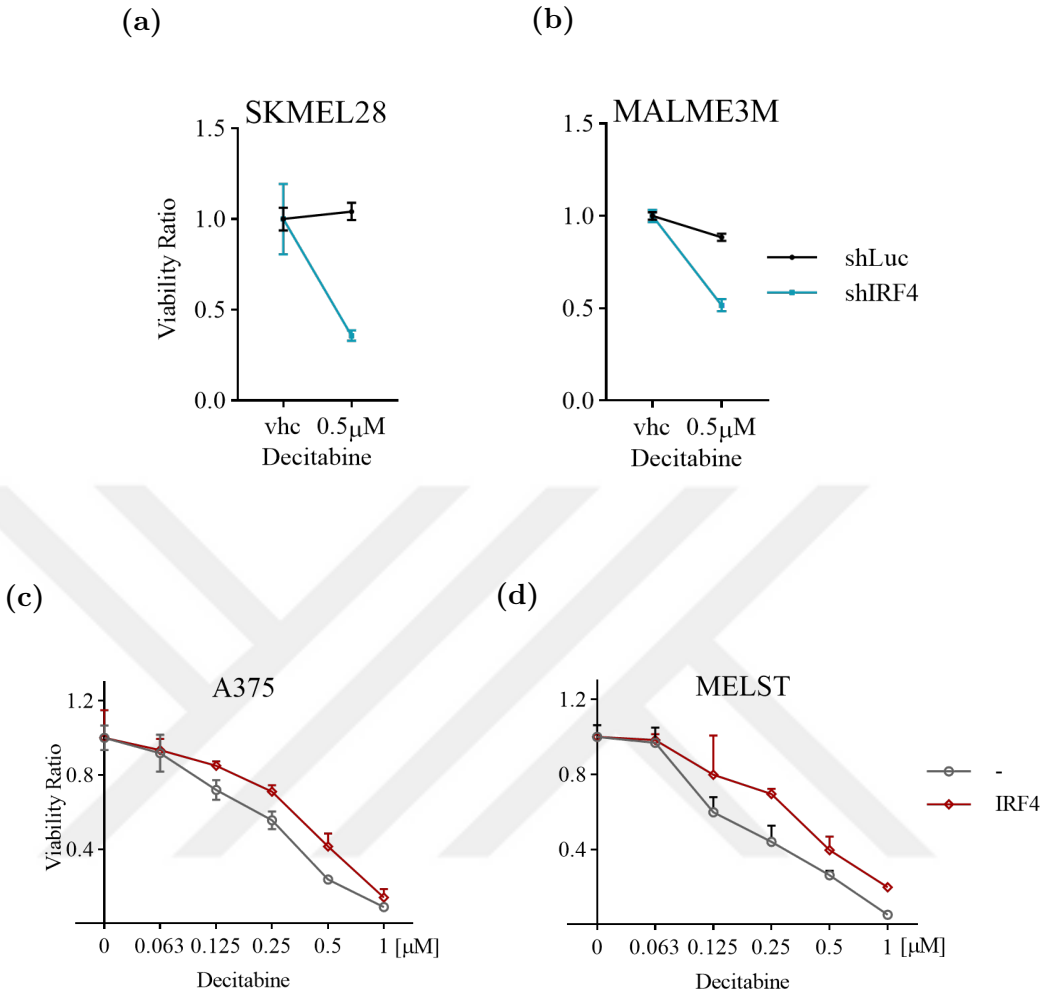

Figure 5.38. XTT assay for Decitabine treatment in (a)IRF4 knockdown cells (b-c) IRF4 overexpression in A375 and MELST (n=2).

5.5.3. IRF4 Modulates Cytotoxic Activity of EZH2 Inhibitor, EPZ-6438, in Melanoma Cells

Although the EZH2 inhibitor was not part of the NCI-60 hit list, the experimental data from previous parts of this thesis suggests a potential link between IRF4 expression and the EZH2i cytotoxic activity. Phenotypic studies reveal the most consistent and significant link between IRF4 and EPZ-6438 in IRF4 overexpressing cells. 5 different

cell lines on day 3 of IRF4 overexpression, were treated with EPZ-6438 for 6 days. At the end of treatment, with XTT assay, we checked for viability of the cells. Results show partial yet significant rescue of the cells from EPZ-6438 cytotoxicity (Figure 5.39, Figure 5.40).

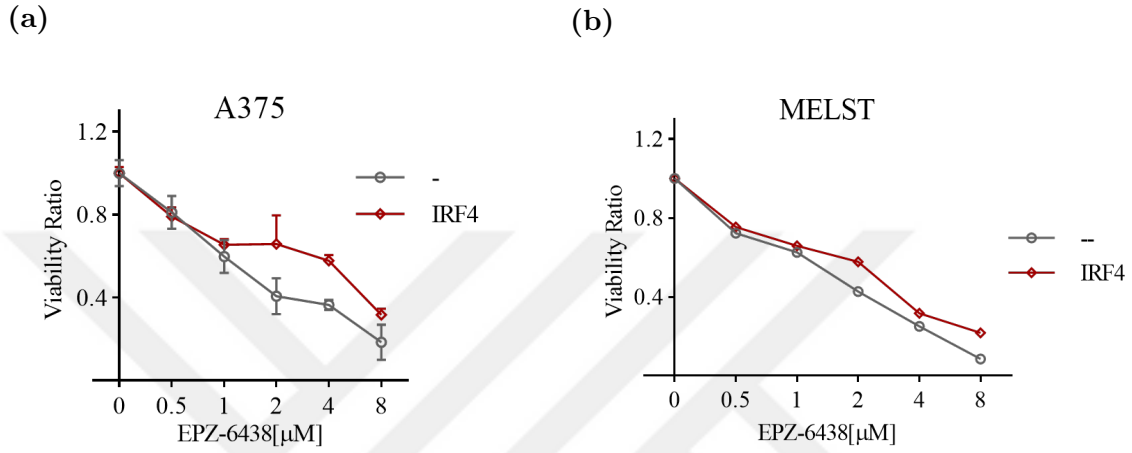

Figure 5.39. XTT assay with multiple doses after 6 days of treatment with EPZ-6438 in IRF4 overexpressing cells (a) A375 (b) MELST.

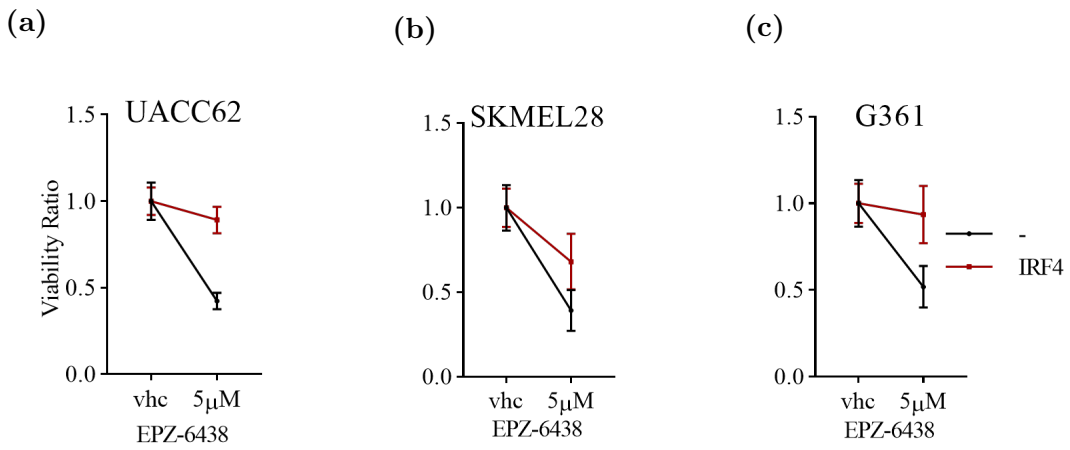

Figure 5.40. XTT assay single-dose after 6 days of treatment with EPZ-6438 in IRF4 overexpressing cells (a) UACC62 (b) SKMEL28 (c) G361.

5.6. In Pursuit of Synthetic Lethal Partners of IRF4 in Melanoma Cells via Focused Pooled CRISPR-Cas9 Loss-of-Function Screen

For years, loss-of-function genetic screens have shed light on gene dependencies in cancers and other diseases. Initially, RNAi screens and then CRISPR-Cas9 screens have been used to identify vulnerabilities in cancers (Zhan et al., 2015; Huang et al., 2020; Zhang et al., 2021). As part of this thesis, we used CRISPR-Cas9 pooled screen to identify IRF4 accomplices in melanoma cells. For this purpose, we used SKMEL28, one of our IRF4-expressing cell lines, to carry out the CRISPR-Cas9 screen. Furthermore, we sought targeted libraries focusing on transcription and gene expression machinery and critical genes and pathways in cancer. We obtained the "Apoptosis and Cancer" (ACOC) and "Gene Expression" gRNA libraries (GEEX) from Michael Bassik (Stanford University) (Morgens et al., 2017). In the last section of the results, the process of setting up the screen and analyzing preliminary data is described.

5.6.1. Analysis of gRNA Representation Post-Transformation

To check the efficiency of transformation and an estimation of the diversity of gRNA vectors, in parallel with overnight liquid culture, a dilution plating assay was carried out (Appendix Figure M.1). To determine gRNA distribution, we prepared next-generation sequencing (NGS) libraries from plasmids extracted from liquid culture and submitted them for sequencing. Upon receiving the NGS results, the Lorenz curve method was used to analyze gRNA distribution. For this analysis, we extracted gRNA data from the raw data files, aligned them, and counted them for every gRNA library. Then, we calculated the area under the curve (AUC) for each library by plotting the Lorenz curve. For example, AUC value of 0.5 means the same frequency for each gRNA, which results in the steady increase in the fraction of sequenced and aligned gRNAs. At this step, an AUC value of 0.5–0.7 is considered acceptable for gRNA library distribution (Addgene Blog, 2016). According to the Lorenz curve, the AUC values for the GEEX and ACOC libraries were 0.66 and 0.63, respectively (Figure 5.41). We concluded that the gRNA distributions in both libraries were acceptable,

and we proceeded with lentiviral production. Since the gRNA vectors contain both mCherry and Puromycin, we have based our flow-cytometry-based titration protocol on the mCherry signal (Appendix Figure N.1, and N.2).

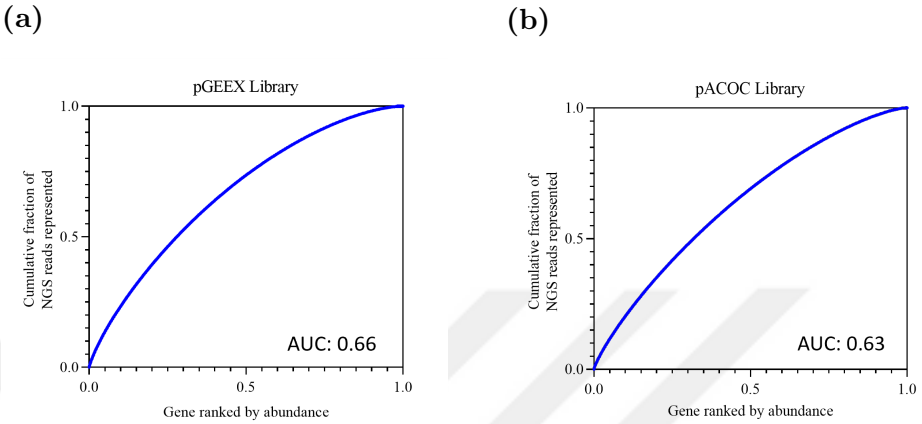

Figure 5.41. gRNA distribution analysis for evaluation of transformation efficiency of (a) GEEX library AUC=0.66 and (b) ACOC Library AUC=0.63.

5.6.2. Preliminary Analysis of CRISPR/Cas9 Library Screening

The purpose of the screening was the identification of negatively selected genes with the context-essentiality factor of being an essential gene only in IRF4-depleted cells and not in the control empty vector cells. For this study, each gene was targeted with 10 gRNAs. Knocking out these genes would result in cell death. Therefore, the population of cells carrying these targeting gRNAs would be in decline at day 21 (the end timepoint). NGS results were analyzed with MAGeCK (Appendix Table O.1, O.2). In the algorithm used in MAGeCK, essential genes are detected by finding genes whose sgRNAs are consistently ranked higher than other sgRNAs, using a method called robust rank aggregation (RRA). This method considers the significance of the rankings so that genes that are ranked higher because of chance are not identified as essential (Li et al., 2014). The preliminary analysis results will be discussed for each gRNA library separately.

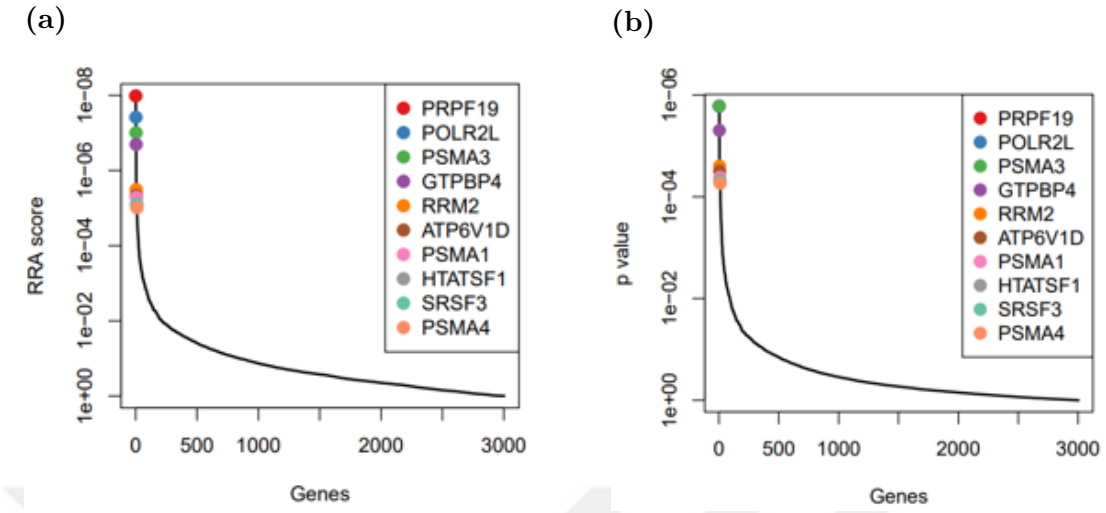

Figure 5.42. CRISPR/Cas9 screening for ACOC library in SKMEL28-Cas9 EV cells. (a) RRA score and (b) p-value of the top 10 negatively selected genes. For full details of the top 5 genes (Appendix Table P.1)

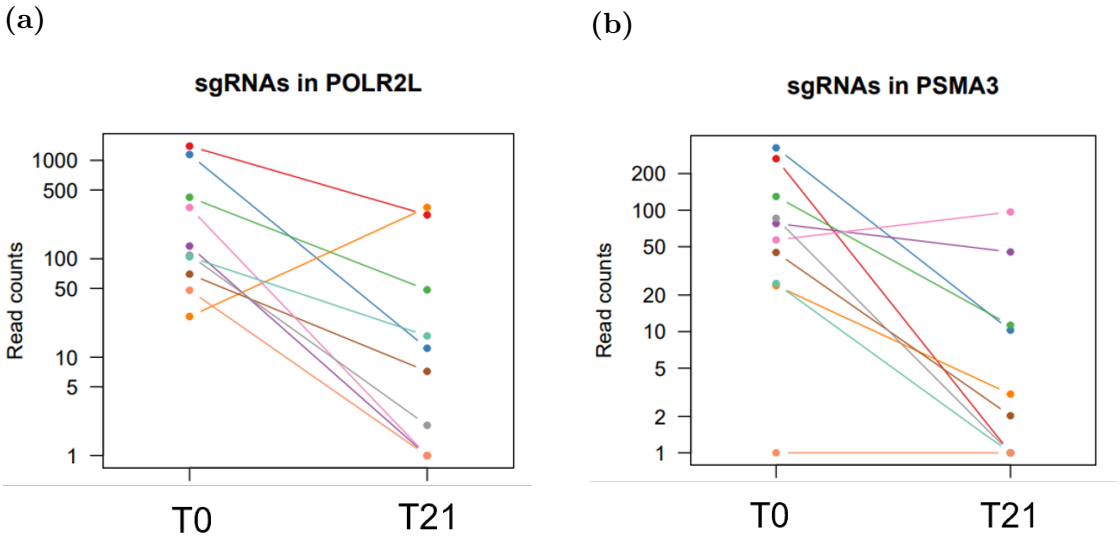

Figure 5.43. Top 2 common genes, gRNA counts in CRISPR screening in EV-ACOC samples. T0: Start of dox-inducible Cas9 expression, T21: Endpoint.

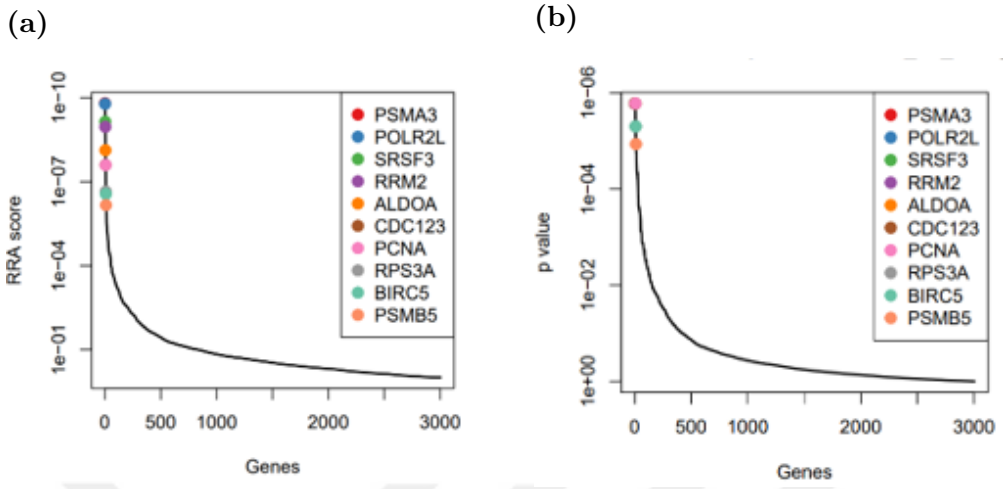

Figure 5.44. CRISPR/Cas9 screening for ACOC library in SKMEL28-Cas9 sgIRF4 KO cells. (a) RRA score and (b) p-value of the top 10 negatively selected genes. For full details of the top 5 genes (Appendix Table P.2).

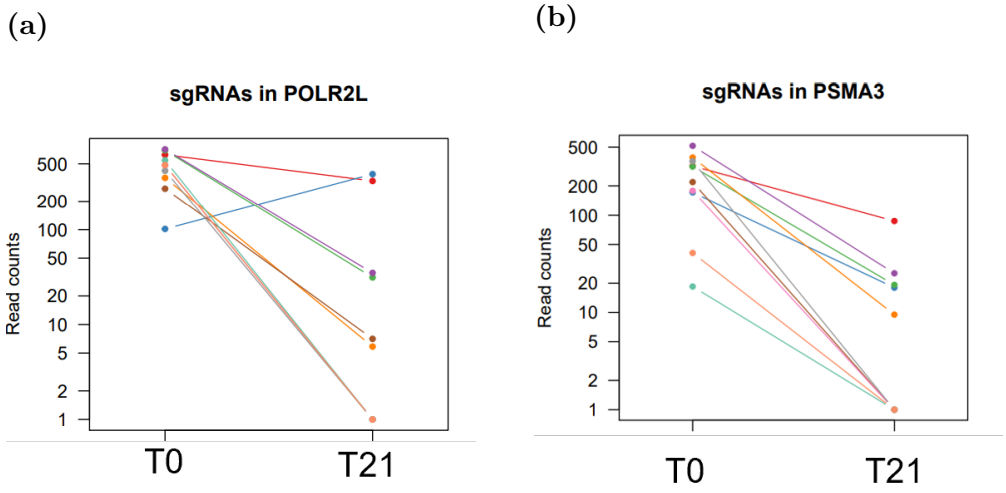

Figure 5.45. CRISPR/Cas9 screening for ACOC library in SKMEL28-Cas9 sgIRF4 KO cells. (a) RRA score and (b) p-value of the top 10 negatively selected genes. For full details of the top 5 genes (Appendix Table P.2).

5.6.2.1. Apoptosis and Cancer Library (ACOC). The analysis results for the ACOC library show that the highest rank among negatively selected genes would be for genes that have core essentiality. The core-essential genes are key genes in the most critical biological processes, such as RNA polymerases and transcription initiation complexes, the proteasome degradation complex, and glycolysis pathway genes. For example, In ACOC results for both EV and sgIRF4 KO, the common genes negatively selected and ranked in the top three genes are POLR2L, an RNA polymerase subunit, and PSMA3, part of the proteasome degradation complex (Figure 5.42, Figure 5.44, and Appendix Table P.1). Zooming in on the gRNAs targeting POLR2L (Figure 5.43a, Figure 5.45a) and PSMA3 (Figure 5.43b, Figure 5.45b) reveals that almost the majority of gRNAs targeting these genes have been depleted or decreased in endpoint samples. The preliminary analysis of the ACOC library indicates that screening has been successful, and samples can be analyzed with the purpose of identifying IRF4 synthetic-lethal partners.

5.6.2.2. Gene Expression (GEEX) Library. In GEEX samples, similar to ACOC, preliminary analysis was performed with MAGeCK. However, among the top three highest-ranked genes in the negatively selected ranked gene list, there is only one common gene between EV and sgIRF4 KO samples. RPL21, a component of 60s ribosomal subunit, has ranked first in both EV and sgIRF4 KO datasets (Figure 5.46, Figure 5.47, and Appendix Table P.2). Taking a closer look at sgRNA changes for RPL21 gene in each dataset, out of 10 RPL21-targetting gRNA, more gRNAs were depleted in the EV dataset than in the sgIRF4 KO dataset (Figure 5.46c, Figure 5.47c). Overall, the gene scores and the fold-change values are higher in ACOC than in GEEX screening.

5.6.3. Pathway Enrichment and Gene Ontology (GO) Analyses

For each of the pooled libraries, based on the MAGeCK-generated ranked gene list for negatively selected genes, genes with a q-value of less than 0.1 and a p-value of less than 0.01 were picked. The common genes in between EV and sgIRF4 sets were filtered out. The final list of genes consisted of all the genes which are negatively selected only

in sgIRF4 KO samples, which means they are only essential genes in IRF4-knockout cells (Appendix Figure Q.1). For gene set enrichment analysis, EnrichR was used, and REACTOME, WikiPathways, and GO Biological Process were chosen to demonstrate IRF4-dependent pathways (Kuleshov et al. 2016, Xie et al. 2021).

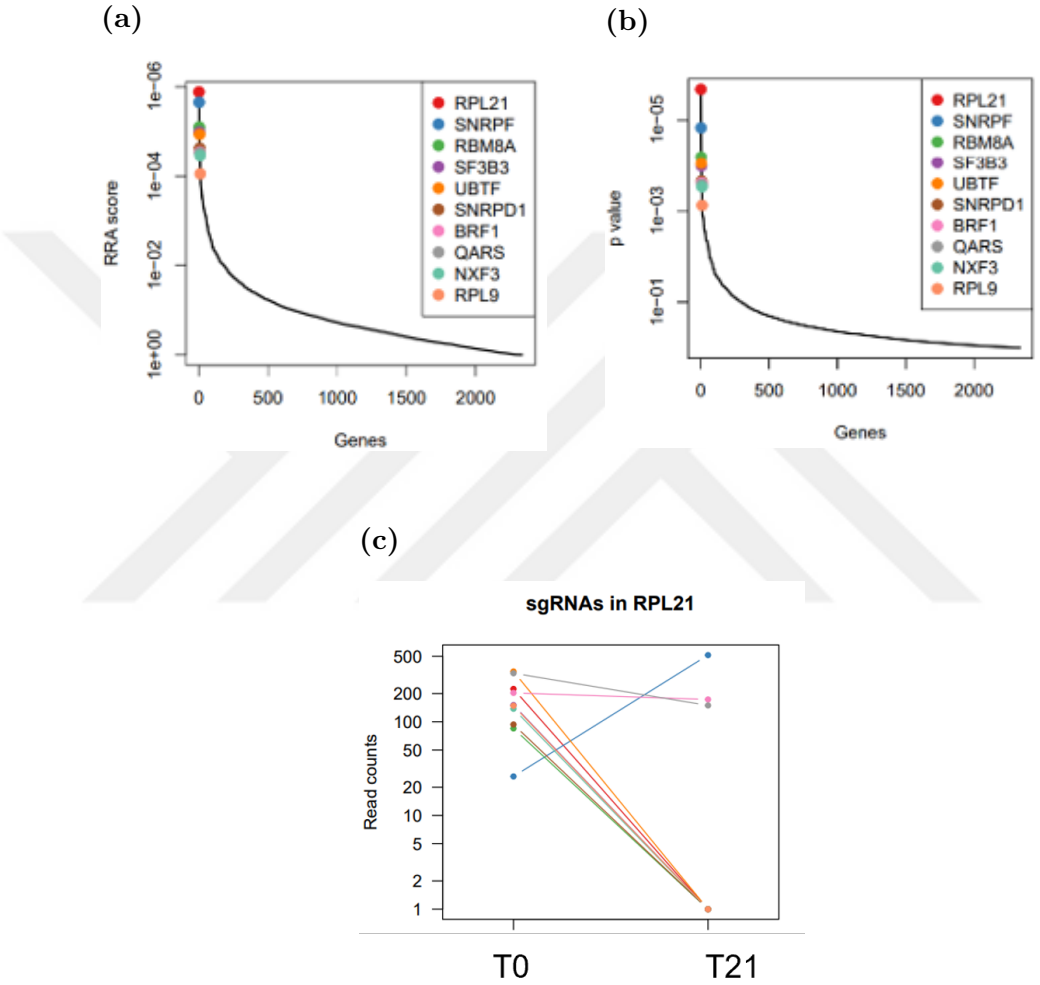

Figure 5.46. Results of CRISPR/Cas9 screening for GEEX library in SKMEL28-Cas9 EV cells. (a) RRA score and (b) p-value of the top 10 negatively selected genes. (c) gRNA counts for RPL21 genes in EV. T0: Start of dox-inducible Cas9 expression, T21: Endpoint (Appendix Table P.3).

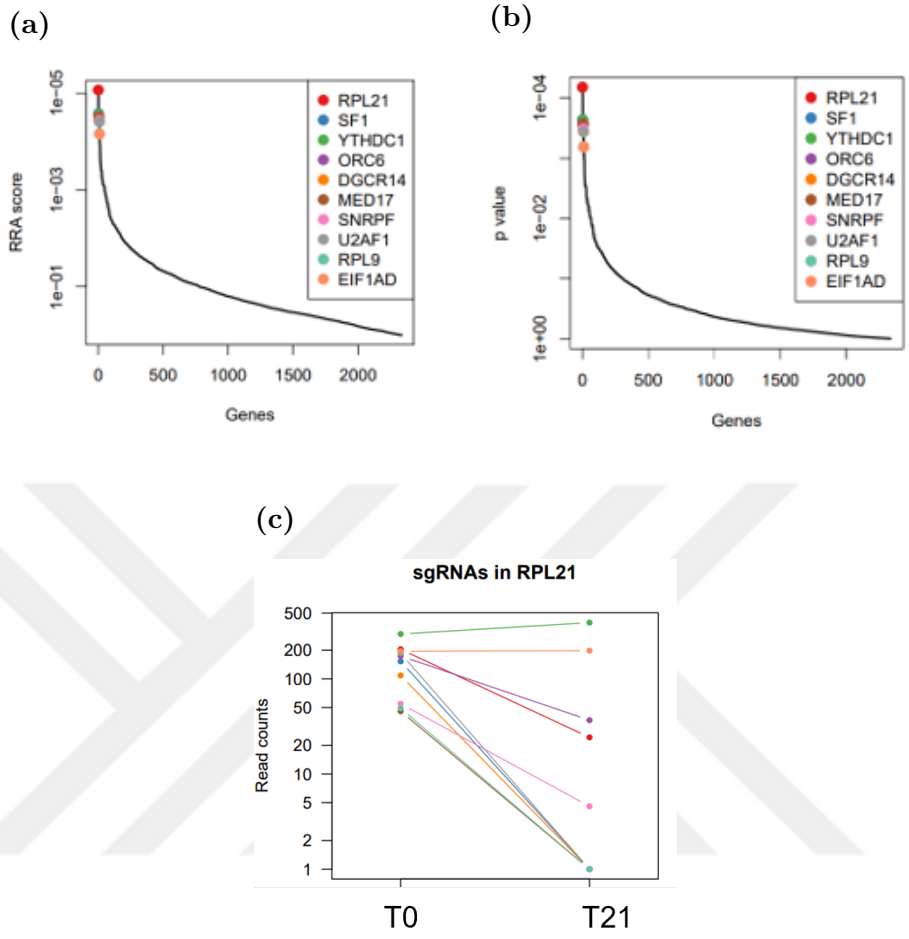

Figure 5.47. Results of CRISPR/Cas9 screening for GEEX library in SKMEL28-Cas9 sgIRF4 KO cells. a) RRA score and p-value of the top 10 negatively selected genes. b) gRNA counts for RPL21 genes in SKMEL28-Cas9 sgIRF4 KO. T0: Start of dox-inducible Cas9 expression, T21: Endpoint of the assay (Appendix Table P.4).

5.6.3.1. Apoptosis and Cancer (ACOC) Library. The most enriched pathway across REACTOME, WikiPathways, and Gene Ontology analysis is the cell cycle and its regulation (Figure 5.48). This is an interesting finding, as the role of IRF4 in the deregulation of the cell cycle has been discussed previously (Figure 5.25, Figure 5.26). The data indicate a further major role for IRF4 in the regulation of cell cycle and proliferative signaling than what we have seen until now. Another noteworthy finding is the significance of the G1/S transition process in REACTOME and WikiPathways

(Figure 5.48a and b). As shown previously, IRF4 downregulation resulted in an increase in the G1 population (Figure 5.25). Finally, the most recurrent non-cell-cycle term in this analysis was related to proteasome degradation and ubiquitin-related processes (Figure 5.48b and c). Overall, the results of screening with ACOC further confirm previous results and give insight into a potential link between IRF4 and the process of protein degradation by proteosomes and ubiquitination.

5.6.3.2. Gene Expression (GEEX) Library. Preliminary analysis of screening with the GEEX library revealed that the most repeated term across all 3 databases was related to Transcription and RNA processes (Figure 5.49, Appendix Figure Q.2). This is to be expected, as the GEEX library is specifically designed to identify genes involved in gene expression. The enrichment analysis was carried out based on genes that were depleted in sgIRF4 KO samples; Even with different genes being depleted in EV samples, the same terms can be encountered. Therefore, it would be better to focus on more specific terms. The other most noteworthy process is the regulation of lipid metabolism and the PPARα-mediated process, which was a hit both in REACTOME and WikiPathways, (Figure 5.49a and b). PPARα is a major transcriptional regulator of lipid metabolism. Studies have shown that IRF4 is a major regulator of lipid metabolism in brown adipocytes (Egouchi et al., 2011). In melanoma, the link between IRF4 and lipid metabolism and how it affects tumorigenesis is poorly understood.

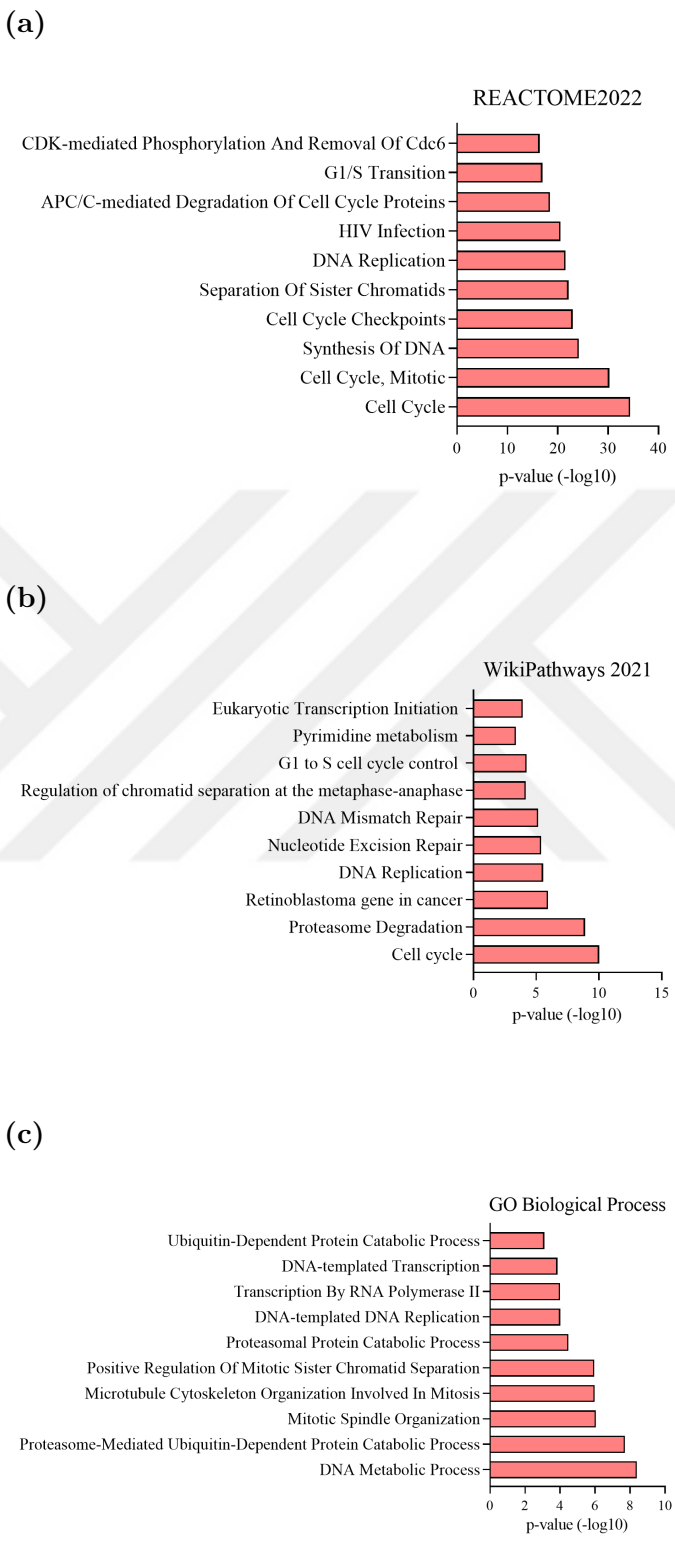

Figure 5.48. GSEA of ACOC results of essential genes in IRF4-KO.

Figure 5.49. GSEA of GEEX results of essential genes in IRF4-KO.

6. DISCUSSION

Research for novel targeted therapies, including those that target cancer cells or modulate the immune system, as well as the repurposing of some renowned therapeutic agents, is at the forefront of cancer therapeutic studies. In parallel, pursuing novel potential prognostic markers, specially in cancers with high metastasis potency, is crucial. The rise in annual melanoma incidences demands better prognostic markers and therapeutic strategies. Although many targeted therapies such as BRAF inhibitors, MEK inhibitors, and checkpoint inhibitors have been effective for melanoma patients, after some time, develop resistance. It has been well-established that the distribution of oncogenes, tumor suppressors, and immune profiles within and across melanoma subtypes can influence tumor behavior and clinical outcomes (Emran et al., 2019; Wagstaff et al., 2022). In addition to the significantly mutated genes and other genomic aberrations in melanomas, the phenotype switching and cell plasticity impact the mechanisms of resistance to both targeted and immune checkpoint blockade (ICB) therapies (Rambow et al., 2019). Taken together, finding new prognostic markers which can also give insight into the most effective combinatory therapeutic protocols is critical for improving the long-term expectancy and the quality of life in melanoma patients.

The role of IRF4 in some lymphoid-origin cancers, such as multiple myeloma, ABC-DLBCL, and ALCL, has been extensively characterized (Shaffer et al., 2008; Yang et al., 2012; Weilemann et al., 2015). Furthermore, the IRF4-dependency and IRF4-mediated drug sensitivities in these cancers are also well-studied. In these cancers, by targeting upstream regulators, IRF4 expression is diminished, and cells become sensitized toward a complementary treatment or die. In multiple myeloma and other mature lymphoid malignancies, treatment with immunomodulatory drugs (IMiD) such as lenalidomide has been shown to decrease IRF4 levels in the cells (Lopez-Girona et al., 2011; Zhang et al., 2013). A more recent study in multiple myeloma reported depletion of IRF4 via targeting with IRF4 antisense oligonucleotides led to cell cycle arrest and impairment in cell growth (Mondala et al., 2021).

Melanoma tumors express the highest levels of IRF4 among all non-hematopoietic malignancies (Figure 5.1, Figure 5.3). DEPMAP CRISPR screening data show IRF4 dependency in IRF4-expressing melanoma cell lines (Figure 5.2). Furthermore, in cutaneous melanoma TCGA patient data, higher IRF4 expression indicates poorer prognosis compared to IRF4 low patients (Figure 5.4). Therefore, IRF4 expression can be used as a prognosis marker in melanoma.

Depletion of IRF4 led to impaired growth and proliferation in melanoma cells (Figure 5.7). To elucidate the IRF4 downstream mechanisms, we went back to the previous RNA-seq data from our group (Yilmaz, 2014). According to RNA-seq data, IRF4 is a potential regulator of a subset of chromatin modifiers responsible for establishing and maintaining epigenetic silencing marks: DNMT1, DNMT3B, and UHRF1 members of DNA methylation machinery, and EZH2 of the polycomb repressive complex 2 (PRC2). RNA-seq data were confirmed with qRT-PCR (Figure 5.10, Figure 5.14) and western blot (Figure 5.11, Figure 5.15). Additionally, analysis of ENCODE data in melanoma suggested potential IRF4 binding regions in DNMT1 and DNMT3B, and EZH2, which was then verified with ChIP-qPCR (Figure 5.12, Figure 5.16). As a result, IRF4 transcriptionally regulates DNMT1, DNMT3B, and EZH2. All these genes are methyltransferase enzymes, DNMT1/DNMT3B responsible for maintenance and de novo DNA methylation, respectively, and EZH2 is the writer enzyme for H3K27me3, a histone modification for gene silencing. As the outcome of IRF4-modulated alterations in the expression of DNMT1, DNMT3B, and UHRF1, the global DNA methylation levels were significantly changed. Similarly, IRF4 depletion led to the downregulation of EZH2 levels, which caused the loss of H3K27me3 in the melanoma cells (Figure 5.17). As a result of IRF4 loss in melanoma cells, global DNA methylation levels were reduced in SKMEL28 cells. Whereas overexpression of IRF4 leads to augmentation of methylation genome-wide (Figure 5.13). However, the overexpression of IRF4 resulted in no significant change in global H3k27me3 levels in A375 cells (Appendix Figure H.2). Overall, we established that in a subset of melanoma cells, there is IRF4-driven epigenetic silencing program, which is diminished upon IRF4 depletion.

Encouraged by the genome-wide results, we focused on a detailed study of some candidate genes downstream of the reshaping of epigenetic silencing in melanoma cells. In melanoma, like many other cancers, the target of epigenetic silencing mechanisms are tumor suppressors and any other gene whose expression would decrease the fitness of the cancer cells. As the outcome of qRT-PCR screening of tumor suppressor genes, which were known to be hypermethylated in melanoma tumors, we focused on three genes with pivotal roles in the regulation of cell cycle, proliferation, and homeostasis of melanoma cells. The two key cell cycle-related genes, CDKN1A/p21 and CDKN1B/p27, are inhibitors of CDK and function as cell cycle checkpoint regulators, and the third gene is PTEN, the negative regulator of the PI3K-AKT pathway. All these three genes are activated upon IRF4 depletion (Figure 5.20, Figure 5.21), whereas an increase in IRF4 levels led to their suppression in melanoma cells (Figure 5.22, Figure 5.23). Furthermore, all these three genes are known to be hypermethylated in melanoma cells (Carnero et al., 2008; Alcazar et al., 2011; Grigore et al., 2020; Zob et al., 2023). Therefore, we checked their methylation levels with the MSRE-qPCR method, and the results demonstrated that IRF4 loss is followed by loss of DNA methylation levels at the promoters of these genes. On the other hand, IRF4 overexpression resulted in the establishment of hypermethylated promoters for p21, p27, and PTEN (Figure 5.24). The phenotypic consequence of these changes was cell cycle arrest at G1 in IRF4-depleted melanoma cells (Figure 5.25). IRF4-mediated PTEN loss led to a decrease in pSer473 AKT (pAKT), the key modification for AKT activity. Consequently, the loss of pAKT levels is followed by the loss of pS6 and pFOXO1 levels. The outcome of pS6 and pFOXO1 loss is dysregulation of translation and stabilization of FOXO1 protein, respectively (Figure 5.27). Furthermore, FOXO1 escapes from degradation, which will activate apoptosis and cell death (Xing et al., 2018; Orea-Soufi et al., 2022). Taken as a whole with other phenotypic data discussed in this thesis, there is an IRF4-linked cell cycle and proliferation program in melanoma cells, and when IRF4 expression is diminished, the melanoma cells cannot proliferate, and subsequently, prolonged loss of IRF4 triggers cell death.

On the other hand, IRF4 overexpression leads to a decrease in p21, p27, and PTEN levels. Also, PTEN depletion leads to replenishment of pAKT and subsequently elevated pS6 levels. Yet, it seems the abundancy of IRF4 in A375 and SKMEL28 cells has implications for the deregulation of the cell cycle, shown as an increase in the percentage of the population at the S phase and slower proliferation in A375 and SKMEL28 cells (Figure 5.8, Figure 5.26). This can be interpreted as two different possible scenarios, first impairment in DNA replication and maybe the accumulation of DNA damage, which leads to an increase in the cell population at S-phase; the second scenario is related to cell plasticity and phenotype switching, but whether it is towards an invasive phenotype or towards a differentiated phenotype is yet to be studied.

As a target of the IRF4-EZH2 axis, we focussed on WDR19, which has already been implicated as the target of EZH2 in melanoma (Zingg et al., 2018). WDR19, known as IFT144, is part of the ciliary transport system and has a function in the maintenance of cilia structure. In this study, we have demonstrated that IRF4 manipulation affects WDR19 expression inversely (Figure 5.29, Figure 5.30). Furthermore, the ChIP-qPCR data indicates that upon IRF4 loss, H3K27me3 levels decrease at WDR19 promoter (Figure 5.31). Overexpression of IRF4 results in depletion of WDR19, leading to loss of cilia in A375 and UACC6. Moreover, the combination of IRF4 overexpression and treatment with EZH2 inhibitor resulted in partial rescue of ciliogenesis in A375 cells (Figure 5.32, Figure 5.33). Zingg et al. reported that the implications of EZH2-mediated cilia deconstruction are exhibited on the canonical WNT-βcatenin pathway (Zingg et al., 2018). In accordance with their data, our results indicate activation of the canonical WNT-βcatenin pathway and upregulation of βcatenin target genes, AXIN2 and MET. Hence, we suggest that through suppression of ciliogenesis genes, and loss of cilia, the IRF4-EZH2 axis through the WNT-βcatenin pathway possibly contributes to melanoma progression.

As the final piece of IRF4-mediated epigenetic silencing, we investigated the relationship between IRF4 and two different epigenetic inhibitors: The DNMT inhibitors

(5-Aza and Decitabine) and the EZH2 inhibitor (Tazmetostat). The XTT results from combining IRF4 manipulation and treatment with DNMT inhibitors have shown that IRF4 contributes to resistance of the melanoma cells toward the effect of these drugs. As IRF4 expression and response to DNMT inhibitor are inversely linked. However, depletion of IRF4 will lead to sensitization of cells to 5-Aza and Decitabine. Furthermore, XTT results from IRF4 overexpression and EZH2 inhibitor treatment indicate aberrant IRF4 levels in the cells have a negative contribution to EPZ-6438 cytotoxic response in melanoma cells. Overall, the XTT assays for both drugs suggest that treatment with these drugs in patients with high IRF4 expression may have lower efficacy at milder doses compared to patients with no IRF4 expression. As the last part of this study, to expand our knowledge on IRF4 partners in melanoma, we carried out CRISPR/Cas9 loss-of-function screening to find IRF4 synthetic lethal partners in SKMEL28 cell lines with two targeted libraries, Apoptosis and Cancer (ACOC) and Gene Expression (GEEX). Due to budget restrictions, we could only process one replicate for each sample. Therefore, the reported results are preliminary.

The results of screening with ACOC showed that in IRF4 knockout samples, gRNA-targeting genes involved in cell cycle regulation and proteasomal degradation were negatively selected. This means that the loss of IRF4 combined with the loss of these genes led to cell death and the depletion of cells carrying the gRNAs related to these pathways. These data further confirm and even expand the role of IRF4 in regulating the cell cycle and, subsequently, proliferation in melanoma cells. Furthermore, it was surprising to see genes related to the proteasomal degradation pathway. One of the possible future directions for this work could be the investigation of the link between IRF4 expression and pathways that lead to proteasomal degradation, such as ubiquitination.

The outcome of screening with the GEEX library generated a smaller number of significantly negatively selected genes. Therefore, the significance of the gene set enrichment analysis results was also lower than that of ACOC. However, the most interesting result was from genes related to lipid metabolism and PPARα-mediated

processing. Previous work from RNA-seq data reported a possible link between IRF4 and lipid metabolism (Yilmaz, 2014). Additionally, studies have shown IRF4 to be a key modulator of lipogenesis and the metabolism of lipids in adipocytes of brown fat tissue (Eguchi et al., 2011; Kong et al., 2014). However, the implication of IRF4 expression on lipid metabolism in melanoma cells still needs to be studied.

In conclusion, there are studies that have shown that through modulation of epigenetic silencing, we can modulate drug efficacy in melanoma patients, in particular the response to immune checkpoint inhibitor (ICB) treatments such as anti-PD-L1 and anti-CTLA-4 (Emran et al., 2019). Also, a recent study has shown that IRF4 expression negatively regulates PDL1 expression through suppression of IRF4 and that IRF4 depletion via downregulation of SOX10, its upstream regulator, could improve response to ICB (Yokoyama et al., 2021). Hence, the link between IRF4 levels and immune response in cancer cells is another promising path to further illuminate if IRF4 expression contributes to poorer prognosis through modulation of immune response in melanoma cells.

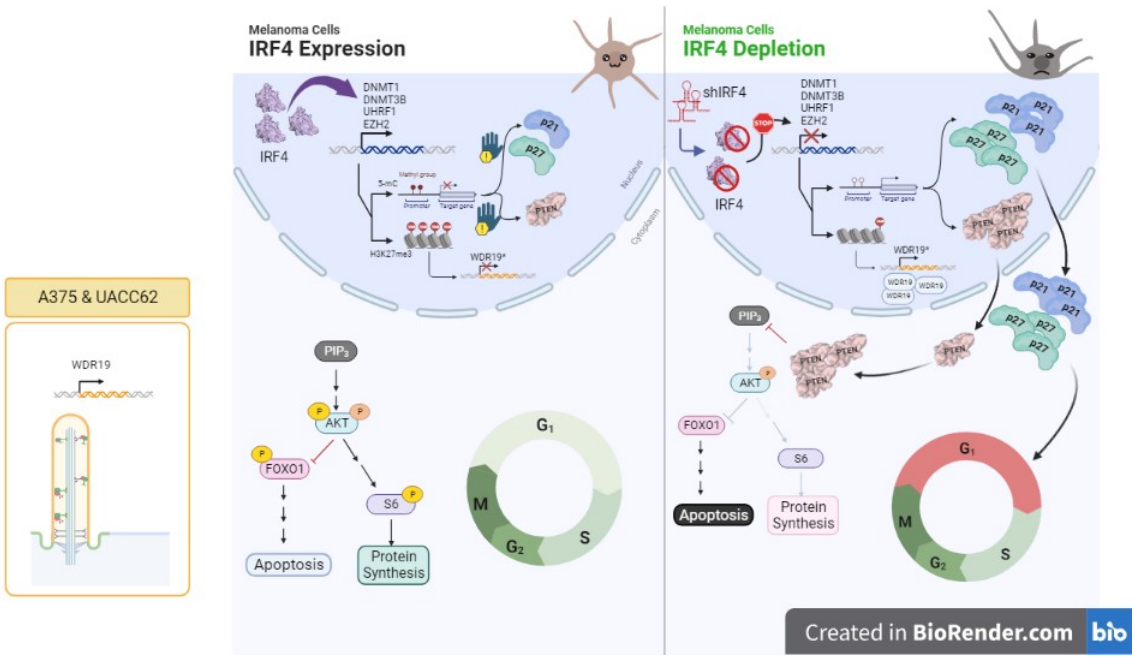

Figure 6.1. The proposed model for role of IRF4 in melanoma

Another noteworthy point regarding epigenetic silencing machinery in cells that we didn't discuss here is H3k9me3 and its multiple writer enzymes. Studies have shown the key writer enzyme for H3K9me3 in melanoma tumors is SETDB1, and its amplified expression is critical for melanoma development (Ceol et al., 2011; Orouji et al., 2019). According to RNA-seq data, we are aware that the only H3K9me3 writer regulated by IRF4 is SETDB1 (Yilmaz, 2014). Although we have acquired preliminary data regarding IRF4's impact on SETDB1 expression and H3K9me3 levels, due to lack of time, we haven't followed up.

Taken together, the experiments in the first part of this thesis and preliminary results from CRISPR/Cas9 screening suggest IRF4's involvement in cell cycle regulation is broader than what we have seen. Moreover, the result of this study implies a potential role for IRF4 in pathways leading to proteasomal degradation and lipid metabolism, which is yet to be studied. Based on the results of this study, we indicate that the impacts of IRF4 expression are broader than what we had foreseen. Also, we propose that one of the ways IRF4 expression regulates cell cycle, proliferation, and cell homeostasis is through modulation of epigenetic silencing marks and subsequently regulating the expression of downstream targets such as p21 and p27 and the PI3K-AKT pathway through PTEN (Figure 6.1).

Finally, our study indicates that in cutaneous melanoma cells, distorted DNA methylation machinery and epigenetic silencing mechanisms can alter the efficacy of specific therapies. Additionally, the determination of IRF4 expression could potentially have implications for diagnosis and choosing a method of treatment in melanoma. Furthermore, regarding the role of IRF4 in cell plasticity and phenotype switching in IRF4-expressing tumors, we need to investigate and characterize whether the downregulation of IRF4 in certain phenotypes could also be an indicator or efficacy of drug response in these patients. As the next step, these results need to be further investigated *in vivo* as xenograft studies or using conditional IRF4 knockout mouse melanoma models.

REFERENCES

1. Abbastabar, M., M. Kheyrollah, K. Azizian, N. Bagherlou, S. S. Tehrani, M. Maniati and A. Karimian, "Multiple Functions of p27 in Cell Cycle, Apoptosis, Epigenetic Modification and Transcriptional Regulation for the Control of Cell Growth: A Double-Edged Sword Protein", *DNA Repair*, Vol. 69, pp. 63–72, 2018.

2. Adamson, B., T. M. Norman, M. Jost, M. Y. Cho, J. K. Nuñez, Y. Chen, J. E. Villalta, L. A. Gilbert, M. A. Horlbeck, M. Y. Hein, R. A. Pak, A. N. Gray, C. A. Gross, A. Dixit, O. Parnas, A. Regev and J. S. Weissman, "A Multiplexed Single-Cell CRISPR Screening Platform Enables Systematic Dissection of the UnfoldedProteinResponse", *Cell*, Vol. 167, No. 7, pp. 1867–1882.e21, 2016.

3. Adzhubei, I. A., S. Schmidt, L. Peshkin, V. E. Ramensky, A. Gerasimova, P. Bork, A. S. Kondrashov and S. R. Sunyaev, "A Method and Server for Predicting Damaging Missense Mutations", *Nature Methods*, Vol. 7, No. 4, pp. 248–249, 2010.

4. Aguirre, A. J., R. M. Meyers, B. A. Weir, F. Vazquez, C.-Z. Zhang, U. Ben-David, A. Cook, G. Ha, W. F. Harrington, M. B. Doshi, M. Kost-Alimova, S. Gill, H. Xu, L. D. Ali, G. Jiang, S. Pantel, Y. Lee, A. Goodale, A. D. Cherniack, C. Oh, G. Kryukov, G. S. Cowley, L. A. Garraway, K. Stegmaier, C. W. Roberts, T. R. Golub, M. Meyerson, D. E. Root, A. Tsherniak and W. C. Hahn, "Genomic Copy Number Dictates a Gene-Independent Cell Response to CRISPR-Cas9 Targeting", *Cancer Discovery*, Vol. 6, No. 8, pp. 914–929, 2016.

5. Akbani, R., K. C. Akdemir, B. A. Aksoy, M. Albert, A. Ally, S. B. Amin, H. Arachchi, A. Arora, J. T. Auman, B. Ayala, J. Baboud, M. Balasundaram, S. Balu, N. Barnabas, J. Bartlett, P. Bartlett, B. C. Bastian, S. B. Baylin, J. N., D. J. Weisenberger, P. White, M. D. Wilkerson, J. S. Wilmott, L. Wise, M. Wiznerowicz, S. E. Woodman, C.-J. Wu, C.-C. Wu, J. Wu, Y. Wu, R. Xi, A. W. Xu, D. Yang, L. Yang, L. Yang, T. I. Zack, J. C. Zenklusen, H. Zhang, J. Zhang,

W. Zhang, X. Zhao, J. Zhu, K. Zhu, L. Zimmer, E. Zmuda and L. Zou, "Genomic Classification of Cutaneous Melanoma", *Cell*, Vol. 161, No. 7, pp. 1681–1696, 2015.

6. Alcazar, O., S. Achberger, W. Aldrich, Z. Hu, S. Negrotto, Y. Saunthararajah and P. Triozzi, "Epigenetic Regulation by Decitabine of Melanoma Differentiation in vitro and in vivo", *International Journal of Cancer*, Vol. 131, No. 1, pp. 18–29, 2012.

7. Aldinucci, D., M. Celegato, C. Borghese, A. Colombatti and A. Carbone, "IRF4 Silencing Inhibits Hodgkin Lymphoma Cell Proliferation, Survival And CCL5 Secretion", *British Journal of Haematology*, Vol. 152, No. 2, pp. 182–190, 2011.

8. Amaral, T., T. Sinnberg, F. Meier, C. Krepler, M. Levesque, H. Niessner and C. Garbe, "The Mitogen-Activated Protein Kinase Pathway in Melanoma Part I – Activation and Primary Resistance Mechanisms to BRAF Inhibition", *European Journal of Cancer*, Vol. 73, pp. 85–92, 2017.

9. Aumer, T., C. B. Gremmelmaier, L. S. Runtsch, J. C. Pforr, G. N. Yeşiltaç, S. Kaiser and F. R. Traube, "Comprehensive Comparison Between Azacytidine and Decitabine Treatment in an Acute Myeloid Leukemia Cell Line", *Clinical Epigenetics*, Vol. 14, No. 1, p. 113, 2022.

10. Ayhan, M. C., *Characterization of IRF4 Dependency in Melanoma Cell Lines*, M.S. Thesis, Boğaziçi University, 2014.

11. Bandini, C., A. Pupuleku, E. Spaccarotella, E. Pellegrino, R. Wang, N. Vitale, C. Duval, D. Cantarella, A. Rinaldi, P. Provero, F. Di Cunto, E. Medico, F. Bertoni, G. Inghirami and R. Piva, "IRF4 Mediates the Oncogenic Effects of STAT3 in Anaplastic Large Cell Lymphomas", *Cancers*, Vol. 10, No. 1, p. 21, 2018.

12. Barth, T. K. and A. Imhof, "Fast Signals and Slow Marks: The Dynamics of Histone Modifications", *Trends in Biochemical Sciences*, Vol. 35, No. 11, pp. 618–626, 2010.

13. Beikircher, G., W. Pulverer, M. Hofner, C. Noehammer and A. Weinhaeusel, "Multiplexed and Sensitive DNA Methylation Testing Using Methylation-Sensitive Restriction Enzymes "MSRE-qPCR"", *Methods in Molecular Biology (Clifton, N.J.)*, Vol. 1708, pp. 407–424, 2018.

14. Bitler, B. G., K. M. Aird, A. Garipov, H. Li, M. Amatangelo, A. V. Kossenkov, D. C. Schultz, Q. Liu, I.-M. Shih, J. R. Conejo-Garcia, D. W. Speicher and R. Zhang, "Synthetic Lethality by Targeting EZH2 Methyltransferase Activity in ARID1A-Mutated Cancers", *Nature Medicine*, Vol. 21, No. 3, pp. 231–238, 2015.

15. Boddicker, R. L., N. S. Kip, X. Xing, Y. Zeng, Z.-Z. Yang, J.-H. Lee, L. L. Almada, S. F. Elsawa, R. A. Knudson, M. E. Law, R. P. Ketterling, J. M. Cunningham, Y. Wu, M. J. Maurer, M. M. O'Byrne, J. R. Cerhan, S. L. Slager, B. K. Link, J. C. Porcher, D. M. Grote, D. F. Jelinek, A. Dogan, S. M. Ansell, M. E. Fernandez-Zapico and A. L. Feldman, "The Oncogenic Transcription Factor IRF4 is Regulated by a Novel CD30/NF-κB Positive Feedback Loop in Peripheral T-Cell Lymphoma", *Blood*, Vol. 125, No. 20, pp. 3118–3127, 2015.

16. Boehm, J. S. and W. C. Hahn, "Towards Systematic Functional Characterization of Cancer Genomes", *Nature Reviews. Genetics*, Vol. 12, No. 7, pp. 487–498, 2011.

17. Broad Institute, "DepMap Portal", 2021, `https://depmap.org/portal/`, accessed on July 15, 2023.

18. Bustin, S. A., V. Benes, J. A. Garson, J. Hellemans, J. Huggett, R. Mueller, T. Nolan, M. W. Pfaffl, G. L. Shipley, J. Vandesompele and C. T. Wittwer, "The MIQE Guidelines: Minimum Information for Publication of Quantitative Real-Time PCR Experiments", *Clinical Chemistry*, Vol. 55, No. 4, pp. 611–622, 2009.

19. Cao, R. and Y. Zhang, "The Functions of E(Z)/EZH2-Mediated Methylation of Lysine 27 in Histone H3", *Current Opinion in Genetics & Development*, Vol. 14, No. 2, pp. 155–164, 2004.

20. Carnero, A., C. Blanco-Aparicio, O. Renner, W. Link and J. F. M. Leal, "The PTEN/PI3K/AKT Signalling Pathway in Cancer, Therapeutic Implications", *Current Cancer Drug Targets*, Vol. 8, No. 3, pp. 187–198, 2008.

21. Ceol, C. J., Y. Houvras, J. Jane-Valbuena, S. Bilodeau, D. A. Orlando, V. Battisti, L. Fritsch, W. M. Lin, T. J. Hollmann, F. Ferré, C. Bourque, C. J. Burke, L. Turner, A. Uong, L. A. Johnson, R. Beroukhim, C. H. Mermel, M. Loda, S. Ait-Si-Ali, L. A. Garraway, R. A. Young and L. I. Zon, "The Histone Methyltransferase SETDB1 Is Recurrently Amplified in Melanoma and Accelerates Its Onset", *Nature*, Vol. 471, No. 7339, pp. 513–517, 2011.

22. Chavez, A., J. Scheiman, S. Vora, B. W. Pruitt, M. Tuttle, E. P R Iyer, S. Lin, S. Kiani, C. D. Guzman, D. J. Wiegand, D. Ter-Ovanesyan, J. L. Braff, N. Davidsohn, B. E. Housden, N. Perrimon, R. Weiss, J. Aach, J. J. Collins and G. M. Church, "Highly Efficient Cas9-Mediated Transcriptional Programming", *Nature Methods*, Vol. 12, No. 4, pp. 326–328, 2015.

23. Chien, A. J., E. C. Moore, A. S. Lonsdorf, R. M. Kulikauskas, B. G. Rothberg, A. J. Berger, M. B. Major, S. T. Hwang, D. L. Rimm and R. T. Moon, "Activated Wnt/*Beta*-Catenin Signaling in Melanoma Is Associated with Decreased Proliferation in Patient Tumors and a Murine Melanoma Model", *Proceedings of the National Academy of Sciences of the United States of America*, Vol. 106, No. 4, pp. 1193–1198, 2009.

24. Chin, L., G. Merlino and R. A. DePinho, "Malignant Melanoma: Modern Black Plague and Genetic Black Box", *Genes & Development*, Vol. 12, No. 22, pp. 3467–3481, 1998.

25. Christodoulou, E., M. Rashid, C. Pacini, A. Droop, H. Robertson, T. van Groningen, A. F. A. S. Teunisse, F. Iorio, A. G. Jochemsen, D. J. Adams and R. van Doorn, "Analysis of CRISPR-Cas9 Screens Identifies Genetic Dependencies in Melanoma", *Pigment Cell & Melanoma Research*, Vol. 34, No. 1, pp. 122–131, 2021.

26. Cowley, G. S., B. A. Weir, F. Vazquez, P. Tamayo, J. A. Scott, S. Rusin, A. East-Seletsky, L. D. Ali, W. F. J. Gerath, S. E. Pantel, P. H. Lizotte, G. Jiang, J. Hsiao, A. Tsherniak, E. Dwinell, S. Aoyama, M. Okamoto, W. Harrington, E. Gelfand, T. M. Green, M. J. Tomko, S. Gopal, T. C. Wong, H. Li, S. Howell, N. Stransky, T. Liefeld, D. Jang, J. Bistline, B. Hill Meyers, S. A. Armstrong, K. C. Anderson, K. Stegmaier, M. Reich, D. Pellman, J. S. Boehm, J. P. Mesirov, T. R. Golub, D. E. Root and W. C. Hahn, "Parallel Genome-Scale Loss of Function Screens in 216 Cancer Cell Lines for the Identification of Context-Specific Genetic Dependencies", *Scientific Data*, Vol. 1, No. 1, p. 140035, 2014.

27. Cronin, K. A., S. Scott, A. U. Firth, H. Sung, S. J. Henley, R. L. Sherman, R. L. Siegel, R. N. Anderson, B. A. Kohler, V. B. Benard, S. Negoita, C. Wiggins, W. G. Cance and A. Jemal, "Annual Report to the Nation on the Status of Cancer, Part 1: National Cancer Statistics", *Cancer*, Vol. 128, No. 24, pp. 4251–4284, 2022.

28. Cui, C., X. Zhou, W. Zhang, Y. Qu and X. Ke, "Is -Catenin a Druggable Target for Cancer Therapy?", *Trends in Biochemical Sciences*, Vol. 43, No. 8, pp. 623–634, 2018.

29. Datlinger, P., A. F. Rendeiro, C. Schmidl, T. Krausgruber, P. Traxler, J. Klughammer, L. C. Schuster, A. Kuchler, D. Alpar and C. Bock, "Pooled CRISPR Screening with Single-Cell Transcriptome Readout", *Nature Methods*, Vol. 14, No. 3, pp. 297–301, 2017.

30. Davies, H., G. R. Bignell, C. Cox, P. Stephens, S. Edkins, S. Clegg, J. Teague, H. Woffendin, M. J. Garnett, W. Bottomley, N. Davis, E. Dicks, R. Ewing,

Y. Floyd, K. Gray, S. Hall, R. Hawes, J. Hughes, V. Kosmidou, A. Menzies, C. Mould, A. Parker, C. Stevens, S. Watt, S. Hooper, R. Wilson, H. Jayatilake, B. A. Gusterson, C. Cooper, J. Shipley, D. Hargrave, K. Pritchard-Jones, N. Maitland, G. Chenevix-Trench, G. J. Riggins, D. D. Bigner, G. Palmieri, A. Cossu, A. Flanagan, A. Nicholson, J. W. C. Ho, S. Y. Leung, S. T. Yuen, B. L. Weber, H. F. Seigler, T. L. Darrow, H. Paterson, R. Marais, C. J. Marshall, R. Wooster, M. R. Stratton and P. A. Futreal, "Mutations of the BRAF Gene in Human Cancer", *Nature*, Vol. 417, No. 6892, pp. 949–954, 2002.

31. Davies, M. A., "The Role of the PI3K-AKT Pathway in Melanoma", *The Cancer Journal*, Vol. 18, No. 2, p. 142, 2012.

32. De Silva, N. S., G. Simonetti, N. Heise and U. Klein, "The Diverse Roles of IRF4 in Late Germinal Center B-Cell Differentiation", *Immunological Reviews*, Vol. 247, No. 1, pp. 73–92, 2012.

33. Delmas, V., F. Beermann, S. Martinozzi, S. Carreira, J. Ackermann, M. Kumasaka, L. Denat, J. Goodall, F. Luciani, A. Viros, N. Demirkan, B. C. Bastian, C. R. Goding and L. Larue, "-Catenin Induces Immortalization of Melanocytes by Suppressing p16INK4a Expression and Cooperates with N-Ras in Melanoma Development", *Genes & Development*, Vol. 21, No. 22, pp. 2923–2935, 2007.

34. Deng, M., J. Brägelmann, I. Kryukov, N. Saraiva-Agostinho and S. Perner, "FirebrowseR: an R Client to the Broad Institute's Firehose Pipeline", *Database: The Journal of Biological Databases and Curation*, Vol. 2017, pp. 154–160, 2017.

35. Diesch, J., A. Zwick, A.-K. Garz, A. Palau, M. Buschbeck and K. S. Götze, "A Clinical-Molecular Update on Azanucleoside-Based Therapy for the Treatment of Hematologic Cancers", *Clinical Epigenetics*, Vol. 8, No. 1, p. 71, 2016.

36. Dixit, A., O. Parnas, B. Li, J. Chen, C. P. Fulco, L. Jerby-Arnon, N. D. Marjanovic, D. Dionne, T. Burks, R. Raychowdhury, B. Adamson, T. M. Norman,

E. S. Lander, J. S. Weissman, N. Friedman and A. Regev, "Perturb-Seq: Dissecting Molecular Circuits with Scalable Single-Cell RNA Profiling of Pooled Genetic Screens", *Cell*, Vol. 167, No. 7, pp. 1853–1866.e17, 2016.

37. Duan, R., W. Du and W. Guo, "EZH2: a Novel Target for Cancer Treatment", *Journal of Hematology & Oncology*, Vol. 13, No. 1, p. 104, 2020.

38. Duffy, D. L., M. M. Iles, D. Glass, G. Zhu, J. H. Barrett, V. Höiom, Z. Z. Zhao, R. A. Sturm, N. Soranzo, C. Hammond, M. Kvaskoff, D. C. Whiteman, M. Mangino, J. Hansson, J. A. Newton-Bishop, GenoMEL, V. Bataille, N. K. Hayward, N. G. Martin, D. T. Bishop, T. D. Spector and G. W. Montgomery, "IRF4 Variants Have Age-Specific Effects on Nevus Count and Predispose to Melanoma", *American Journal of Human Genetics*, Vol. 87, No. 1, pp. 6–16, 2010.

39. Duffy, D. L., G. Zhu, X. Li, M. Sanna, M. M. Iles, L. C. Jacobs, D. M. Evans, S. Yazar, J. Beesley, M. H. Law, P. Kraft, A. Visconti, J. C. Taylor, F. Liu, M. J. Wright, A. K. Henders, L. Bowdler, D. Glass, M. A. Ikram, A. G. Uitterlinden, P. A. Madden, A. C. Heath, E. C. Nelson, A. C. Green, S. Chanock, J. H. Barrett, M. A. Brown, N. K. Hayward, S. MacGregor, R. A. Sturm, A. W. Hewitt, Melanoma GWAS Consortium, M. Kayser, D. J. Hunter, J. A. Newton Bishop, T. D. Spector, G. W. Montgomery, D. A. Mackey, G. D. Smith, T. E. Nijsten, D. T. Bishop, V. Bataille, M. Falchi, J. Han and N. G. Martin, "Novel Pleiotropic Risk Loci for Melanoma and Nevus Density Implicate Multiple Biological Pathways", *Nature Communications*, Vol. 9, No. 1, p. 4774, 2018.

40. Dzobo, K., N. E. Thomford and D. A. Senthebane, "Targeting the Versatile Wnt/-Catenin Pathway in Cancer Biology and Therapeutics: From Concept to Actionable Strategy", *OMICS: A Journal of Integrative Biology*, Vol. 23, No. 11, pp. 517–538, 2019.

41. Eguchi, J., X. Wang, S. Yu, E. E. Kershaw, P. C. Chiu, J. Dushay, J. L. Estall,

U. Klein, E. Maratos-Flier and E. D. Rosen, "Transcriptional Control of Adipose Lipid Handling by IRF4", *Cell Metabolism*, Vol. 13, No. 3, pp. 249–259, 2011.

42. Eguchi, J., Q.-W. Yan, D. E. Schones, M. Kamal, C.-H. Hsu, M. Q. Zhang, G. E. Crawford and E. D. Rosen, "Interferon Regulatory Factors Are Transcriptional Regulators of Adipogenesis", *Cell Metabolism*, Vol. 7, No. 1, pp. 86–94, 2008.

43. Emran, A. A., A. Chatterjee, E. J. Rodger, J. C. Tiffen, S. J. Gallagher, M. R. Eccles and P. Hersey, "Targeting DNA Methylation and EZH2 Activity to Overcome Melanoma Resistance to Immunotherapy", *Trends in Immunology*, Vol. 40, No. 4, pp. 328–344, 2019.

44. European Cancer Information System, "Skin Melanoma Burden in EU-27", 2021, `https://visitors-centre.jrc.ec.europa.eu/en/media/infographics/skin-melanoma-burden-eu-27`, accessed on July 15, 2023.

45. Fan, T., S. Jiang, N. Chung, A. Alikhan, C. Ni, C.-C. R. Lee and T. J. Hornyak, "EZH2-Dependent Suppression of a Cellular Senescence Phenotype in Melanoma Cells by Inhibition of p21/CDKN1A Expression", *Molecular Cancer Research*, Vol. 9, No. 4, pp. 418–429, 2011.

46. Forsea, A.-M., "Melanoma Epidemiology and Early Detection in Europe: Diversity and Disparities", *Dermatology Practical & Conceptual*, Vol. 10, No. 3, p. e2020033, 2020.

47. Fu, S., H. Wu, H. Zhang, C. G. Lian and Q. Lu, "DNA Methylation/Hydroxymethylation in Melanoma", *Oncotarget*, Vol. 8, No. 44, pp. 78163–78173, 2017.

48. Fujii, K., S. Tanaka, T. Hasegawa, H. Koseki, T. Kurosaki and W. Ise, "TET is Required for Plasma Cell Differentiation by Controlling Expression Levels of IRF4", *International Immunology*, Vol. 32, No. 10, pp. 683–690, 2020.

49. Gan, L., Y. Yang, Q. Li, Y. Feng, T. Liu and W. Guo, "Epigenetic Regulation of Cancer Progression by EZH2: From Biological Insights to Therapeutic Potential", *Biomarker Research*, Vol. 6, No. 1, p. 10, 2018.

50. Gandini, S., F. Sera, M. S. Cattaruzza, P. Pasquini, D. Abeni, P. Boyle and C. F. Melchi, "Meta-Analysis of Risk Factors for Cutaneous Melanoma: I. Common and Atypical Naevi", *European Journal of Cancer (Oxford, England: 1990)*, Vol. 41, No. 1, pp. 28–44, 2005.

51. Garman, B., I. N. Anastopoulos, C. Krepler, P. Brafford, K. Sproesser, Y. Jiang, B. Wubbenhorst, R. Amaravadi, J. Bennett, M. Beqiri, D. Elder, K. T. Flaherty, D. T. Frederick, T. C. Gangadhar, M. Guarino, D. Hoon, G. Karakousis, Q. Liu, N. Mitra, N. J. Petrelli, L. Schuchter, B. Shannan, C. L. Shields, J. Wargo, B. Wenz, M. A. Wilson, M. Xiao, W. Xu, X. Xu, X. Yin, N. R. Zhang, M. A. Davies, M. Herlyn and K. L. Nathanson, "Genetic and Genomic Characterization of 462 Melanoma Patient-Derived Xenografts, Tumor Biopsies, and Cell Lines", *Cell Reports*, Vol. 21, No. 7, pp. 1936–1952, 2017.

52. Gauzzi, M. C., C. Purificato, L. Conti, L. Adorini, F. Belardelli and S. Gessani, "IRF-4 Expression in the Human Myeloid Lineage: Upregulation During Dendritic Cell Differentiation and Inhibition by 1α, 25-Dihydroxyvitamin D3", *Journal of Leukocyte Biology*, Vol. 77, No. 6, pp. 944–947, 2005.

53. Gerami, P., R. W. Cook, M. C. Russell, J. Wilkinson, R. N. Amaria, R. Gonzalez, S. Lyle, G. L. Jackson, A. J. Greisinger, C. E. Johnson, K. M. Oelschlager, J. F. Stone, D. J. Maetzold, L. K. Ferris, J. D. Wayne, C. Cooper, R. Obregon, K. A. Delman and D. Lawson, "Gene Expression Profiling for Molecular Staging of Cutaneous Melanoma in Patients Undergoing Sentinel Lymph Node Biopsy", *Journal of the American Academy of Dermatology*, Vol. 72, No. 5, pp. 780–785.e3, 2015.

54. Gilbert, L. A., M. A. Horlbeck, B. Adamson, J. E. Villalta, Y. Chen, E. H.

Whitehead, C. Guimaraes, B. Panning, H. L. Ploegh, M. C. Bassik, L. S. Qi, M. Kampmann and J. S. Weissman, "Genome-Scale CRISPR-Mediated Control of Gene Repression and Activation", *Cell*, Vol. 159, No. 3, pp. 647–661, 2014.

55. Gillespie, M., B. Jassal, R. Stephan, M. Milacic, K. Rothfels, A. Senff-Ribeiro, J. Griss, C. Sevilla, L. Matthews, C. Gong, C. Deng, T. Varusai, E. Ragueneau, Y. Haider, B. May, V. Shamovsky, J. Weiser, T. Brunson, N. Sanati, L. Beckman, X. Shao, A. Fabregat, K. Sidiropoulos, J. Murillo, G. Viteri, J. Cook, S. Shorser, G. Bader, E. Demir, C. Sander, R. Haw, G. Wu, L. Stein, H. Hermjakob and P. D'Eustachio, "The Reactome Pathway Knowledgebase 2022", *Nucleic Acids Research*, Vol. 50, No. D1, pp. D687–D692, 2022.

56. Goff, L. A. and J. L. Rinn, "Polycombing the Genome for RNA", *Nature Structural & Molecular Biology*, Vol. 20, No. 12, pp. 1344–1346, 2013.

57. Goldman, M. J., B. Craft, M. Hastie, K. Repečka, F. McDade, A. Kamath, A. Banerjee, Y. Luo, D. Rogers, A. N. Brooks, J. Zhu and D. Haussler, "Visualizing and Interpreting Cancer Genomics Data via The Xena Platform", *Nature Biotechnology*, Vol. 38, No. 6, pp. 675–678, 2020.

58. Grigore, F., H. Yang, N. D. Hanson, M. W. VanBrocklin, A. L. Sarver and J. P. Robinson, "BRAF Inhibition in Melanoma Is Associated with the Dysregulation of Histone Methylation and Histone Methyltransferases", *Neoplasia (New York, N.Y.)*, Vol. 22, No. 9, pp. 376–389, 2020.

59. Grossman, A., H. W. Mittrücker, J. Nicholl, A. Suzuki, S. Chung, L. Antonio, S. Suggs, G. R. Sutherland, D. P. Siderovski and T. W. Mak, "Cloning of Human Lymphocyte-Specific Interferon Regulatory Factor (hLSIRF/hIRF4) and Mapping of the Gene to 6p23-p25", *Genomics*, Vol. 37, No. 2, pp. 229–233, 1996.

60. Grossman, R. L., A. P. Heath, V. Ferretti, H. E. Varmus, D. R. Lowy, W. A. Kibbe and L. M. Staudt, "Toward a Shared Vision for Cancer Genomic Data",

The New England Journal of Medicine, Vol. 375, No. 12, pp. 1109–1112, 2016.

61. Guo, S., Z.-Z. Li, D.-S. Jiang, Y. Y. Lu, Y. Liu, L. Gao, S.-M. Zhang, H. Lei, L.-H. Zhu, X.-D. Zhang, D.-P. Liu and H. Li, "IRF4 is a Novel Mediator for Neuronal Survival in Ischaemic Stroke", *Cell Death and Differentiation*, Vol. 21, No. 6, pp. 888–903, 2014.

62. Gupta, S., M. Jiang, A. Anthony and A. B. Pernis, "Lineage-Specific Modulation of Interleukin 4 Signaling by Interferon Regulatory Factor 4", *The Journal of Experimental Medicine*, Vol. 190, No. 12, pp. 1837–1848, 1999.

63. Güvenç, C., F. Neckebroeck, A. Antoranz, M. Garmyn, J. van den Oord and F. M. Bosisio, "Bona Fide Tumor Suppressor Genes Hypermethylated in Melanoma: A Narrative Review", *International Journal of Molecular Sciences*, Vol. 22, No. 19, p. 10674, 2021.

64. Han, J., P. Kraft, H. Nan, Q. Guo, C. Chen, A. Qureshi, S. E. Hankinson, F. B. Hu, D. L. Duffy, Z. Z. Zhao, N. G. Martin, G. W. Montgomery, N. K. Hayward, G. Thomas, R. N. Hoover, S. Chanock and D. J. Hunter, "A Genome-Wide Association Study Identifies Novel Alleles Associated with Hair Color and Skin Pigmentation", *PLoS Genetics*, Vol. 4, No. 5, p. e1000074, 2008.

65. Hart, T., M. Chandrashekhar, M. Aregger, Z. Steinhart, K. R. Brown, G. MacLeod, M. Mis, M. Zimmermann, A. Fradet-Turcotte, S. Sun, P. Mero, P. Dirks, S. Sidhu, F. P. Roth, O. S. Rissland, D. Durocher, S. Angers and J. Moffat, "High-Resolution CRISPR Screens Reveal Fitness Genes and Genotype-Specific Cancer Liabilities", *Cell*, Vol. 163, No. 6, pp. 1515–1526, 2015.

66. Hartenian, E. and J. G. Doench, "Genetic Screens and Functional Genomics Using CRISPR/Cas9 Technology", *The FEBS Journal*, Vol. 282, No. 8, pp. 83–93, 2015.

67. Hatzimichael, E., K. Lagos, V. R. Sim, E. Briasoulis and T. Crook, "Epigenetics in

Diagnosis, Prognostic Assessment and Treatment of Cancer: An Update", *EXCLI Journal*, Vol. 13, pp. 954–976, 2014.

68. Hayward, N. K., J. S. Wilmott, N. Waddell, P. A. Johansson, M. A. Field, K. Nones, A.-M. Patch, H. Kakavand, L. B. Alexandrov, H. Burke, V. Jakrot, S. Kazakoff, O. Holmes, C. Leonard, R. Sabarinathan, L. Mularoni, S. Wood, Q. Xu, N. Waddell, V. Tembe, G. M. Pupo, R. De Paoli-Iseppi, R. E. Vilain, P. Shang, L. M. S. Lau, R. A. Dagg, S.-J. Schramm, A. Pritchard, K. Dutton-Regester, F. Newell, A. Fitzgerald, C. A. Shang, S. M. Grimmond, H. A. Pickett, J. Y. Yang, J. R. Stretch, A. Behren, R. F. Kefford, P. Hersey, G. V. Long, J. Cebon, M. Shackleton, A. J. Spillane, R. P. M. Saw, N. López-Bigas, J. V. Pearson, J. F. Thompson, R. A. Scolyer and G. J. Mann, "Whole-Genome Landscapes of Major Melanoma Subtypes", *Nature*, Vol. 545, No. 7653, pp. 175–180, 2017.

69. Heimes, A.-S., K. Madjar, K. Edlund, M. J. Battista, K. Almstedt, S. Gebhard, S. Foersch, J. Rahnenführer, W. Brenner, A. Hasenburg, J. G. Hengstler and M. Schmidt, "Prognostic Significance of Interferon Regulating Factor 4 (IRF4) in Node-Negative Breast Cancer", *Journal of Cancer Research and Clinical Oncology*, Vol. 143, No. 7, pp. 1123–1131, 2017.

70. Heintel, D., N. Zojer, M. Schreder, K. Strasser-Weippl, B. Kainz, M. Vesely, H. Gisslinger, J. Drach, A. Gaiger, U. Jäger and H. Ludwig, "Expression of MUM1/IRF4 mRNA as a Prognostic Marker in Patients with Multiple Myeloma", *Leukemia*, Vol. 22, No. 2, pp. 441–445, 2008.

71. Hernando, B., M. V. Ibañez, J. A. Deserio-Cuesta, R. Soria-Navarro, I. Vilar-Sastre and C. Martinez-Cadenas, "Genetic Determinants of Freckle Occurrence in the Spanish Population: Towards Ephelides Prediction from Human DNA Samples", *Forensic Science International: Genetics*, Vol. 33, pp. 38–47, 2018.

72. Hernando, B., E. Sanz-Page, G. Pitarch, L. Mahiques, F. Valcuende-Cavero and C. Martinez-Cadenas, "Genetic Variants Associated with Skin Photosensitivity in

a Southern European Population from Spain", *Photodermatology, Photoimmunology & Photomedicine*, Vol. 34, No. 6, pp. 415–422, 2018.

73. Hers, I., E. E. Vincent and J. M. Tavaré, "AKT Signalling in Health and Disease", *Cellular Signalling*, Vol. 23, No. 10, pp. 1515–1527, 2011.

74. Hervouet, E., P. Peixoto, R. Delage-Mourroux, M. Boyer-Guittaut and P.-F. Cartron, "Specific or Not Specific Recruitment of DNMTs for DNA Methylation, an Epigenetic Dilemma", *Clinical Epigenetics*, Vol. 10, No. 1, p. 17, 2018.

75. Hiremath, I. S., A. Goel, S. Warrier, A. P. Kumar, G. Sethi and M. Garg, "The Multidimensional Role of the Wnt/β-Catenin Signaling Pathway in Human Malignancies", *Journal of Cellular Physiology*, Vol. 237, No. 1, pp. 199–238, 2022.

76. Hou, P., D. Liu, J. Dong and M. Xing, "The BRAFV600E Causes Widespread Alterations in Gene Methylation in the Genome of Melanoma Cells", *Cell Cycle*, Vol. 11, No. 2, pp. 286–295, 2012.

77. Huang, A., L. A. Garraway, A. Ashworth and B. Weber, "Synthetic Lethality as an Engine for Cancer Drug Target Discovery", *Nature Reviews Drug Discovery*, Vol. 19, No. 1, pp. 23–38, 2020.

78. Huang, X., M. Di Liberto, D. Jayabalan, J. Liang, S. Ely, J. Bretz, A. L. Shaffer, T. Louie, I. Chen, S. Randolph, W. C. Hahn, L. M. Staudt, R. Niesvizky, M. A. S. Moore and S. Chen-Kiang, "Prolonged Early G(1) Arrest by Selective CDK4/CDK6 Inhibition Sensitizes Myeloma Cells to Cytotoxic Killing Through Cell Cycle-Coupled Loss of IRF4", *Blood*, Vol. 120, No. 5, pp. 1095–1106, 2012.

79. Jaitin, D. A., A. Weiner, I. Yofe, D. Lara-Astiaso, H. Keren-Shaul, E. David, T. M. Salame, A. Tanay, A. van Oudenaarden and I. Amit, "Dissecting Immune Circuits by Linking CRISPR-Pooled Screens with Single-Cell RNA-Seq", *Cell*, Vol. 167, No. 7, pp. 1883–1896, 2016.

80. Jiang, D.-S., Z.-Y. Bian, Y. Zhang, S.-M. Zhang, Y. Liu, R. Zhang, Y. Chen, Q. Yang, X.-D. Zhang, G.-C. Fan and H. Li, "Role of Interferon Regulatory Factor 4 in the Regulation of Pathological Cardiac Hypertrophy", *Hypertension (Dallas, Tex.: 1979)*, Vol. 61, No. 6, pp. 1193–1202, 2013.

81. Jo, S.-H. and R. Ren, "IRF-4 Suppresses BCR/ABL Transformation of Myeloid Cells in a DNA Binding-Independent Manner", *The Journal of Biological Chemistry*, Vol. 287, No. 3, pp. 1770–1778, 2012.

82. Jo, S.-H., J. H. Schatz, J. Acquaviva, H. Singh and R. Ren, "Cooperation Between Deficiencies of IRF-4 and IRF-8 Promotes Both Myeloid and Lymphoid Tumorigenesis", *Blood*, Vol. 116, No. 15, pp. 2759–2767, 2010.

83. Joung, J., S. Konermann, J. S. Gootenberg, O. O. Abudayyeh, R. J. Platt, M. D. Brigham, N. E. Sanjana and F. Zhang, "Genome-Scale CRISPR-Cas9 Knockout and Transcriptional Activation Screening", *Nature Protocols*, Vol. 12, No. 4, pp. 828–863, 2017.

84. Kataoka, K., Y. Nagata, A. Kitanaka, Y. Shiraishi, T. Shimamura, J.-I. Yasunaga, Y. Totoki, K. Chiba, A. Sato-Otsubo, G. Nagae, R. Ishii, S. Muto, S. Kotani, Y. Watatani, J. Takeda, M. Sanada, H. Tanaka, H. Suzuki, Y. Sato, Y. Shiozawa, T. Yoshizato, K. Yoshida, H. Makishima, M. Iwanaga, G. Ma, K. Nosaka, M. Hishizawa, H. Itonaga, Y. Imaizumi, W. Munakata, H. Ogasawara, T. Sato, K. Sasai, K. Muramoto, M. Penova, T. Kawaguchi, H. Nakamura, N. Hama, K. Shide, Y. Kubuki, T. Hidaka, T. Kameda, T. Nakamaki, K. Ishiyama, S. Miyawaki, S.-S. Yoon, K. Tobinai, Y. Miyazaki, A. Takaori-Kondo, F. Matsuda, K. Takeuchi, O. Nureki, H. Aburatani, T. Watanabe, T. Shibata, M. Matsuoka, S. Miyano, K. Shimoda and S. Ogawa, "Integrated Molecular Analysis of Adult T Cell Leukemia/Lymphoma", *Nature Genetics*, Vol. 47, No. 11, pp. 1304–1315, 2015.

85. Kim, K. H. and C. W. M. Roberts, "Targeting EZH2 in Cancer", *Nature Medicine*,

Vol. 22, No. 2, pp. 128–134, 2016.

86. Klein, U., S. Casola, G. Cattoretti, Q. Shen, M. Lia, T. Mo, T. Ludwig, K. Rajewsky and R. Dalla-Favera, "Transcription Factor IRF4 Controls Plasma Cell Differentiation and Class-Switch Recombination", *Nature Immunology*, Vol. 7, No. 7, pp. 773–782, 2006.

87. Knutson, S. K., T. J. Wigle, N. M. Warholic, C. J. Sneeringer, C. J. Allain, C. R. Klaus, J. D. Sacks, A. Raimondi, C. R. Majer, J. Song, M. P. Scott, L. Jin, J. J. Smith, E. J. Olhava, R. Chesworth, M. P. Moyer, V. M. Richon, R. A. Copeland, H. Keilhack, R. M. Pollock and K. W. Kuntz, "A Selective Inhibitor of EZH2 Blocks H3K27 Methylation and Kills Mutant Lymphoma Cells", *Nature Chemical Biology*, Vol. 8, No. 11, pp. 890–896, 2012.

88. Koike-Yusa, H., Y. Li, E.-P. Tan, M. D. C. Velasco-Herrera and K. Yusa, "Genome-Wide Recessive Genetic Screening in Mammalian Cells with a Lentiviral CRISPR-Guide RNA Library", *Nature Biotechnology*, Vol. 32, No. 3, pp. 267–273, 2014.

89. Konermann, S., M. D. Brigham, A. E. Trevino, J. Joung, O. O. Abudayyeh, C. Barcena, P. D. Hsu, N. Habib, J. S. Gootenberg, H. Nishimasu, O. Nureki and F. Zhang, "Genome-Scale Transcriptional Activation by an Engineered CRISPR-Cas9 Complex", *Nature*, Vol. 517, No. 7536, pp. 583–588, 2015.

90. Kong, X., A. Banks, T. Liu, L. Kazak, R. R. Rao, P. Cohen, X. Wang, S. Yu, J. C. Lo, Y.-H. Tseng, A. M. Cypess, R. Xue, S. Kleiner, S. Kang, B. M. Spiegelman and E. D. Rosen, "IRF4 Is a Key Thermogenic Transcriptional Partner of PGC-1α", *Cell*, Vol. 158, No. 1, pp. 69–83, 2014.

91. Körner, A. and J. Pawelek, "Mammalian Tyrosinase Catalyzes Three Reactions in the Biosynthesis of Melanin", *Science (New York, N.Y.)*, Vol. 217, No. 4565, pp. 1163–1165, 1982.

92. Kuleshov, M. V., M. R. Jones, A. D. Rouillard, N. F. Fernandez, Q. Duan, Z. Wang, S. Koplev, S. L. Jenkins, K. M. Jagodnik, A. Lachmann, M. G. McDermott, C. D. Monteiro, G. W. Gundersen and A. Ma'ayan, "Enrichr: A Comprehensive Gene Set Enrichment Analysis Web Server 2016 Update", *Nucleic Acids Research*, Vol. 44, No. W1, pp. 90–97, 2016.

93. Kvaskoff, M., D. C. Whiteman, Z. Z. Zhao, G. W. Montgomery, N. G. Martin, N. K. Hayward and D. L. Duffy, "Polymorphisms in Nevus-Associated Genes MTAP, PLA2G6, and IRF4 and the Risk of Invasive Cutaneous Melanoma", *Twin Research and Human Genetics: The Official Journal of the International Society for Twin Studies*, Vol. 14, No. 5, pp. 422–432, 2011.

94. Kwong, L. N. and M. A. Davies, "Navigating the Therapeutic Complexity of PI3K Pathway Inhibition in Melanoma", *Clinical Cancer Research*, Vol. 19, No. 19, pp. 5310–5319, 2013.

95. Laga, A. C. and G. F. Murphy, "Cellular Heterogeneity in Vertical Growth Phase Melanoma", *Archives of Pathology & Laboratory Medicine*, Vol. 134, No. 12, pp. 1750–1757, 2010.

96. Landi, M. T., D. T. Bishop, S. MacGregor, M. J. Machiela, A. J. Stratigos, P. Ghiorzo, Brossard, GenoMEL Consortium, Q-MEGA and QTWIN Investigators, ATHENS Melanoma Study Group, 23andMe, SDH Study Group, IBD Investigators, Essen-Heidelberg Investigators, AMFS Investigators, MelaNostrum Consortium, K. Peris, S. J. Chanock, F. Demenais, K. M. Brown, S. Puig, E. Nagore, J. Shi, M. M. Iles and M. H. Law, "Genome-Wide Association Meta-Analyses Combining Multiple Risk Phenotypes Provide Insights into the Genetic Architecture of Cutaneous Melanoma Susceptibility", *Nature Genetics*, Vol. 52, No. 5, pp. 494–504, 2020.

97. Li, W., H. Xu, T. Xiao, L. Cong, M. I. Love, F. Zhang, R. A. Irizarry, J. S. Liu, M. Brown and X. S. Liu, "MAGeCK Enables Robust Identification of Essential

Genes from Genome-Scale CRISPR/Cas9 Knockout Screens", *Genome Biology*, Vol. 15, No. 12, p. 554, 2014.

98. Liu, X., Q. Gao, P. Li, Q. Zhao, J. Zhang, J. Li, H. Koseki and J. Wong, "UHRF1 Targets DNMT1 for DNA Methylation Through Cooperative Binding of Hemi-Methylated DNA and Methylated H3K9", *Nature Communications*, Vol. 4, p. 1563, 2013.

99. Luna, A., F. Elloumi, S. Varma, Y. Wang, V. N. Rajapakse, M. I. Aladjem, J. Robert, C. Sander, Y. Pommier and W. C. Reinhold, "CellMiner Cross-Database (CellMinerCDB) Version 1.2: Exploration of Patient-Derived Cancer Cell Line Pharmacogenomics", *Nucleic Acids Research*, Vol. 49, No. D1, pp. D1083–D1093, 2021.

100. Man, K., M. Miasari, W. Shi, A. Xin, D. C. Henstridge, S. Preston, M. Pellegrini, G. T. Belz, G. K. Smyth, M. A. Febbraio, S. L. Nutt and A. Kallies, "The Transcription Factor IRF4 is Essential for TCR Affinity-Mediated Metabolic Programming and Clonal Expansion of T Cells", *Nature Immunology*, Vol. 14, No. 11, pp. 1155–1165, 2013.

101. Mangiavacchi, A., M. Sorci, S. Masciarelli, S. Larivera, I. Legnini, I. Iosue, I. Bozzoni, F. Fazi and A. Fatica, "The miR-223 Host Non-Coding Transcript linc-223 Induces IRF4 Expression in Acute Myeloid Leukemia by Acting as a Competing Endogenous RNA", *Oncotarget*, Vol. 7, No. 37, pp. 60155–60168, 2016.

102. Marecki, S., M. L. Atchison and M. J. Fenton, "Differential Expression and Distinct Functions of IFN Regulatory Factor 4 and IFN Consensus Sequence Binding Protein in Macrophages", *Journal of Immunology (Baltimore, Md.: 1950)*, Vol. 163, No. 5, pp. 2713–2722, 1999.

103. Martin, M., "Cutadapt Removes Adapter Sequences from High-Throughput Sequencing Reads", *EMBnet Journal*, Vol. 17, No. 1, pp. 10–12, 2011.

104. Meyers, R. M., J. G. Bryan, J. M. McFarland, B. A. Weir, A. E. Sizemore, H. Xu, N. V. Dharia, P. G. Montgomery, G. S. Cowley, S. Pantel, A. Goodale, Y. Lee, L. D. Ali, G. Jiang, R. Lubonja, W. F. Harrington, M. Strickland, T. Wu, D. C. Hawes, V. A. Zhivich, M. R. Wyatt, Z. Kalani, J. J. Chang, M. Okamoto, K. Stegmaier, T. R. Golub, J. S. Boehm, F. Vazquez, D. E. Root, W. C. Hahn and A. Tsherniak, "Computational Correction of Copy Number Effect Improves Specificity of CRISPR–Cas9 Essentiality Screens in Cancer Cells", *Nature Genetics*, Vol. 49, No. 12, pp. 1779–1784, 2017.

105. Mitra, D., X. Luo, A. Morgan, J. Wang, M. P. Hoang, J. Lo, C. R. Guerrero, J. K. Lennerz, M. C. Mihm, J. A. Wargo, K. C. Robinson, S. P. Devi, J. C. Vanover, J. A. D'Orazio, M. McMahon, M. W. Bosenberg, K. M. Haigis, D. A. Haber, Y. Wang and D. E. Fisher, "An Ultraviolet-Radiation-Independent Pathway to Melanoma Carcinogenesis in the Red Hair/Fair Skin Background", *Nature*, Vol. 491, No. 7424, pp. 449–453, 2012.

106. Mobley, A. K., R. R. Braeuer, T. Kamiya, E. Shoshan and M. Bar-Eli, "Driving Transcriptional Regulators in Melanoma Metastasis", *Cancer Metastasis Reviews*, Vol. 31, No. 3-4, pp. 621–632, 2012.

107. Mondala, P. K., A. A. Vora, T. Zhou, E. Lazzari, L. Ladel, X. Luo, Y. Kim, C. Costello, A. R. MacLeod, C. H. M. Jamieson and L. A. Crews, "Selective Antisense Oligonucleotide Inhibition of Human IRF4 Prevents Malignant Myeloma Regeneration via Cell Cycle Disruption", *Cell Stem Cell*, Vol. 28, No. 4, pp. 623–636, 2021.

108. Munoz, D. M., P. J. Cassiani, L. Li, E. Billy, J. M. Korn, M. D. Jones, J. Golji, D. A. Ruddy, K. Yu, G. McAllister, A. DeWeck, D. Abramowski, J. Wan, M. D. Shirley, S. Y. Neshat, D. Rakiec, R. de Beaumont, O. Weber, A. Kauffmann, E. R. McDonald III, N. Keen, F. Hofmann, W. R. Sellers, T. Schmelzle, F. Stegmeier and M. R. Schlabach, "CRISPR Screens Provide a Comprehensive Assessment of Cancer Vulnerabilities but Generate False-Positive Hits for Highly Amplified

Genomic Regions", *Cancer Discovery*, Vol. 6, No. 8, pp. 900–913, 2016.

109. Muris, J. J. F., C. J. L. M. Meijer, W. Vos, J. H. J. M. van Krieken, N. M. Jiwa, G. J. Ossenkoppele and J. J. Oudejans, "Immunohistochemical Profiling Based on Bcl-2, CD10 and MUM1 Expression Improves Risk Stratification in Patients with Primary Nodal Diffuse Large B Cell Lymphoma", *The Journal of Pathology*, Vol. 208, No. 5, pp. 714–723, 2006.

110. Nakagawa, M., A. L. Shaffer, M. Ceribelli, M. Zhang, G. Wright, D. W. Huang, W. Xiao, J. Powell, M. N. Petrus, Y. Yang, J. D. Phelan, H. Kohlhammer, S. P. Dubois, H. M. Yoo, E. Bachy, D. E. Webster, Y. Yang, W. Xu, X. Yu, H. Zhao, B. R. Bryant, J. Shimono, T. Ishio, M. Maeda, P. L. Green, T. A. Waldmann and L. M. Staudt, "Targeting the HTLV-I-Regulated BATF3/IRF4 Transcriptional Network in Adult T Cell Leukemia/Lymphoma", *Cancer Cell*, Vol. 34, No. 2, pp. 286–297, 2018.

111. National Cancer Institute, "TCGA", 2018, `https://www.cancer.gov/ccg/research/genome-sequencing/tcga/studied-cancers`, accessed on July 15, 2023.

112. National Institute of Health, "Annual Report to the Nation 2022: Overall Cancer Statistics", 2022, `https://seer.cancer.gov/report_to_nation/statistics.html`, accessed on June 21, 2023.

113. Natkunam, Y., R. A. Warnke, K. Montgomery, B. Falini and M. van De Rijn, "Analysis of MUM1/IRF4 Protein Expression Using Tissue Microarrays and Immunohistochemistry", *Modern Pathology: An Official Journal of the United States and Canadian Academy of Pathology, Inc*, Vol. 14, No. 7, pp. 686–694, 2001.

114. Nissan, M. H., C. A. Pratilas, A. M. Jones, R. Ramirez, H. Won, C. Liu, S. Tiwari, L. Kong, A. J. Hanrahan, Z. Yao, T. Merghoub, A. Ribas, P. B. Chapman, R. Yaeger, B. S. Taylor, N. Schultz, M. F. Berger, N. Rosen and D. B. Solit,

"Loss of NF1 in Cutaneous Melanoma Is Associated with RAS Activation and MEK Dependence", *Cancer Research*, Vol. 74, No. 8, pp. 2340–2350, 2014.

115. Norton, H. L., M. Edwards, S. Krithika, M. Johnson, E. A. Werren and E. J. Parra, "Quantitative Assessment of Skin, Hair, and Iris Variation in a Diverse Sample of Individuals and Associated Genetic Variation", *American Journal of Physical Anthropology*, Vol. 160, No. 4, pp. 570–581, 2016.

116. Okano, M., D. W. Bell, D. A. Haber and E. Li, "DNA Methyltransferases Dnmt3a and Dnmt3b Are Essential for de novo Methylation and Mammalian Development", *Cell*, Vol. 99, No. 3, pp. 247–257, 1999.

117. Orea-Soufi, A., J. Paik, J. Bragança, T. A. Donlon, B. J. Willcox and W. Link, "FOXO Transcription Factors as Therapeutic Targets in Human Diseases", *Trends in Pharmacological Sciences*, Vol. 43, No. 12, pp. 1070–1084, 2022.

118. Orlow, I., J. M. Satagopan, M. Berwick, H. L. Enriquez, K. a. M. White, K. Cheung, S. W. Dusza, S. A. Oliveria, M. A. Marchetti, A. Scope, A. A. Marghoob and A. C. Halpern, "Genetic Factors Associated with Naevus Count and Dermoscopic Patterns: Preliminary Results from the Study of Nevi in Children (SONIC)", *The British Journal of Dermatology*, Vol. 172, No. 4, pp. 1081–1089, 2015.

119. Orouji, E., A. Federico, L. Larribère, D. Novak, D. B. Lipka, Y. Assenov, S. Sachindra, L. Hüser, K. Granados, C. Gebhardt, C. Plass, V. Umansky and J. Utikal, "Histone Methyltransferase SETDB1 Contributes to Melanoma Tumorigenesis and Serves as a New Potential Therapeutic Target", *International Journal of Cancer*, Vol. 145, No. 12, pp. 3462–3477, 2019.

120. Pang, S. H. M., M. Minnich, P. Gangatirkar, Z. Zheng, A. Ebert, G. Song, R. A. Dickins, L. M. Corcoran, C. G. Mullighan, M. Busslinger, N. D. Huntington, S. L. Nutt and S. Carotta, "PU.1 Cooperates with IRF4 and IRF8 to Suppress Pre-B-Cell Leukemia", *Leukemia*, Vol. 30, No. 6, pp. 1375–1387, 2016.

121. Paraiso, K. H. T., Y. Xiang, V. W. Rebecca, E. V. Abel, Y. A. Chen, A. C. Munko, E. Wood, I. V. Fedorenko, V. K. Sondak, A. R. A. Anderson, A. Ribas, M. D. Palma, K. L. Nathanson, J. M. Koomen, J. L. Messina and K. S. M. Smalley, "PTEN Loss Confers BRAF Inhibitor Resistance to Melanoma Cells Through the Suppression of BIM Expression", *Cancer Research*, Vol. 71, No. 7, pp. 2750–2760, 2011.

122. Pathak, S., S. Ma, L. Trinh, J. Eudy, K.-U. Wagner, S. S. Joshi and R. Lu, "IRF4 Is a Suppressor of c-Myc Induced B Cell Leukemia", *PloS One*, Vol. 6, No. 7, p. e22628, 2011.

123. Peña-Chilet, M., M. Blanquer-Maceiras, M. Ibarrola-Villava, C. Martinez-Cadenas, M. Martin-Gonzalez, C. Gomez-Fernandez, M. Mayor, J. A. Aviles, A. Lluch and G. Ribas, "Genetic Variants in PARP1 (rs3219090) and IRF4 (rs12203592) Genes Associated with Melanoma Susceptibility in a Spanish Population", *BMC Cancer*, Vol. 13, p. 160, 2013.

124. Penna, I., A. Molla, G. Grazia, L. Cleris, G. Nicolini, F. Perrone, B. Picciani, M. Del Vecchio, F. de Braud, R. Mortarini and A. Anichini, "Primary Cross-Resistance to BRAFV600E-, MEK1/2- and PI3K/mTOR-Specific Inhibitors in BRAF-Mutant Melanoma Cells Counteracted by Dual Pathway Blockade", *Oncotarget*, Vol. 7, No. 4, pp. 3947–3965, 2015.

125. Pirini, F., S. Noazin, M. H. Jahuira-Arias, S. Rodriguez-Torres, L. Friess, C. Michailidi, J. Cok, J. Combe, G. Vargas, W. Prado, E. Soudry, J. Pérez, T. Yudin, A. Mancinelli, H. Unger, C. Ili-Gangas, P. Brebi-Mieville, D. E. Berg, M. Hayashi, D. Sidransky, R. H. Gilman and R. Guerrero-Preston, "Early Detection of Gastric Cancer Using Global, Genome-Wide and IRF4, ELMO1, CLIP4 and MSC DNA Methylation in Endoscopic Biopsies", *Oncotarget*, Vol. 8, No. 24, pp. 38501–38516, 2017.

126. Praetorius, C., C. Grill, S. N. Stacey, A. M. Metcalf, D. U. Gorkin, K. C. Robin-

son, E. Van Otterloo, R. S. Q. Kim, K. Bergsteinsdottir, M. H. Ogmundsdottir, E. Magnusdottir, P. J. Mishra, S. R. Davis, T. Guo, M. R. Zaidi, A. S. Helgason, M. I. Sigurdsson, P. S. Meltzer, G. Merlino, V. Petit, L. Larue, S. K. Loftus, D. R. Adams, U. Sobhiafshar, N. C. T. Emre, W. J. Pavan, R. Cornell, A. G. Smith, A. S. McCallion, D. E. Fisher, K. Stefansson, R. A. Sturm and E. Steingrimsson, "A Polymorphism in IRF4 Affects Human Pigmentation Through a Tyrosinase-Dependent MITF/TFAP2A Pathway", *Cell*, Vol. 155, No. 5, pp. 1022–1033, 2013.

127. Qian, Y., Z. Du, Y. Xing, T. Zhou, T. Chen and M. Shi, "Interferon Regulatory Factor 4 (IRF4) Is Overexpressed in Human Non-Small Cell Lung Cancer (NSCLC) and Activates the Notch Signaling Pathway", *Molecular Medicine Reports*, Vol. 16, No. 5, pp. 6034–6040, 2017.

128. Rambow, F., J.-C. Marine and C. R. Goding, "Melanoma Plasticity and Phenotypic Diversity: Therapeutic Barriers and Opportunities", *Genes & Development*, Vol. 33, No. 19-20, pp. 1295–1318, 2019.

129. Rebecca, V. W., V. K. Sondak and K. S. M. Smalley, "A Brief History of Melanoma: from Mummies to Mutations", *Melanoma Research*, Vol. 22, No. 2, pp. 114–122, 2012.

130. Ribas, A. and K. T. Flaherty, "BRAF Targeted Therapy Changes the Treatment Paradigm in Melanoma", *Nature Reviews Clinical Oncology*, Vol. 8, No. 7, pp. 426–433, 2011.

131. Ribas, A., R. Gonzalez, A. Pavlick, O. Hamid, T. F. Gajewski, A. Daud, L. Flaherty, T. Logan, B. Chmielowski, K. Lewis, D. Kee, P. Boasberg, M. Yin, I. Chan, L. Musib, N. Choong, I. Puzanov and G. A. McArthur, "Combination of Vemurafenib and Cobimetinib in Patients with Advanced BRAFV600-Mutated Melanoma: A Phase 1b Study", *The Lancet Oncology*, Vol. 15, No. 9, pp. 954–965, 2014.

132. Saginala, K., A. Barsouk, J. S. Aluru, P. Rawla and A. Barsouk, "Epidemiology of Melanoma", *Medical Sciences*, Vol. 9, No. 4, p. 63, 2021.

133. Sambrook, J. and D. W. Russell, *Molecular Cloning: A Laboratory Manual*, CSHL Press, 2001.

134. Sanson, K. R., R. E. Hanna, M. Hegde, K. F. Donovan, C. Strand, M. E. Sullender, E. W. Vaimberg, A. Goodale, D. E. Root, F. Piccioni and J. G. Doench, "Optimized Libraries for CRISPR-Cas9 Genetic Screens with Multiple Modalities", *Nature Communications*, Vol. 9, No. 1, p. 5416, 2018.

135. Schaefer, M., S. Hagemann, K. Hanna and F. Lyko, "Azacytidine Inhibits RNA Methylation at DNMT2 Target Sites in Human Cancer Cell Lines", *Cancer Research*, Vol. 69, No. 20, pp. 8127–8132, 2009.

136. Schmidt, M., A. Hochhaus, S. A. König-Merediz, C. Brendel, J. Proba, G. J. Hoppe, B. Wittig, G. Ehninger, R. Hehlmann and A. Neubauer, "Expression of Interferon Regulatory Factor 4 in Chronic Myeloid Leukemia: Correlation with Response to Interferon Alfa Therapy", *Journal of Clinical Oncology: Official Journal of the American Society of Clinical Oncology*, Vol. 18, No. 19, pp. 3331–3338, 2000.

137. Shaffer, A. L., N. C. T. Emre, L. Lamy, V. N. Ngo, G. Wright, W. Xiao, J. Powell, S. Dave, X. Yu, H. Zhao, Y. Zeng, B. Chen, J. Epstein and L. M. Staudt, "IRF4 Addiction in Multiple Myeloma", *Nature*, Vol. 454, No. 7201, pp. 226–231, 2008.

138. Shalem, O., N. E. Sanjana, E. Hartenian, X. Shi, D. A. Scott, T. Mikkelson, D. Heckl, B. L. Ebert, D. E. Root, J. G. Doench and F. Zhang, "Genome-Scale CRISPR-Cas9 Knockout Screening in Human Cells", *Science (New York, N.Y.)*, Vol. 343, No. 6166, pp. 84–87, 2014.

139. Shi, H., W. Hugo, X. Kong, A. Hong, R. C. Koya, G. Moriceau, T. Chodon,

R. Guo, D. B. Johnson, K. B. Dahlman, M. C. Kelley, R. F. Kefford, B. Chmielowski, J. A. Glaspy, J. A. Sosman, N. van Baren, G. V. Long, A. Ribas and R. S. Lo, "Acquired Resistance and Clonal Evolution in Melanoma During BRAF Inhibitor Therapy", *Cancer Discovery*, Vol. 4, No. 1, pp. 80–93, 2014.

140. Sigalotti, L., A. Covre, E. Fratta, G. Parisi, P. Sonego, F. Colizzi, S. Coral, S. Massarut, J. M. Kirkwood and M. Maio, "Whole Genome Methylation Profiles as Independent Markers of Survival in Stage IIIC Melanoma Patients", *Journal of Translational Medicine*, Vol. 10, No. 1, p. 185, 2012.

141. Snedecor, E. R., C. C. Sung, A. Moncayo, B. E. Rothstein, D. C. Mockler, M. G. Tonnesen, E. C. Jones, M. Fujita, R. A. Clark, K. R. Shroyer and J. Chen, "Loss of Primary Cilia in Melanoma Cells Is Likely Independent of Proliferation and Cell Cycle Progression", *The Journal of Investigative Dermatology*, Vol. 135, No. 5, pp. 1456–1458, 2015.

142. Sobhi Afshar, U., *Genome-Wide Localisation Analysis for IRF4 Target Gene Identification in Melanoma Cell Lines*, M.S. Thesis, Boğaziçi University, 2015.

143. Stomper, J., J. C. Rotondo, G. Greve and M. Lübbert, "Hypomethylating Agents (HMA) for the Treatment of Acute Myeloid Leukemia and Myelodysplastic Syndromes: Mechanisms of Resistance and Novel HMA-Based Therapies", *Leukemia*, Vol. 35, No. 7, pp. 1873–1889, 2021.

144. Straining, R. and W. Eighmy, "Tazemetostat: EZH2 Inhibitor", *Journal of the Advanced Practitioner in Oncology*, Vol. 13, No. 2, pp. 158–163, 2022.

145. Stresemann, C. and F. Lyko, "Modes of Action of the DNA Methyltransferase Inhibitors Azacytidine and Decitabine", *International Journal of Cancer*, Vol. 123, No. 1, pp. 8–13, 2008.

146. Sulem, P., D. F. Gudbjartsson, S. N. Stacey, A. Helgason, T. Rafnar, K. P. Mag-

nusson, A. Manolescu, A. Karason, A. Palsson, G. Thorleifsson, M. Jakobsdottir, S. Steinberg, S. Pálsson, F. Jonasson, B. Sigurgeirsson, K. Thorisdottir, R. Ragnarsson, K. R. Benediktsdottir, K. K. Aben, L. A. Kiemeney, J. H. Olafsson, J. Gulcher, A. Kong, U. Thorsteinsdottir and K. Stefansson, "Genetic Determinants of Hair, Eye and Skin Pigmentation in Europeans", *Nature Genetics*, Vol. 39, No. 12, pp. 1443–1452, 2007.

147. Sundram, U., J. D. Harvell, R. V. Rouse and Y. Natkunam, "Expression of the B-Cell Proliferation Marker MUM1 by Melanocytic Lesions and Comparison with S100, gp100 (HMB45), and MelanA", *Modern Pathology: An Official Journal of the United States and Canadian Academy of Pathology, Inc*, Vol. 16, No. 8, pp. 802–810, 2003.

148. The Galaxy Community, "The Galaxy Platform for Accessible, Reproducible and Collaborative Biomedical Analyses: 2022 Update", *Nucleic Acids Research*, Vol. 50, No. W1, pp. W345–W351, 2022.

149. Tiffen, J. C., S. J. Gallagher, H.-Y. Tseng, F. V. Filipp, B. de St Groth and P. Hersey, "EZH2 as a Mediator of Treatment Resistance in Melanoma", *Pigment Cell & Melanoma Research*, Vol. 29, No. 5, pp. 500–507, 2016.

150. Tiffen, J. C., D. Gunatilake, S. J. Gallagher, K. Gowrishankar, A. Heinemann, C. Cullinane, K. Dutton-Regester, G. M. Pupo, D. Strbenac, J. Y. Yang, J. Madore, G. J. Mann, N. K. Hayward, G. A. McArthur, F. V. Filipp and P. Hersey, "Targeting Activating Mutations of EZH2 Leads to Potent Cell Growth Inhibition in Human Melanoma by Derepression of Tumor Suppressor Genes", *Oncotarget*, Vol. 6, No. 29, pp. 27023–27036, 2015.

151. Tiffen, J., S. J. Gallagher and P. Hersey, "EZH2: An Emerging Role in Melanoma Biology and Strategies for Targeted Therapy", *Pigment Cell & Melanoma Research*, Vol. 28, No. 1, pp. 21–30, 2015.

152. Trujillo, J. A., J. J. Luke, Y. Zha, J. P. Segal, L. L. Ritterhouse, S. Spranger, K. Matijevich and T. F. Gajewski, "Secondary Resistance to Immunotherapy Associated with β-Catenin Pathway Activation or PTEN Loss in Metastatic Melanoma", *Journal for ImmunoTherapy of Cancer*, Vol. 7, No. 1, p. 295, 2019.

153. Tsherniak, A., F. Vazquez, P. G. Montgomery, B. A. Weir, G. Kryukov, G. S. Cowley, S. Gill, W. F. Harrington, S. Pantel, J. M. Krill-Burger, R. M. Meyers, L. Ali, A. Goodale, Y. Lee, G. Jiang, J. Hsiao, W. F. J. Gerath, S. Howell, E. Merkel, M. Ghandi, L. A. Garraway, D. E. Root, T. R. Golub, J. S. Boehm and W. C. Hahn, "Defining a Cancer Dependency Map", *Cell*, Vol. 170, No. 3, pp. 564–576, 2017.

154. Tsoi, J., L. Robert, K. Paraiso, C. Galvan, K. M. Sheu, J. Lay, D. J. L. Wong, M. Atefi, R. Shirazi, X. Wang, D. Braas, C. S. Grasso, N. Palaskas, A. Ribas and T. G. Graeber, "Multi-stage Differentiation Defines Melanoma Subtypes with Differential Vulnerability to Drug-Induced Iron-Dependent Oxidative Stress", *Cancer Cell*, Vol. 33, No. 5, pp. 890–904, 2018.

155. Tsuboi, K., S. Iida, H. Inagaki, M. Kato, Y. Hayami, I. Hanamura, K. Miura, S. Harada, M. Kikuchi, H. Komatsu, S. Banno, A. Wakita, S. Nakamura, T. Eimoto and R. Ueda, "MUM1/IRF4 Expression as a Frequent Event in Mature Lymphoid Malignancies", *Leukemia*, Vol. 14, No. 3, pp. 449–456, 2000.

156. Tumeh, P. C., C. L. Harview, J. H. Yearley, I. P. Shintaku, E. J. M. Taylor, L. Robert, B. Chmielowski, M. Spasic, G. Henry, V. Ciobanu, A. N. West, M. Carmona, C. Kivork, E. Seja, G. Cherry, A. J. Gutierrez, T. R. Grogan, C. Mateus, G. Tomasic, J. A. Glaspy, R. O. Emerson, H. Robins, R. H. Pierce, D. A. Elashoff, C. Robert and A. Ribas, "PD-1 Blockade Induces Responses by Inhibiting Adaptive Immune Resistance", *Nature*, Vol. 515, No. 7528, pp. 568–571, 2014.

157. Uebel, A., S. Kewitz-Hempel, E. Willscher, K. Gebhardt, C. Sunderkötter and D. Gerloff, "Resistance to BRAF Inhibitors: EZH2 and Its Downstream Targets as

Potential Therapeutic Options in Melanoma", *International Journal of Molecular Sciences*, Vol. 24, No. 3, p. 1963, 2023.

158. Uranishi, M., S. Iida, T. Sanda, T. Ishida, E. Tajima, M. Ito, H. Komatsu, H. Inagaki and R. Ueda, "Multiple Myeloma Oncogene 1 (MUM1)/Interferon Regulatory Factor 4 (IRF4) Upregulates Monokine Induced by Interferon-gamma (MIG) Gene Expression in B-Cell Malignancy", *Leukemia*, Vol. 19, No. 8, pp. 1471–1478, 2005.

159. Urteaga, O. and G. T. Pack, "On the Antiquity of Melanoma", *Cancer*, Vol. 19, No. 5, pp. 607–610, 1966.

160. Van Allen, E. M., N. Wagle, A. Sucker, D. J. Treacy, C. M. Johannessen, E. M. Goetz, C. S. Place, A. Taylor-Weiner, S. Whittaker, G. V. Kryukov, E. Hodis, M. Rosenberg, A. McKenna, K. Cibulskis, D. Farlow, L. Zimmer, U. Hillen, R. Gutzmer, S. M. Goldinger, S. Ugurel, H. J. Gogas, F. Egberts, C. Berking, U. Trefzer, C. Loquai, B. Weide, J. C. Hassel, S. B. Gabriel, S. L. Carter, G. Getz, L. A. Garraway, D. Schadendorf and Dermatologic Cooperative Oncology Group of Germany (DeCOG), "The Genetic Landscape of Clinical Resistance to RAF Inhibition in Metastatic Melanoma", *Cancer Discovery*, Vol. 4, No. 1, pp. 94–109, 2014.

161. Vaughan, R. M., B. M. Dickson, E. M. Cornett, J. S. Harrison, B. Kuhlman and S. B. Rothbart, "Comparative Biochemical Analysis of UHRF Proteins Reveals Molecular Mechanisms That Uncouple UHRF2 from DNA Methylation Maintenance", *Nucleic Acids Research*, Vol. 46, No. 9, pp. 4405–4416, 2018.

162. Visser, M., R.-J. Palstra and M. Kayser, "Allele-Specific Transcriptional Regulation of IRF4 in Melanocytes Is Mediated by Chromatin Looping of the Intronic rs12203592 Enhancer to the IRF4 Promoter", *Human Molecular Genetics*, Vol. 24, No. 9, pp. 2649–2661, 2015.

163. Wang, L., Z. Q. Yao, J. P. Moorman, Y. Xu and S. Ning, "Gene Expression Profiling Identifies IRF4-Associated Molecular Signatures in Hematological Malignancies", *PloS One*, Vol. 9, No. 9, p. e106788, 2014.

164. Webster, M. R., C. H. Kugel and A. T. Weeraratna, "The Wnts of Change: How Wnts Regulate Phenotype Switching in Melanoma", *Biochimica et Biophysica Acta (BBA) - Reviews on Cancer*, Vol. 1856, No. 2, pp. 244–251, 2015.

165. Weilemann, A., M. Grau, T. Erdmann, O. Merkel, U. Sobhiafshar, I. Anagnostopoulos, M. Hummel, A. Siegert, C. Hayford, H. Madle, B. Wollert-Wulf, I. Fichtner, B. Dörken, S. Dirnhofer, S. Mathas, M. Janz, N. C. T. Emre, A. Rosenwald, G. Ott, P. Lenz, A. Tzankov and G. Lenz, "Essential Role of IRF4 and MYC Signaling for Survival of Anaplastic Large Cell Lymphoma", *Blood*, Vol. 125, No. 1, pp. 124–132, 2015.

166. Whiteman, D. C., A. C. Green and C. M. Olsen, "The Growing Burden of Invasive Melanoma: Projections of Incidence Rates and Numbers of New Cases in Six Susceptible Populations Through 2031", *Journal of Investigative Dermatology*, Vol. 136, No. 6, pp. 1161–1171, 2016.

167. Wong, R. W. J., T. K. Tan, S. Amanda, P. C. T. Ngoc, W. Z. Leong, S. H. Tan, K. Asamitsu, Y. Hibi, R. Ueda, T. Okamoto, T. Ishida, S. Iida and T. Sanda, "Feed-Forward Regulatory Loop Driven by IRF4 and NF-κB in Adult T-Cell Leukemia/Lymphoma", *Blood*, Vol. 135, No. 12, pp. 934–947, 2020.

168. Wu, H., V. Goel and F. G. Haluska, "PTEN Signaling Pathways in Melanoma", *Oncogene*, Vol. 22, No. 20, pp. 3113–3122, 2003.

169. Xerri, L., E. Bachy, B. Fabiani, D. Canioni, C. Chassagne-Clément, P. Dartigues-Cuilléres, F. Charlotte, N. Brousse, M.-C. Rousselet, C. Foussard, P. Brice, P. Feugier, F. Morschhauser, A. Sonet, D. Olive, G. Salles and L. study, "Identification of MUM1 as a Prognostic Immunohistochemical Marker in Follicular

Lymphoma Using Computerized Image Analysis", *Human Pathology*, Vol. 45, No. 10, pp. 2085–2093, 2014.

170. Xie, Z., A. Bailey, M. V. Kuleshov, D. J. B. Clarke, J. E. Evangelista, S. L. Jenkins, A. Lachmann, M. L. Wojciechowicz, E. Kropiwnicki, K. M. Jagodnik, M. Jeon and A. Ma'ayan, "Gene Set Knowledge Discovery with Enrichr", *Current Protocols*, Vol. 1, No. 3, p. e90, 2021.

171. Xing, Y.-Q., A. Li, Y. Yang, X.-X. Li, L.-N. Zhang and H.-C. Guo, "The Regulation of FOXO1 and Its Role in Disease Progression", *Life Sciences*, Vol. 193, pp. 124–131, 2018.

172. Yang, Y., A. L. Shaffer, N. C. T. Emre, M. Ceribelli, M. Zhang, G. Wright, W. Xiao, J. Powell, J. Platig, H. Kohlhammer, R. M. Young, H. Zhao, Y. Yang, W. Xu, J. J. Buggy, S. Balasubramanian, L. A. Mathews, P. Shinn, R. Guha, M. Ferrer, C. Thomas, T. A. Waldmann and L. M. Staudt, "Exploiting Synthetic Lethality for the Therapy of ABC Diffuse Large B Cell Lymphoma", *Cancer Cell*, Vol. 21, No. 6, pp. 723–737, 2012.

173. Yerinde, C., *Implementation of Crispr Based Technologies for Genome and Gene Expression Manipulation of IRF4 in Melanoma Cells*, M.S. Thesis, Boğaziçi University,, 2016.

174. Yildiz-Ayhan, N., *NFAT and IRF4: The Characterization of a New Regulatory Axis in SK-MEL-28 Melanoma Cell Line*, Ph.D. Thesis, Boğaziçi University, 2023.

175. Yilmaz, E., *Characterization of Interferon Regulatory Factor 4 Target Genes in Melanoma Cell Lines*, M.S. Thesis, Boğaziçi University,, 2014.

176. Yokoyama, S., A. Takahashi, R. Kikuchi, S. Nishibu, J. A. Lo, M. Hejna, W. M. Moon, S. Kato, Y. Zhou, F. S. Hodi, J. S. Song, H. Sakurai, D. E. Fisher

and Y. Hayakawa, "SOX10 Regulates Melanoma Immunogenicity Through an IRF4–IRF1 Axis", *Cancer Research*, Vol. 81, No. 24, pp. 6131–6141, 2021.

177. Zalatan, J. G., M. E. Lee, R. Almeida, L. A. Gilbert, E. H. Whitehead, M. La Russa, J. C. Tsai, J. S. Weissman, J. E. Dueber, L. S. Qi and W. A. Lim, "Engineering Complex Synthetic Transcriptional Programs with CRISPR RNA Scaffolds", *Cell*, Vol. 160, No. 1-2, pp. 339–350, 2015.

178. Zhan, T. and M. Boutros, "Towards a Compendium of Essential Genes – From Model Organisms to Synthetic Lethality in Cancer Cells", *Critical Reviews in Biochemistry and Molecular Biology*, Vol. 51, No. 2, pp. 74–85, 2016.

179. Zhang, B., C. Tang, Y. Yao, X. Chen, C. Zhou, Z. Wei, F. Xing, L. Chen, X. Cai, Z. Zhang, S. Sun and Q. Liu, "The Tumor Therapy Landscape of Synthetic Lethality", *Nature Communications*, Vol. 12, No. 1, p. 1275, 2021.

180. Zhang, H., Y. P. Liu, A. Q. Ge, X. Wang, H. R. Sun, H. R. Bi, D. Pang and Y. S. Zhao, "[Association Between AOX1, IRF4 Methylation in Peripheral Blood Leukocyte DNA and the Risks of Breast Cancer: A Case-Control Study]", *Zhonghua Liu Xing Bing Xue Za Zhi = Zhonghua Liuxingbingxue Zazhi*, Vol. 39, No. 9, pp. 1265–1269, 2018.

181. Zhang, L.-H., J. Kosek, M. Wang, C. Heise, P. H. Schafer and R. Chopra, "Lenalidomide Efficacy in Activated B-Cell-Like Subtype Diffuse Large B-Cell Lymphoma Is Dependent Upon IRF4 and Cereblon Expression", *British Journal of Haematology*, Vol. 160, No. 4, pp. 487–502, 2013.

182. Zingg, D., N. Arenas-Ramirez, D. Sahin, R. A. Rosalia, A. T. Antunes, J. Haeusel, L. Sommer and O. Boyman, "The Histone Methyltransferase Ezh2 Controls Mechanisms of Adaptive Resistance to Tumor Immunotherapy", *Cell Reports*, Vol. 20, No. 4, pp. 854–867, 2017.

183. Zingg, D., J. Debbache, R. Peña-Hernández, A. T. Antunes, S. M. Schaefer, P. F. Cheng, D. Zimmerli, J. Haeusel, R. R. Calçada, E. Tuncer, Y. Zhang, R. Bossart, K.-K. Wong, K. Basler, R. Dummer, R. Santoro, M. P. Levesque and L. Sommer, "EZH2-Mediated Primary Cilium Deconstruction Drives Metastatic Melanoma Formation", *Cancer Cell*, Vol. 34, No. 1, pp. 69–84, 2018.

184. Zob, D. L., I. Augustin, L. Caba, M.-C. Panzaru, S. Popa, A. D. Popa, L. Florea and E. V. Gorduza, "Genomics and Epigenomics in the Molecular Biology of Melanoma-A Prerequisite for Biomarkers Studies", *International Journal of Molecular Sciences*, Vol. 24, No. 1, p. 716, 2022.

APPENDIX A: KH1 PLASMID

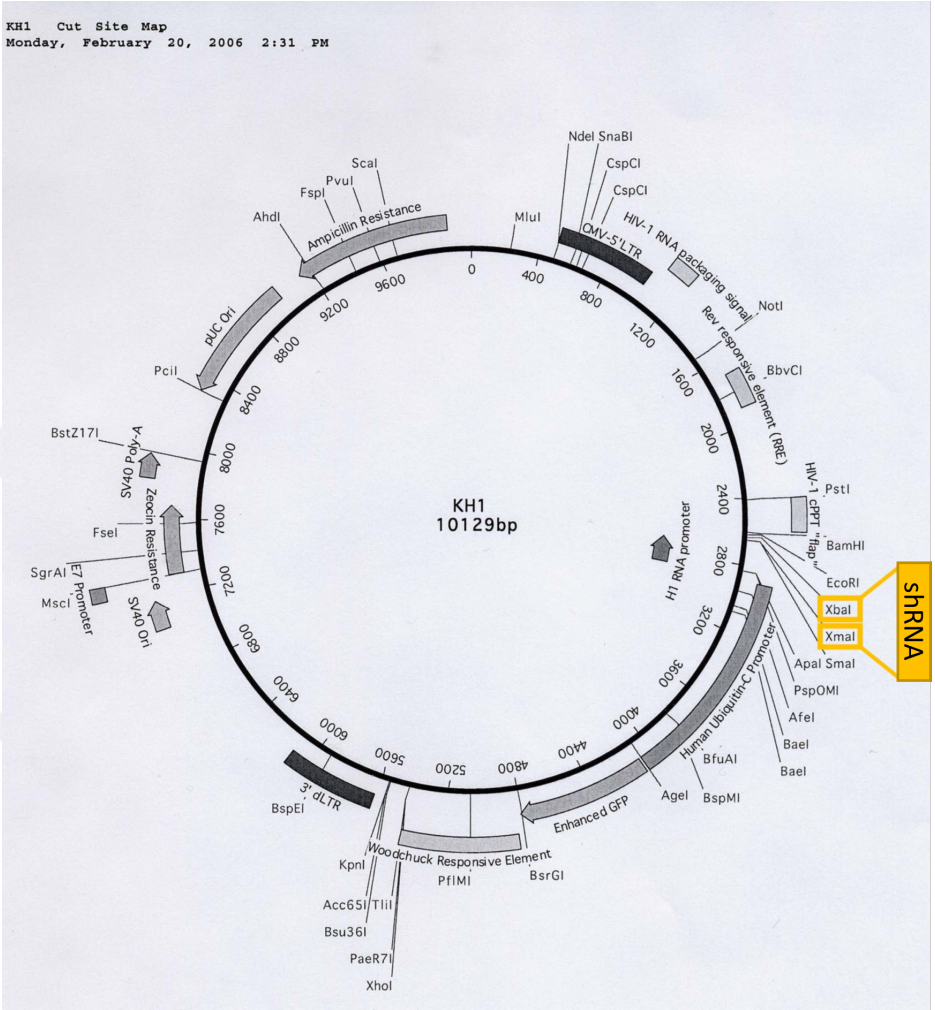

Figure A.1. KH1 plasmid map. The region where shLuc, shIRF4-1, or shIRF4-2 inserts were cloned is indicated in yellow (Yildiz-Ayhan, 2023).

APPENDIX B: pINDUCER20 VECTOR

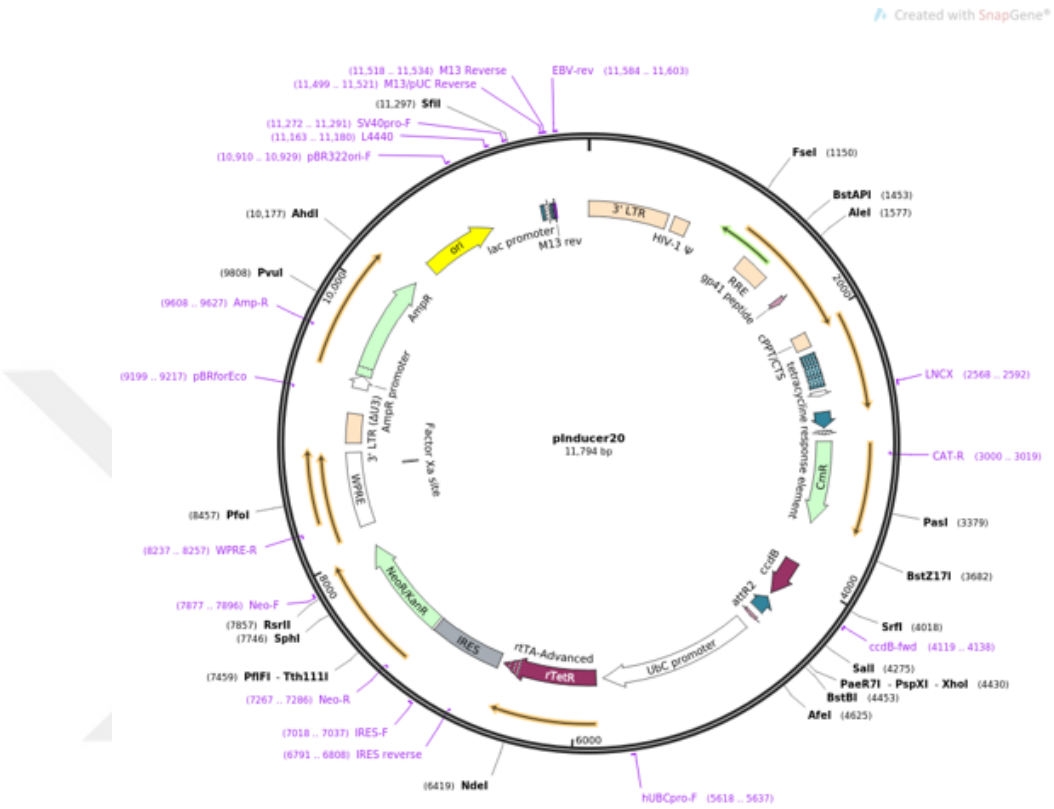

Figure B.1. pInducer20 map. With Gateway cloning, IRF4 cDNA was cloned in between attR elements replacing the ccdB resistance element (Yildiz-Ayhan, 2023).

APPENDIX C: CRISPR/CAS9 VECTORS

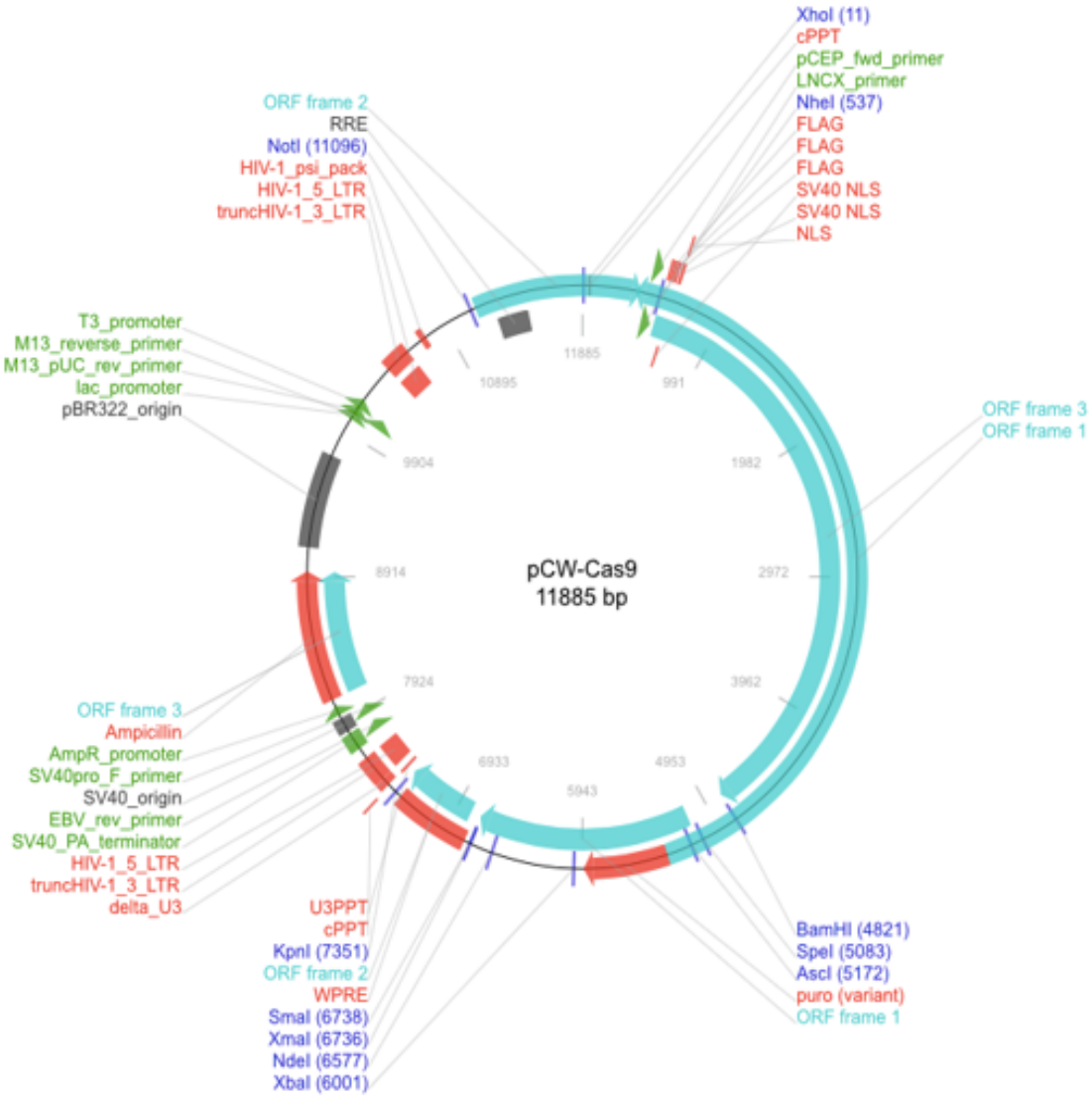

Figure C.1. pCW-Cas9 (Addgene: 50661) plasmid used in generation of Cas9 stable melanoma cell lines (from Wang et al., 2014).

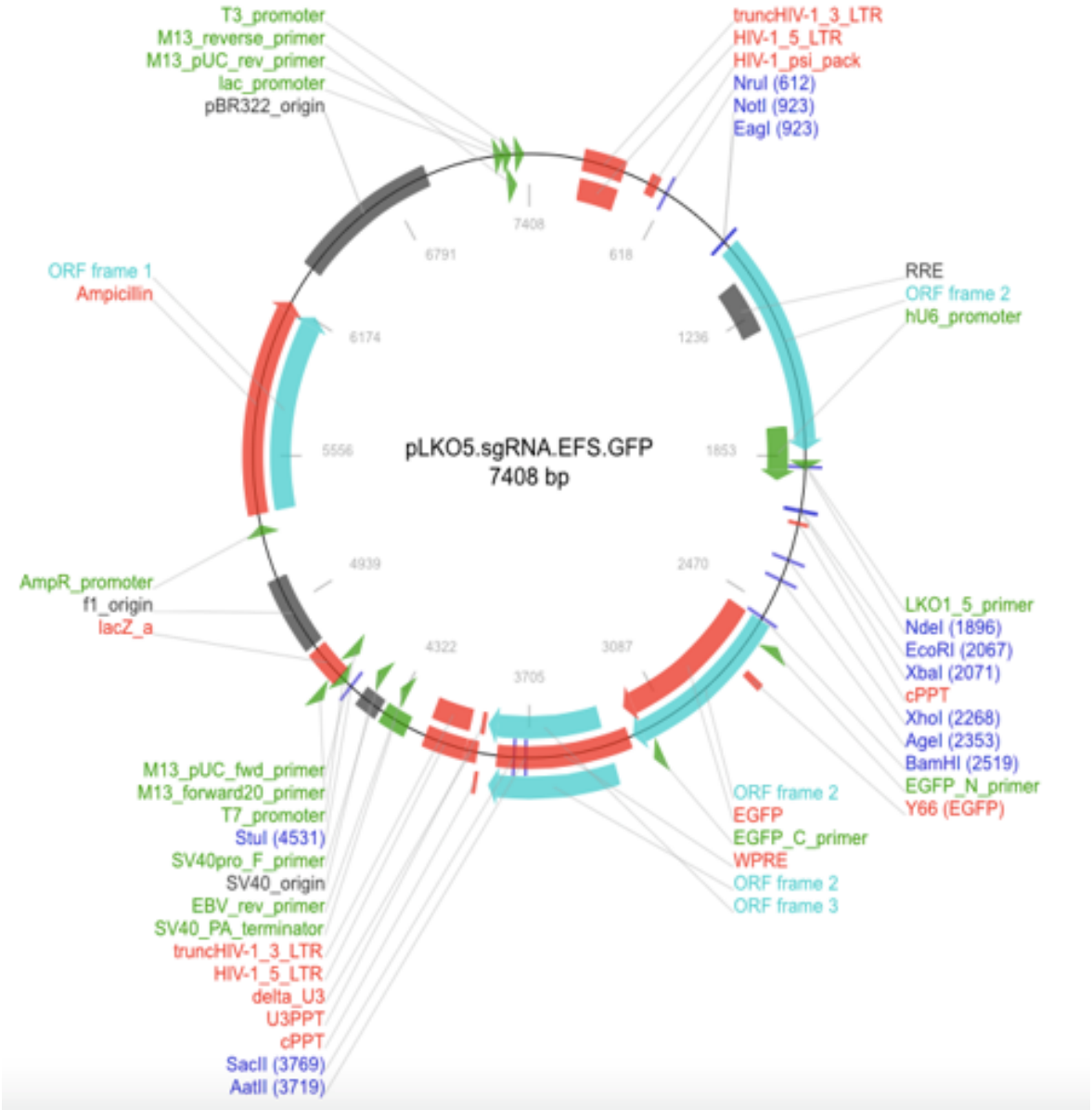

Figure C.2. pLKO5.sgRNA.EFS.GFP plasmid (Addgene 57822) used to express sgRNAs in stable melanoma cell lines (Heckl et al., 2015; Yerinde, 2016).

APPENDIX D: IRF4 EXPRESSION IN MELANOMA CELL LINES

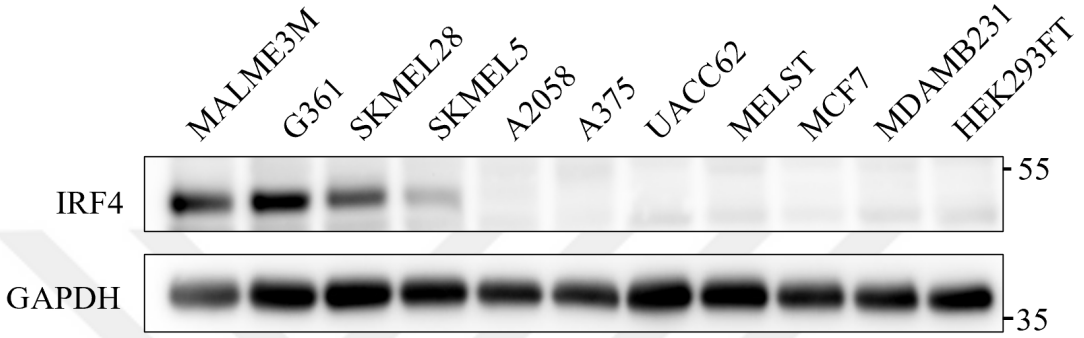

Figure D.1. Western blot for IRF4 expression across melanoma cell lines with non-melanoma cells as controls (MCF7, MDA-MB231, HEK293FT).

APPENDIX E: IRF4 OVEREXPRESSION-PHENOTYPIC ASSAY

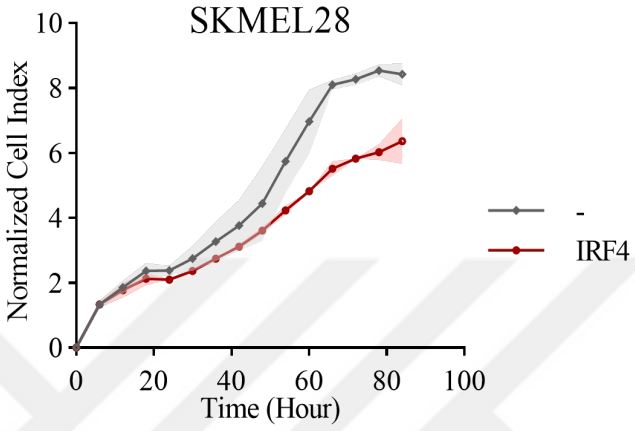

Figure E.1. Real-time cell analysis with XCELLigence in IRF4 overexpressing in SKMEL28 cells.

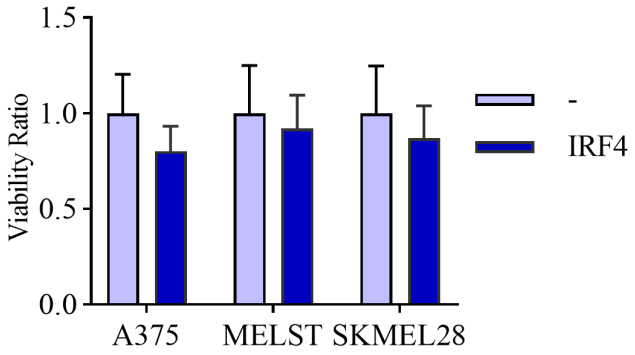

Figure E.2. XTT assay for 3 IRF4-overexpressing cell lines. n=3

APPENDIX F: WESTERN BLOT FOR DNMTS IN OTHER CELL LINES

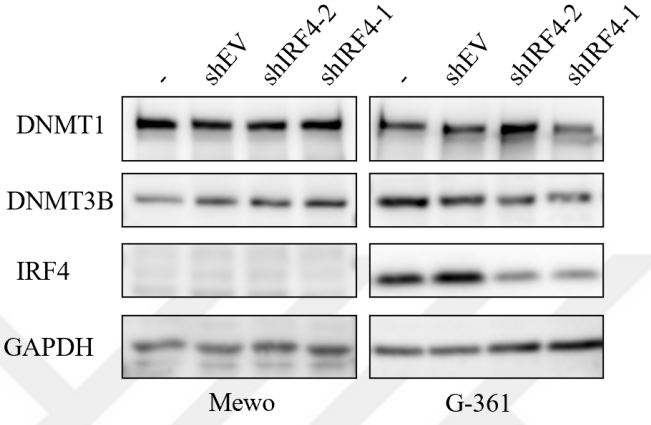

Figure F.1. Western blot for DNMT1, and DNMT3B in IRF4-depleted G361. MEWO, with IRF4 expression, is used as a negative control.

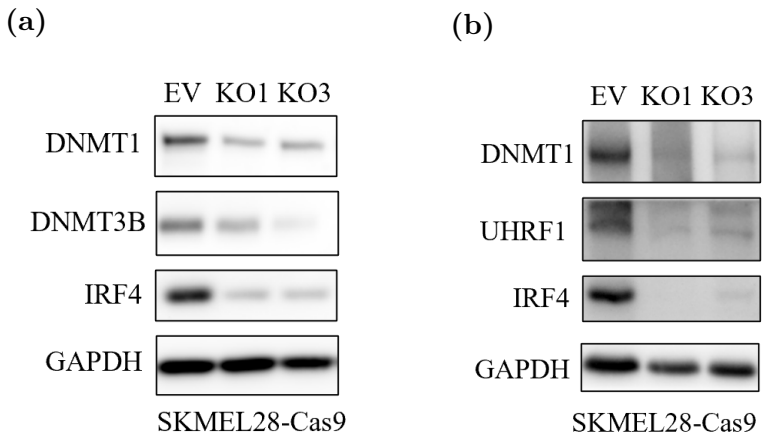

Figure F.2. Western blot in IRF4 KO cells for DNMT1, DNMT3B, UHRF1.

APPENDIX G: IRF4-BINDING SITES AT DNMT1 AND DNMT3B LOCI

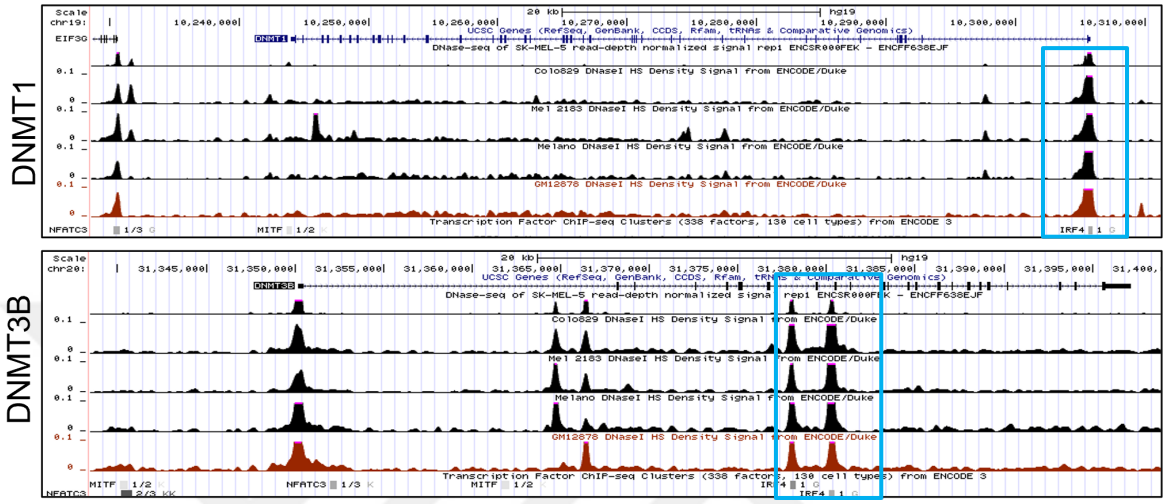

Figure G.1. UCSC genome browser shot. IRF4-binding site for DNMT1 promoter and intronic site at DNMT3B loci. The open chromatin region is from DNaseI assay in SKMEL-5, COLO829, MEL2183, and MELANO cell lines.

APPENDIX H: WESTERN BLOT FOR HISTONE MODIFICATIONS

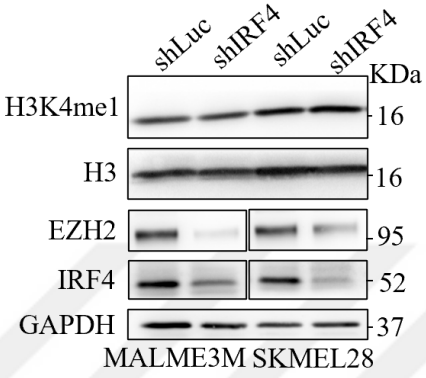

Figure H.1. Western blot for EZH2 and H3K4me1. Related to Figure 5.17

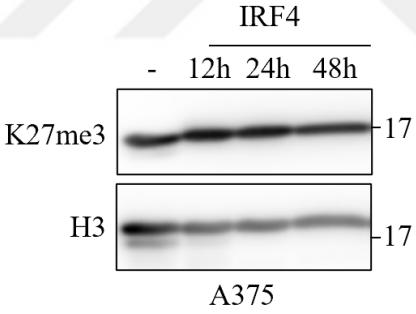

Figure H.2. Western blot for H3K27me3 IRF4 overexpressing A375 cell line.

APPENDIX I: IMMUNO BLOTS OF P21, P27, PTEN

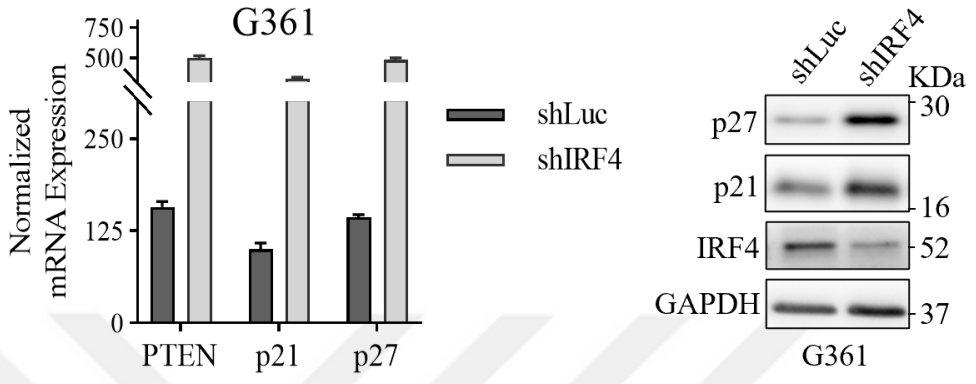

Figure I.1. PTEN, p21 and p27 expression upon IRF4 knockdown.

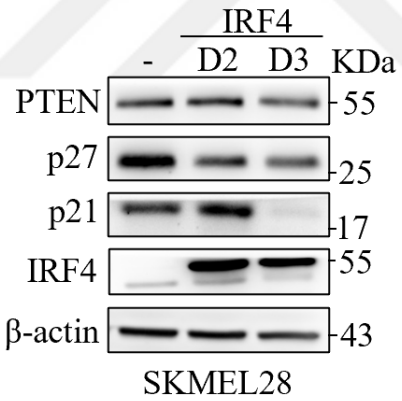

Figure I.2. Western blot for PTEN, p21 and p27 expression in SKMEL28 cell line overexpressing IRF4.

APPENDIX J: MSRE-QPCR- THE UNDIGESTED CONTROLS

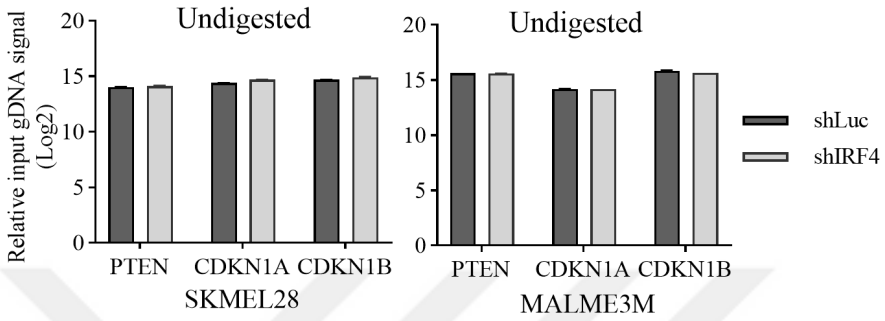

Figure J.1. qPCR for undigested controls in IRF4 knockdown melanoma cells.

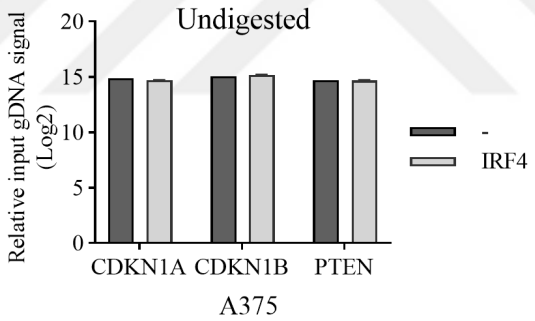

Figure J.2. qPCR for undigested controls in IRF4 overexpressing cells.

APPENDIX K: IMMUNOBLOT OF PI3K-AKT PATHWAY

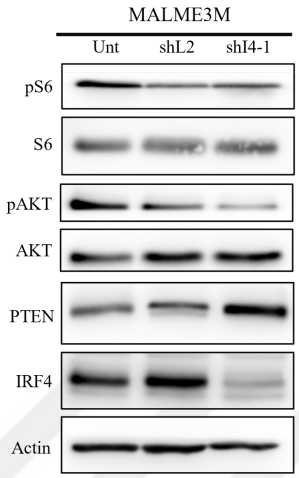

Figure K.1. Immunoblot for PI3K-AKT pathways and its downstream targets upon IRF4 depletion.

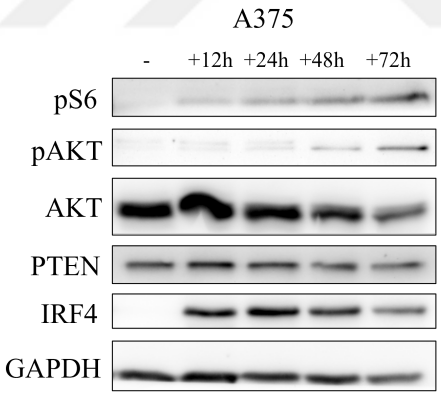

Figure K.2. Immunoblot for PI3K-AKT pathways and its downstream targets in IRF4 overexpressing A375 cell line at multiple timepoints.

APPENDIX L: 5-AZA AND DECITABINE

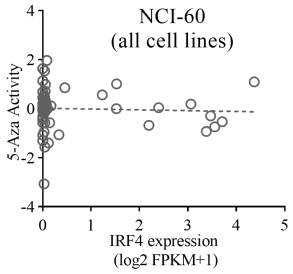

Figure L.1. Correlation analysis for all NCI-60 cell lines panel and 5-Aza cytostatic activity versus IRF4 expression. R = -0.04, linear regression p = 0.76.

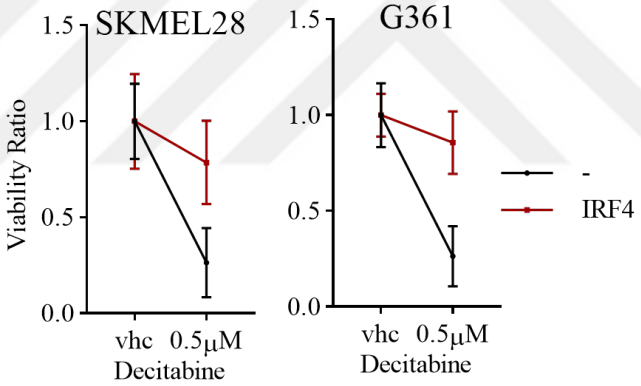

Figure L.2. XTT assay results of Decitabine treatment in IRF4 overexpressing melanoma cell lines.

APPENDIX M: DILUTION PLATING ASSAY FOR QUALITY CONTROL

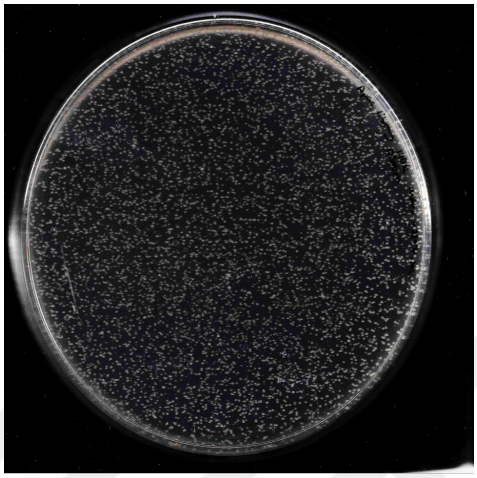

1:10,000

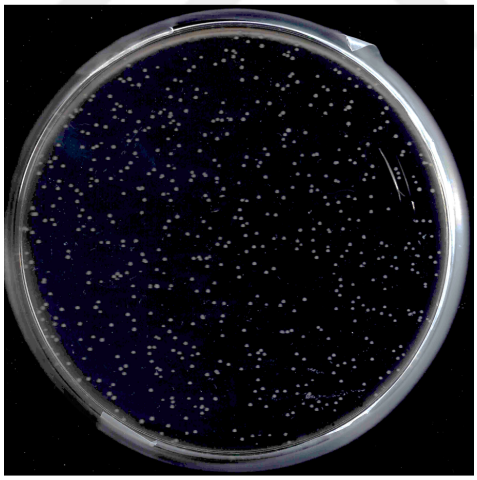

1:100,000

Figure M.1. Representative presentation of dilution plating assay for ACOC library.

APPENDIX N: VIRUS TITRATION OF ACOC AND GEEX LIBRARIES

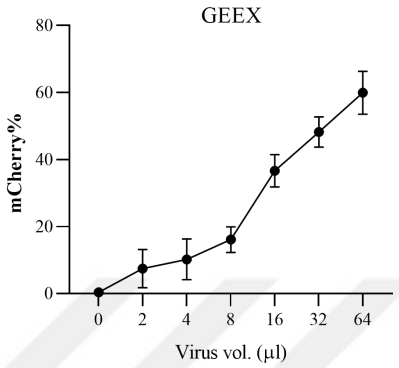

Figure N.1. mCherry-based titration for viruses produced for GEEX libraries screening in SKMEL28-Cas9 cells.

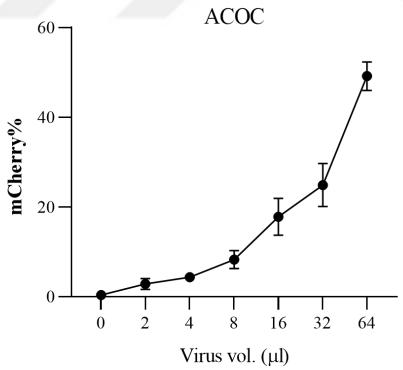

Figure N.2. mCherry-based titration for viruses produced for ACOC libraries screening in SKMEL28-Cas9 cells.

APPENDIX O: MAPPING STATISTICS FOR CRISPR/CAS9 SCREENING

Table O.1 Mapping statistics for NGS results of screening with ACOC library

Label	Percentage	Total sgRNAs	Zero counts	Gini Index
ACOC-EV-1	0.65	31324	610	0.126
ACOC-EV-2	0.75	31324	1049	0.1589
ACOC-KO3-2	0.75	31324	1049	0.1606
ACOC-KO3-1	0.78	31324	851	0.1027

Table O.2 Mapping statistics for NGS results of screening with GEEX library

Label	Percentage	Total sgRNAs	Zero counts	Gini Index
GEEX-EV-1	0.62	24449	520	0.09623
GEEX-EV-2	0.59	24449	2786	0.2084
GEEX-KO3-1	0.61	24449	451	0.0945
GEEX-KO3-2	0.49	24449	1639	0.227

APPENDIX P: TOP 5 GENES IN ACOC AND GEEX LIBRARIES

Table P.1. Statistics of top 5 ranked genes for ACOC libraries in SKMEL28-Cas9 EV samples.

id	num	neg—score	neg—p-value	neg—fdr	neg—rank	neg—lfc
PRPF19	10	1,03E-05	1,65E-03	0.00165	1	-44.434
POLR2L	10	3,83E-05	1,65E-03	0.00165	2	-44.308
PSMA3	9	9,90E-04	1,65E-03	0.00165	3	-44.661
GTPBP4	10	2,02E-03	4,94E-02	0.003713	4	-2.557
RRM2	10	3,23E-02	2,47E-02	0.014851	5	-30.506

Table P.2. Statistics of top 5 ranked genes for ACOC libraries in SKMEL28-Cas9 sgIRF4 KO samples.

id	num	neg—score	neg—p-value	neg—fdr	neg—rank	neg—lfc
PSMA3	10	1,57E-06	1,65E-03	0.000707	1	-48.568
POLR2L	10	1,65E-07	1,65E-03	0.000707	2	-55.981
SRSF3	10	7,19E-06	1,65E-03	0.000707	3	-65.889
RRM2	10	1,10E-06	1,65E-03	0.000707	4	-51.881
ALDOA	10	7,52E-05	1,65E-03	0.000707	5	-33.287

Table P.3. Statistics of top 5 ranked genes for GEEX libraries in SKMEL28-Cas9 EV samples.

id	num	neg—score	neg—p-value	neg—fdr	neg—rank	neg—lfc
RPL21	10	1,32E-02	2,12E-02	0.00495	1	-48.568
SNRPF	10	2,24E-02	1,48E-01	0.017327	2	-55.981
RBM8A	10	8,03E-02	6,57E-01	0.048515	3	-65.889
SF3B3	9	1,04E-01	0.00010389	0.048515	4	-51.881
UBTF	10	1,17E-01	9,12E-01	0.048515	5	-33.287

Table P.4. Statistics of top 5 ranked genes for GEEX libraries in SKMEL28-Cas9 sgIRF4 KO samples.

id	num	neg—score	neg—p-value	neg—fdr	neg—rank	neg—lfc
RPL21	10	8,51E-03	6,57E-01	0.0105817	1	-48.568
SF1	10	2,60E-01	0.00022685	0.0105817	2	-55.981
YTHDC1	10	2,74E-01	0.00023109	0.0105817	3	-65.889
ORC6	10	3,03E-01	0.00026078	0.0105817	4	-51.881
DGCR14	10	3,11E-02	0.0002735	0.0105817	5	-33.287

APPENDIX Q: VENN DIAGRAM RELATED TO CRISPR SCREENING

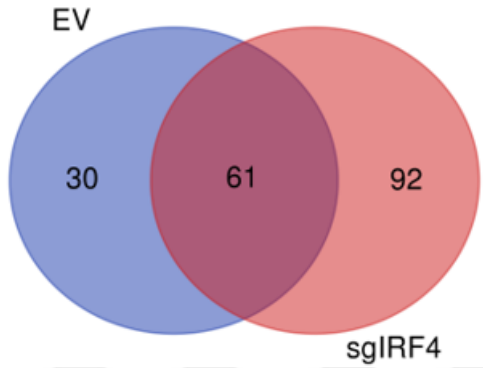

Figure Q.1. Venn diagram for filtering out common genes between EV and sgIRF4 KO in ACOC libraries. 92 genes only present in sgIRF4 KO samples used for further analysis.

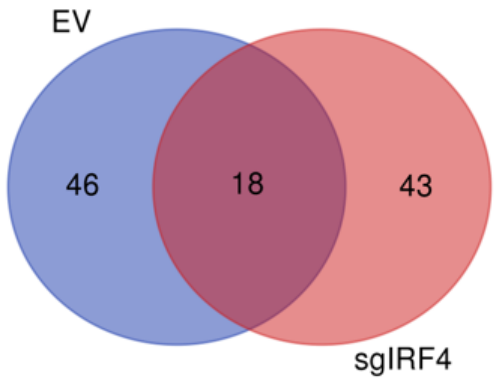

Figure Q.2. Venn diagram for filtering out common genes between EV and sgIRF4 KO in GEEX libraries. 43 genes only present in sgIRF4 KO samples used for further analysis.